

ABSTRACT

RUMBAUGH, BROOKE ALICIA. Impact of storm events on density stratification in the Pamlico and Albemarle Estuarine System. (Under the direction of Casey Dietrich).

Tropical cyclones and other coastal storms have multiple effects on estuaries. They create storm surge, or the rise of water levels above the normal tides, which can cause flooding of coastal areas, including communities near estuaries. They can also alter ecosystems, including in estuaries with changes to nutrient loading and regeneration, abrupt changes in salinity, increases in the mixed-layer depth, decreases in sea-surface temperature, and breakdowns in water column stratification. The interactions between surge and estuarine circulation can enhance the storm effects. And with the increasing intensity of tropical cyclones, these effects will be further enhanced.

Numerical models can represent the coastal environment and its response to the combined effects of tides, river flows, and winds. It is especially challenging for numerical models to represent the response of estuaries to storms, due to the complex interactions of fresh and saline waters, and thus relatively few studies have used models to represent both storm- and density-driven circulation in estuaries. These few studies have shown that salinities and temperatures of estuaries can change significantly during storms and may require weeks to recover, depending on the amount of freshwater discharge. However, these studies have been limited in number and geographic coverage, relied on coupling to other models for baroclinic inputs, did not have the estuarine mixing and stratification as a focus, or were missing physics. Much is still uncertain about how estuarine circulation evolves during a storm event. How quickly do the horizontal salinities respond to the storm? How does the salinity transport vary through an estuary? How do freshwater discharges due to rainfall affect the mixing? Another uncertainty is the salinity response after the storm. How quickly does a system recover? Do the freshwater discharges interrupt the recovery? In this thesis, *it is hypothesized that, for a large and shallow estuarine system with minimal connections to the open ocean, the storm forcing will cause large brackish and freshwater intrusions and recoveries that vary through the system.*

To investigate this hypothesis, we developed a three-dimensional model of storm- and density-driven circulation in the Albemarle-Pamlico Estuarine System (APES) in North Carolina. Irene (2011) was used as the basis for storm event simulations to examine the evolution of the horizontal salinity distribution. Included in this model were hurricane-strength winds and pressures, tides, river discharges, and density circulation. Using this

model, it was determined that during Irene, APES experienced movements of brackish water into the estuaries and saline water into the sounds. These movements were heavily dependent on the winds. After the storm simulation, the large river discharges produced intrusions of fresher water into major areas of the sound, and after two weeks, the system was not fully regulated.

From this research, we have developed a better understanding of the horizontal salinity distribution of APES as well as how the system reacts to a single storm event. This research allows for future studies to consider different types of storms along with refinement of the river forcings, to understand better the full range of estuarine responses.

© Copyright 2021 by Brooke Alicia Rumbaugh

All Rights Reserved

Impact of storm events on density stratification in the Pamlico and Albemarle Estuarine
System

by
Brooke Alicia Rumbaugh

A thesis submitted to the Graduate Faculty of
North Carolina State University
in partial fulfillment of the
requirements for the degree of
Master of Science

Civil Engineering

Raleigh, North Carolina

2021

APPROVED BY:

Katherine Anarde

Cheryl Ann Blain

Elizabeth Sciaudone

Casey Dietrich
Chair of Advisory Committee

DEDICATION

To my husband, Kyle, my parents, Todd and Lorie, and siblings, Steffan and Alaina. For supporting me all these years, listening to countless presentations, and reading multiple papers.

BIOGRAPHY

Brooke Rumbaugh was born in Charleston, West Virginia in 1996 to Todd and Lorie Rumbaugh. In 2015, she graduated from Riverside High School and decided to follow in her father's footsteps and become a civil engineer. To do this, she decided to attend Marshall University to pursue a B.S. in engineering. It was during this time she discovered a love of hydraulic engineering, which, combined with her love of the beach, led to her pursuing a M.S. in civil engineering with a coastal emphasis. She graduated from Marshall University in May 2019 and started attending, and researching, at North Carolina State University in Spring 2020. Outside of research and school, she enjoys spending time with her family and pets, reading, trying new foods, and visiting the beach.

ACKNOWLEDGEMENTS

The past two years have been a whirlwind; a good one, but a whirlwind nonetheless. Due to the global pandemic, the support provided to me was invaluable. In all aspects of my life, by numerous people, this support helped me make it through a completely unexpected situation. I would like to take the time to thank everyone for all of the support.

I would first like to thank my amazing advisor, Dr. Casey Dietrich. Without his guidance, I would have never decided to go into the field of coastal engineering, let alone do a thesis based masters program. His dedication to his students is something I admire greatly, as he always has time to help a student in need. If I ever had issues, he would find a way to help me.

Next I would like to thank my committee. Dr. Elizabeth Sciaudone for providing great feedback and ideas for adding depth to my research. Dr. Katherine Anarde for always being involved and willing to go the extra mile to support me. Dr. Cheryl Ann Blain for helping with 3D ADCIRC and her wonderful questions that prompted me to gain more insight to my research.

My next thanks goes to the Coastal Engineering Team. While we did not get to see each other in person as much as I would have liked, we were still able to connect, develop great friendships, and help each other. From helping with Python codes to providing great feedback during research updates, I am immensely grateful for each of you.

For the feedback and assistance provided during the 3D ADCIRC calls, you all have my most sincere thanks. With the feedback I was able to gain further understanding into the world of ADCIRC, as well as into my research. The recommendations that ranged from data sources to delving more into certain areas of the research, assisted me in developing a more complete story. I wholeheartedly thank each one of you for all of the assistance.

And, finally, to my family, I extend my thanks for being with me at every step. To my husband, Kyle, I am so thankful that you put up with me practicing all my presentations with you for hours. My parents, Lorie and Todd, for encouraging me to pursue my goals. My siblings, Steffan and Alaina, for taking the time to check in on me whenever they could.

TABLE OF CONTENTS

List of Tables	vii
List of Figures	viii
Chapter 1 INTRODUCTION	1
1.1 Funding Acknowledgment	7
Chapter 2 BACKGROUND	8
2.1 Study Area and Major Forcings	9
2.1.1 Albemarle-Pamlico Estuarine System (APES)	9
2.1.2 Density Drivers	9
2.1.3 Irene (2011)	11
2.2 Technologies to Describe Circulation in APES	12
2.2.1 SalWise	13
2.2.2 ADCIRC applied to APES	15
2.3 Motivation	18
2.3.1 Remaining Questions	18
2.3.2 Objectives	19
Chapter 3 METHODS	21
3.1 Mesh Development	21
3.1.1 NC9 Mesh	22
3.1.2 Trimmed Mesh for APES	23
3.1.3 Bathymetry Smoothing	24
3.2 Physical Forcings	27
3.2.1 Tides	28
3.2.2 Atmospheric	29
3.2.3 Rivers	31
3.2.4 Density	32
3.3 Simulation Setup	37
3.4 Analyses	39
3.4.1 Salinity Contours	39
3.4.2 Analysis Methods	42
Chapter 4 RESULTS AND DISCUSSION	46
4.1 Synoptic History of Irene in APES	47
4.1.1 During Irene	47
4.1.2 Before Landfall	47
4.1.3 During Landfall	50
4.1.4 After Landfall	52
4.1.5 After Irene	54

4.2	Irene's Effects on Surface Salinities	56
4.2.1	Albemarle Sound	56
4.2.2	Pamlico Sound and Hatteras and Ocracoke Inlets	60
4.2.3	Roanoke Island and Oregon Inlet	64
4.2.4	Neuse and Tar-Pamlico Rivers	68
4.3	Oyster Sanctuaries	73
Chapter 5	Conclusions and Future Work	75
References	78
APPENDIX	85
Appendix A	ADCIRC Model Parameters	86

LIST OF TABLES

Table 2.1	Each major river’s approximate drainage area, mean annual flow, and maximum flow recorded and date of maximum flow (U.S. Geological Survey 2021; North Carolina Department of Environmental Quality 2021)	10
Table 3.1	Bathymetric depth ranges for which bathymetry was utilized to develop the combined mesh.	27
Table 3.2	USGS stream gauges selected at the four river boundaries for the NC9-APES mesh. The flow rates are the average values of the simulation before the storm segment, 0000 UTC 6 August to 0000 UTC 21 August. These values will be used during the no-storm simulation.	32
Table 3.3	Biologically based estuarine salinity zones from Bulger et al. (1993). The salinities shown are in ppt and are the lower and upper limits of each zone.	40
Table 3.4	Coordinates and geographic regions for the synthetic stations to be used in later analyses.	43
Table 3.5	Coordinates and geographic regions for the oyster sanctuary stations to be used in later analyses.	45

LIST OF FIGURES

Figure 2.1	Map of the Albemarle-Pamlico Estuary System (APES) in coastal North Carolina. The red outline show the extents of the study area. Labeled are the major rivers, inlets, and key areas that will be referenced in this study. The blue outline is a zoomed in area near Roanoke Island.	10
Figure 2.2	The path of Irene through the area of study from the National Hurricane Center best-track file, which records the location of the eye at 6-hr intervals. It made landfall at 1200 UTC 27 August and left the area by 28 August. During this time, it was a Category-1 hurricane.	13
Figure 2.3	Fish kill locations during Irene (2011), as reported by the North Carolina Department of Environmental Quality. The color of marker indicates the amount of fish killed, with red being greater than 1000 kills.	14
Figure 2.4	Distributions of observations collected in the month of August in any year, as reported in the SalWise database, for (left) surface and (right) bottom.	16
Figure 3.1	The NC9 mesh encompasses a large domain, which includes the entire Atlantic coast of the United States.	23
Figure 3.2	The NC9-APES mesh (left) was cut from NC9 and encompasses the Albemarle and Pamlico Sounds and the four key river estuaries. Bathymetry (m, positive downward, right) was interpolated from NC9.	24
Figure 3.3	Bathymetry (m, positive downward) near the Oregon Inlet, as represented in the original mesh (top left), smoothed mesh (top right), and final mesh (bottom). Notice the steep gradients near either side of the inlet in the original mesh. In the smoothed mesh, these are removed. The final mesh is a combination of both.	26
Figure 3.4	The final bathymetry (m, positive downward), after the smoothing, was used for simulation.	28
Figure 3.5	Surface canopy coefficient values for the area of study. Blue indicates a value of 1, showing wind stress is applied, while red indicates a value of 0, with no applied wind stress.	31
Figure 3.6	Flux rates ($\text{m}^3/\text{s}/\text{m}$) applied to each river boundary internal vertex. The largest flux is on the Neuse River, while the smallest is on the Chowan River.	33
Figure 3.7	Square grid used for binning of the SalWise observational data. The blue lines are the 0.05-degree bins, with blue dots at the center of each bin. Within each bin, SalWise observations from August in any year were averaged.	34

Figure 3.8	Sensitivity of interpolated surface to tension and smoothing parameters. The x -axis in both graphs represents the salinity values for each bin. The y -axis is the value taken from the developed salinity surface at the bin location. For both graphs, if the surface was a perfect match to the observational values, the points would fall on the one-to-one line. The left graph depicts variations within the tension parameter between values of 0 and 100. The right graph shows variations with the smoothing parameter, with a tension parameter set to 100. This is due to higher tension value more closely resembling the observational values, the blue dots.	36
Figure 3.9	Initial conditions for (top) salinities and (bottom) temperatures, shown at both the (left) surface and (right) bottom. The salinities have dimensions of ppt, and the temperatures have units of degrees Celsius.	37
Figure 3.10	Timeline of simulation with corresponding dates, types, and forcings. The storm simulation (top) includes the atmospheric forcing and changing river discharges. The no-storm simulation (bottom) does not include atmospheric forcing and constant discharges.	38
Figure 3.11	Average surface salinities for the month of August, developed using the method in Section 3.2.4, with contour values to show the selected salinity zones.	41
Figure 3.12	Locations of synthetic stations (top) and oyster sanctuaries (bottom) to be used to analyze time series of surface salinities.	44
Figure 4.1	Timeline for Irene (2011) to indicate timesnaps shown in later figures.	48
Figure 4.2	Irene's effects on (left) surface salinities (ppt) and (right) water levels (m relative to mean sea level), with time snaps of (top row) 0200 UTC 21 August, (second row) 0400 UTC 26 August, (third row) 0600 UTC 27 August, and (bottom row) 1000 UTC 27 August. For the surface salinities, the colors indicate zones of (light blue) mesohaline, (yellow) polyhaline, and (purple) euhaline.	49
Figure 4.3	Irene's effects on (left) surface salinities (ppt) and (right) water levels (m relative to mean sea level), with time snaps of (top row) 1200 UTC 27 August, (second row) 1600 UTC 27 August, (third row) 2000 UTC 27 August, and (bottom row) 2200 UTC 27 August. For the surface salinities, the colors indicate zones of (light blue) mesohaline, (yellow) polyhaline, and (purple) euhaline.	51
Figure 4.4	Irene's effects on (left) surface salinities (ppt) and (right) water levels (m relative to mean sea level), with time snaps of (top row) 0200 UTC 28 August, (second row) 0600 UTC 28 August, (third row) 1000 UTC 28 August, and (bottom row) 0000 UTC 29 August. For the surface salinities, the colors indicate zone of (light blue) mesohaline, (yellow) polyhaline, and (purple) euhaline.	53

Figure 4.5	Irene's effects on (left) surface salinities (ppt) and (right) water levels (m relative to mean sea level), with time snaps of (top row) 1200 UTC 31 August, (second row) 0000 UTC 5 September, (third row) 1200 UTC 7 September, and (bottom row) 0000 UTC 12 September. For the surface salinities, the colors indicate zones of (light blue) mesohaline, (yellow) polyhaline, and (purple) euhaline.	55
Figure 4.6	Irene's effects on the Albemarle Sound: (left) surface salinities (ppt) and (right) differences (ppt) from a non-storm simulation. Rows correspond to: (top row) 0200 UTC 21 August, (second row) 0800 UTC 27 August, (third row) 1800 UTC 27 August, (fourth row) 0800 UTC 28 August, and (last row) 0000 UTC 5 September.	57
Figure 4.7	Time series of surface salinities (ppt) in Albemarle Sound at synthetic stations: 16 (top left), 17 (top right), 18 (middle left), 19 (middle right), 20 (bottom left), and 21 (bottom right). Details listed in Table 3.4 and shown in Figure 3.12.	58
Figure 4.8	Irene forced effects on the Pamlico Sound, Hatteras Inlet, and Ocracoke Inlet: (left) surface salinities (ppt) and (right) differences (ppt) from a non-storm simulation. Rows correspond to: (top row) 0200 UTC 21 August, (second row) 0800 UTC 27 August, (third row) 2200 UTC 27 August, (fourth row) 0000 UTC 29 August, and (last row) 0000 UTC 12 September.	61
Figure 4.9	Time series of surface salinities (ppt) near Pamlico Sound and Hatteras and Ocracoke Inlets at synthetic stations: 12 (top left), 13 (top right), 14 (middle left), 15 (middle right), 9 (bottom left), and 10 (bottom right). Details listed in Table 3.4 and shown in Figure 3.12.	62
Figure 4.10	Irene forced effects on the Roanoke Island and Oregon Inlet: (left) surface salinities (ppt) and (right) differences (ppt) from a non-storm simulation. Rows correspond to: (top row) 0200 UTC 21 August, (second row) 0600 UTC 27 August, (third row) 1600 UTC 27 August, (fourth row) 0600 UTC 28 August, and (last row) 0000 UTC 12 September.	65
Figure 4.11	Time series of surface salinities (ppt) near Roanoke Island and Oregon Inlet at synthetic stations: 5 (top left), 6 (top right), 7 (middle left), 8 (middle right), and 11 (bottom). Details listed in Table 3.4 and shown in Figure 3.12.	66
Figure 4.12	Irene forced effects on the Neuse and Tar-Pamlico Rivers: (left) surface salinities (ppt) and (right) differences (ppt) from a non-storm simulation. Rows correspond to: (top row) 0200 UTC 21 August, (second row) 1200 UTC 27 August, (third row) 0800 UTC 28 August, (fourth row) 0000 UTC 29 August, and (last row) 0000 UTC 12 September.	69
Figure 4.13	Time series of surface salinities (ppt) in the Neuse and Tar-Pamlico Rivers at synthetic stations: 1 (top left), 2 (top right), 3 (bottom left), and 4 (bottom right). Details listed in Table 3.4 and shown in Figure 3.12.	70

Figure 4.14 Time series of surface salinities (ppt) at the oyster sanctuaries stations:
22 (top left), 25 (top right), 26 (bottom left), and 34 (bottom right).
Locations listed in Table 3.4 and shown in Figure 3.12. 73

CHAPTER

1

INTRODUCTION

Tropical cyclones, which can strengthen into hurricanes, continue to be major natural disasters. Their intense winds, large amounts of rainfall, and flooding all contribute to their destructive capability, both in loss of life and in damages to infrastructure. From 1980 to 2020, tropical cyclones have caused more damage than any other type of weather disaster in the U.S. During this time period, several tropical cyclones each caused more than \$1 billion of damages in the U.S., and those cyclones together caused about \$990 billion in damages (National Oceanic and Atmospheric Administration 2021a). This destruction then translates into a loss of life, with more than 6,500 deaths due to tropical cyclones between 1980 and 2020 (National Oceanic and Atmospheric Administration 2021a).

With increasing climate change, tropical cyclone activity is predicted to increase globally (Emanuel 2013). This activity includes stronger storms and higher precipitation events (Emanuel 2013, 2017). This increased activity of tropical cyclones has been observed since the mid-1990s (Paerl et al. 2018). With the predictions of increasing intensity and frequency of the strongest storms, damages in the North America due to tropical storms are also predicted to increase (Mendelsohn et al. 2012). It has been noted that climate change has more of an effect on the larger storms, thus increasing their relative damage (Mendelsohn et al. 2012). This can be seen within the past four years of hurricane seasons in

the U.S. In 2017, the Atlantic hurricane season was among the top seven most intense seasons ever recorded (National Oceanic and Atmospheric Administration 2021a). For the hurricane seasons of 2018 and 2019, more than \$136 billion of damages were reported. The hurricane season of 2020 was the second time in U.S. history that the Greek alphabet was used to name storms, extending to the ninth letter (National Oceanic and Atmospheric Administration 2021a).

When tropical cyclones approach or make landfall, they create *storm surge* – the rise of ocean waters above the regular tide levels. The changing climate will contribute to a significant increase in storm surge flood levels (Lin et al. 2012). Storm surge can cause flooding of coastal areas, which can lead to fatalities due to drowning, damage to structures and infrastructure, erosion of beaches, and even damage to coastal habitats (National Oceanic and Atmospheric Administration’s Climate Program Office 2020). Storm surge and associated flooding can also disturb estuaries and alter ecosystems. Examples of this include changes to nutrient loading and regeneration, development of harmful algal blooms, habitat degradation, fish mortalities, abrupt changes in salinity, increases in the mixed-layer depth, decreases in sea-surface temperature, and breakdown in water column stratification (Paerl et al. 2018; D’Sa et al. 2019; Williams et al. 2001; Davis and Yan 2004; Black and Dickey 2008). These changes, combined with the projected increases in precipitation and storm surge, could result in large-scale changes in coastal ecosystems (D’Sa et al. 2019). Tropical cyclones cause extensive damages for both human and natural environments.

To understand these hazards and mitigate their risks, coastal stakeholders rely on numerical models, which can represent the coastal environment and its response to the combined effects of tides, rivers, winds, and other forcings. However, to simplify their simulations and thus complete them in a reasonable time, most models do not include the full range of possible physical drivers during a storm. For example, models for storm surge and coastal flooding often assume that the water column is well-mixed, (e.g. Jelesnianski et al. (1992) and Westerink et al. (2008)), and thus they represent the coastal ocean with uniform water densities and depth-averaged currents. With this assumption, these models have been used successfully for real-time forecasting (Blanton et al. 2012b), evaluation and design of flood mitigation systems (Interagency Performance Evaluation Task Force 2008), and mapping of flood risk (FEMA 2021).

Even in estuaries, where the simplifying assumptions can be violated due to density stratification, these models have been successful in evaluating the storm-driven circulation. Maskell et al. (2014) used the Finite Volume Community Ocean Model (FVCOM) with an idealized estuary to investigate the effect of estuary geometry and storm surge against river

discharge. It was found that the interactions between surge and river discharge increased residual elevations, but the storm surge was the dominant mechanism. In real estuaries, the river interaction may have a more significant role, due to up-estuary flooding defenses. Peng et al. (2004) applied the nonlinear, three-dimensional Princeton Ocean Model (POM) for the Croatan-Albemarle-Pamlico estuary system in North Carolina, with forcings from 10 hypothetical Category 2 and 3 hurricanes and the historical Emily (1993). POM was able to accurately reproduce the peak surge in the sounds. Familkhalili and Talke (2016) used Delft3D to investigate storm surge in the Cape Fear River estuary, also in North Carolina. The results suggested that the storm surge was sensitive to bathymetry changes. Dinápoli et al. (2020) validated a modified version of Coastal and Regional Ocean COmmunity Model (CROCO) for simulations in the Río de la Plata Estuary. It was determined that the modified model was able to reproduce the water levels and depth averaged currents, including extreme storm surges for hindcasts. Hu et al. (2015) used Delft3D to study how vegetation can reduce storm surge and the effect of wind intensity and forward speed in the Breton Sound, Louisiana. It was determined that in the upper Breton Sound, with increasing stem height and stem density the reduction and reduction rate of storm surge increased as was seen for increased forward speed, but when wind intensity increased these decreased.

For many studies of storm surge and coastal flooding, the ADvanced CIRCulation (ADCIRC) model has gained prominence. ADCIRC is an unstructured-mesh, finite element, hydrodynamic model. The two-dimensional version is used widely for storm surge applications and have been applied for numerous storm surge studies (Bunya et al. 2010; Cyriac et al. 2018; Dietrich et al. 2012). ADCIRC has been applied in estuaries to examine storm surge, often coupled with the Simulating WAVes Nearshore (SWAN) model. Yin et al. (2017) applied it to the Pearl River Estuary in China to investigate the effect of sea level rise and typhoon intensification on storm surge. It was found that typhoon intensification had the larger effect on the storm surge. Cheng et al. (2015) used it to hindcast the Great Coastal Gale of 2007 at Pacific Northwest estuaries to examine the contribution of physical processes to storm surge. It was determined that large storm waves are the largest contributing process. Sebastian et al. (2014) also used it to investigate maximum water levels and behavior of storm surge in Galveston Bay, Texas. Ike (2008) and stronger perturbations of Ike were simulated. It was found that water levels began rising in Galveston Bay almost a full day before landfall and storm surge in the bay was dependent upon the landfall location.

For all of these studies (ADCIRC or other models), while they investigated the storm-driven circulation, they did not include density-driven circulation and stratification. These studies assumed a well-mixed water column in the coastal regions, so the mixing and

corresponding regulation are not well-represented during storms.

Separately, other studies have focused on the density-driven circulation, often with emphasis on key factors pertaining to specific estuaries. Xie and Li (2018) used a three-dimensional model combined with observational data to examine the along-channel winds in the Chesapeake Bay affect the density stratification. The model was based on the Regional Ocean Modeling System (ROMS) and focused on wind events that were dominated by wind forcing in the along-channel direction. It was determined that the stratification in the mid and upper bay decreased under up-estuary winds and the down-estuary winds created a response that was dependent upon the Wedderburn number, with increases in stratification at moderate values and decreases at large values. The lower bay had responses that were opposite: decreases with down-estuary winds and increases with the up-estuary winds. Rayson et al. (2015) examined density-driven circulation in Galveston Bay. The model Stanford Unstructured Nonhydrostatic Terrain-following Adaptive Navier–Stokes Simulator (SUNTANS) was coupled with the ROMS for the application of tidal, riverine, and atmospheric physical forcings. It was found that the salinity variations in Galveston Bay were due to large river discharges. Lin et al. (2007) used a model based on three-dimensional hydrodynamic-eutrophication model (HEM-3D) to investigate the basic climatologic water quality features for CAPES, North Carolina. It was found that model, along with field data, showed seasonal variations in five different water quality parameters. Also, it was shown that in winter months, the waters are relatively fresher compared to the summer months.

ADCIRC has also been used for simulations of density-driven circulation. One example was for the validation of the three-dimensional, baroclinic version of ADCIRC by using the lock exchange problem (Kolar et al. 2009). In this model, the vertical closure schemes were also examined. It was found that ADCIRC was able to adequately reproduce the mixing of fluids in a laboratory-scale experiment and the Mellor-Yamada 2.5 closure scheme developed the most consistent description. Dresback et al. (2010) applied ADCIRC, coupled with HYbrid Coordinate Ocean Model (HYCOM), to the Northern Gulf of Mexico. The model was initialized by using results from HYCOM for the densities, velocities, and elevations. Wind stress and heat flux were taken from an atmospheric model and the tidal forcing from a tidal database. There were 21 equally spaced vertical layers in the ADCIRC model. It was found that the coupled model's results were qualitatively acceptable. Blain et al. (2009) used ADCIRC to simulate circulation in the Dardanelles Strait. The model was coupled with Coupled Ocean–Atmosphere Mesoscale Prediction System (COAMPS) for surface meteorological forcing and HYCOM for the boundary conditions. There were 41 vertical layers. It was found that the initial conditions had a strong impact on the spread

of the Dardanelles plume into the Aegean Sea and interpolated measurements were able to develop a realistic depth variation for the salinity. Cyriac et al. (2020) investigated the tidal, wind, and density-driven circulation at Choctawhatchee Bay, Florida. There were 21 vertical layers. The model results had a high degree of correlation with observed salinity profiles at most locations. Also in good agreement were the regions where the water column was fully mixed.

While all these studies focused on density-driven circulation, none of the models were forced with tropical-cyclone strength winds. Recently, there have been studies in which the two types of circulation have been combined in the same model; however, most relied on coupling to a larger baroclinic ocean model, some examined the density stratification as an additional goal and not the main goal, most were not in our study area, or some were missing relevant physics.

Liu et al. (2019) used the West Florida Coastal Ocean Model (WFCOM) and in-situ data to investigate impacts on the circulation and the memory of the system in response to Irma (2017) at Florida Bay and Charlotte Harbor Estuary. This model was coupled with HYCOM. The results found that the temperature regulated after about three days, but the salinity was highly dependent up on location. D'Sa et al. (2019) studied the response of dissolved and particulate organic carbon in the Apalachicola Bay, Florida, by using NCOM. This model was nested, using a higher resolution in the study area and a lower resolution for the surrounding northern Gulf of Mexico. It was found that the storm had strong hydrologic and hydrodynamic controls on the response of the carbon. For the salinities, changes began four days before the storm, experienced changes from 0 ppt to 30 ppt, and took up to four days to return to pre-storm levels. Brown et al. (2014) used Delft3D to examine the transport of the dissolved organic carbon in the Neuse River, North Carolina, during Irene (2011). This model had high resolution for the river and a lower resolution of the Albemarle-Pamlico Estuary System. The lower resolution was used to develop wind-driven currents and water levels for the higher resolution nested mesh. Salinities were applied using observations from the Neuse River Estuary Modeling and Monitoring Project (ModMon) taken from before the storm and after the storm. It was determined that the model was able to simulate the horizontal and vertical salinity distribution, and the freshwater plumes progressed along the southern shore of the river.

There have been attempts to develop a combined model for APES, but each attempt had missing physics or a lack of storm-driven circulation (Lin et al. 2007). Amein and Airan (1976) developed a two-dimensional, time-dependent, shallow-water model to investigate storm surge and circulation in the Pamlico Sound. This model did not include the full

area and lacked bottom friction and wind-induced vertical variations. This model was developed into a three-dimensional, time-dependent, shallow-water model to examine the circulation (Pietrafesa et al. 1986; Lin 1992; Pietrafesa and Janowitz 1991). This model was shown to have good predictions of surge for winter and tropical storms (Peng et al. 2004; Pietrafesa et al. 1997; Neuherz et al. 1992), but the two major sounds were simulated separately. Also, in the Lin (1992); Pietrafesa et al. (1986) models, nonlinear advection terms were not included. Xie and Pietrafesa (1999), to overcome these issues, used POM for the entire CAPES. This model was not applied to study the impacts of a storm event and did not include inundation or wetting and drying. Peng et al. (2004) included these missing physics, but did not include density-driven circulation and focused on storm-driven circulation. Lin et al. (2007) was able to include spatial distribution of flows, temperature, salinity, and water quality variables, but the study was focused on developing the basic climatologic water quality features. Jia and Li (2012) used the Regional Ocean Modeling System (ROMS) to hindcast 2003 for the investigation of the mean circulation dynamics and salt balance. This study, while included investigated the entire year of 2003, did not examine the influence of the storm-driven circulation.

Although there have been studies that have investigated separately the storm-driven and density-driven circulation in estuaries and a select few studies that included both, their combination is necessary to understand the full effects of tropical cyclones on these critical systems. Cheng et al. (2015) note that the use of the barotropic, vertically-integrated model may contribute to differences between modeled and observed results, and that a baroclinic model would include the potentially missing vertical variations. Much is still uncertain about how the estuary evolves during a storm event. How quickly do the horizontal salinities respond to the storm? How does the salinity transport vary through the estuary? How do freshwater discharges due to rainfall affect the mixing? Another uncertainty is the salinity response to the storm. How quickly does a system recover? Do the freshwater discharges interrupt the recovery?

These questions are the main basis of this thesis. *It is hypothesized that, for a large and shallow estuarine system with minimal connections to the open ocean, the storm forcing will cause large brackish and freshwater intrusions and recoveries that vary through the system.* To investigate this hypothesis, we will develop a three-dimensional model of storm- and density-driven circulation in the Albemarle-Pamlico Estuarine System (APES) in North Carolina. Irene (2011) will be used as the storm event for simulations to examine the evolution of the horizontal salinity stratification. With this model and application, we will quantify the speed and distribution of salinity transport during a storm, as well as the return

to pre-storm conditions.

1.1 Funding Acknowledgment

The funding for this research was provided by North Carolina Sea Grant, which is part of the National Sea Grant College Program. This program's mission is to enhance the conservation of coastal resources in order to develop a sustainable economy and environment.

CHAPTER

2

BACKGROUND

This research will examine questions about storm-induced mixing and restratification of coastal waters in North Carolina (NC). In this region, the interactions of fresh and saline waters lead to stratification, which can vary both horizontally and vertically and is important for coastal ecosystems, but which can be disrupted due to mixing by storms. This stratification is described by observations collected over decades, but with relatively sparse resolution in space and time. It is also described by numerical models, which have been used typically for separate simulations of storm-driven flooding or non-storm circulation.

In this chapter, we examine elements that led to this research. First, we describe the study area of the Albemarle-Pamlico Estuarine System (APES), including the major drivers of density differences, and how it responded to Irene (2011). Although Irene had hurricane-strength winds as it passed over NC, it was not classified as a hurricane for its full existence, so we refer to the tropical cyclone as only 'Irene' in this thesis. Then, we describe the observations that show how the stratification can vary in the system, and the ADCIRC model that has been developed for storm surge predictions. Last, gaps in these technologies will lead to questions about how the system responds to and recovers from storm forcing. These questions will be developed to motivate the research goals and objectives in this thesis.

2.1 Study Area and Major Forcings

To explore the effects of storm forcing on a stratified estuarine system, this research will consider Irene (2011) in coastal North Carolina (NC). This region is characterized by large estuaries with multiple river inputs, wide sounds with shallow bathymetry, and limited connections to the open ocean. Irene moved directly over the estuarine system, driving circulation in multiple directions as its winds shifted.

2.1.1 Albemarle-Pamlico Estuarine System (APES)

APES is the second-largest estuarine system in the United States, being designated as “an estuary of national significance” in 1987 (Albemarle-Pamlico National Estuary Partnership 2021). It covers a drainage area of approximately 72,000 square kilometers, has approximately 16,000 km of rivers and streams flowing into the 8,000 km estuary. It is comprised of two shallow lagoonal sounds bounded by the Outer Banks barrier island chain and multiple river estuaries (Figure 2.1).

Pamlico Sound is the larger of the two sounds, with an approximate area of 120 km by 40 km and an average depth of 4.5 m (Luettich et al. 2002). Albemarle Sound has an approximate area of 85 km by 12 km and an average depth of 5 m. These two sounds are connected through the Croatan and Roanoke Sounds on either side of Roanoke Island. The Croatan and Roanoke Sounds have a combined area of 20 km by 7 km and an average depth of 2.5 m (Luettich et al. 2002). There are three smaller sounds: Currituck, Bogue, and Core Sounds (Albemarle-Pamlico National Estuary Partnership 2021).

For ocean water exchange, there are three small inlets: Oregon, Hatteras, and Ocracoke. The inlets are small with widths of about 1 km (Luettich et al. 2002). For Ocracoke and Hatteras Inlets, the average depths are shallow about 3.7 m and 3.2 m, respectively. Oregon Inlet has an average depth of about 5 m. Because these inlets are small and so few in number, APES circulation is minimally influenced by tides. Instead, APES circulation is heavily dependent on winds. There are also four major rivers: Chowan, Roanoke, Tar-Pamlico, and Neuse. The rivers provide freshwater discharges into the APES.

2.1.2 Density Drivers

The four rivers discharge freshwater into the APES, thus driving density differences through the system. Out of the four, the Roanoke River has the largest drainage area, mean annual flow rate, and largest maximum flow recorded (Table 2.1). Compared to the annual average,



Figure 2.1: Map of the Albemarle-Pamlico Estuary System (APES) in coastal North Carolina. The red outline show the extents of the study area. Labeled are the major rivers, inlets, and key areas that will be referenced in this study. The blue outline is a zoomed in area near Roanoke Island.

Table 2.1: Each major river’s approximate drainage area, mean annual flow, and maximum flow recorded and date of maximum flow (U.S. Geological Survey 2021; North Carolina Department of Environmental Quality 2021)

River	Drainage Area km ²	Mean Flow m ³ /s	Maximum Flow m ³ /s	Date
Chowan	12,000	21.89	320	11 October 2016
Roanoke	25,000	226.68	7,300	18 August 1940
Tar-Pamlico	16,500	70.35	1,000	22 August 1940
Neuse	16,100	117.30	1,600	20 September 1999

the Roanoke River’s largest recorded flow rate is more than 32 times larger. For the Neuse River, it has the second largest annual mean flow rate and the second highest recorded maximum. The annual flow is more than 13 times smaller than the maximum flow rate recorded. The Tar-Pamlico River has the second largest drainage area, but the third largest mean annual flow rate and maximum flow rate recorded. Between the annual flow rate and the maximum, the annual rate is 14 times smaller than the maximum. The river with the smallest annual mean flow rate, drainage area, and maximum flow rate is the Chowan River. Its maximum flow rate is 14 times larger than the annual flow rate. It should be noted that the drainage area is for the entire river, while the annual mean flows and maximum flow rates are calculated for the United States Geological Survey (USGS) stations listed in Chapter 3.

APES is also influenced by saline inflows through the three ocean inlets. These three inlets have remained dominant waterways in the Outer Banks and are fundamental to the transport of saline water and other materials from the ocean into the sound (Dolan and Lins 2000). These inlets see an average tidal range of about 1 m. The tides inside APES are weak due to the restrictive connections to the Atlantic Ocean, and thus winds are the major forcing of the system (Peng et al. 2004).

With the fresh water discharges from the rivers and the saline water inflows from the ocean inlets, APES has a very diverse salinity distribution. The vertical salinity stratification (between top and bottom) ranges between 0.1 and 2 ppt in the Pamlico Sound, indicating a weak stratification due to the winds mixing the water column well (Luettich et al. 2002; Jia and Li 2012). The Pamlico Sound has an average salinity of about 20 ppt, while the Albemarle is fresher, with values less than 1 ppt (Albemarle-Pamlico National Estuary Partnership 2019; Jia and Li 2012). The Currituck Sound, which is directly connected to the Albemarle, has an average salinity of about 3 ppt (Albemarle-Pamlico National Estuary Partnership 2021). These regions do experience a seasonality to their salinity values. This seasonality is highly dependent on the salt flux balance between the inlet inflow and the river discharges. The river salt flux (a reduction due to being fresh water) increases during the spring and is at a low during the summer, corresponding with the high and low river discharges. This indicates that salinities are lowest during the spring and highest during the summer (Jia and Li 2012).

2.1.3 Irene (2011)

Irene was a destructive tropical cyclone that made landfall in NC and caused extensive flood and wind damage as well as damage to ecosystems (North Carolina Department of Environmental Quality 2011; National Weather Service 2018). The storm began to develop on 15 August 2011 on the west coast of Africa (Avila and Cangialosi 2013). The system became a tropical storm before 0000 UTC on 21 August. Irene progressed west-northwest across the Caribbean Sea and gained strength. On 22 August at 0535 UTC, the storm passed over Puerto Rico and then became a hurricane. By 24 August, Irene had moved past Hispaniola and began to strengthen again. On the same day, by 1200 UTC in the Bahamas, Irene had become a Category-3 hurricane with a peak intensity of about 54 m/s. Keeping the same direction of movement, Irene crossed Acklins and Crooked Islands about 1500 UTC on 24 August. Passing the northwestern Bahamas at 1800 UTC on 25 August, Irene was downgraded to a Category-2 hurricane. While the winds decreased at this point, the circulation expanded

and the central pressure kept falling.

Irene continued northward, progressing past Florida and Georgia to make landfall at Cape Lookout, NC (Figure 2.1). Landfall occurred at 1200 UTC 27 August, and Irene had a peak wind speed of about 38 m/s. It was then classified as a Category-1 hurricane on the Saffir-Simpson scale. These peak winds were located over the eastern sides of the sounds and the Outer Banks. After moving out of coastal NC, Irene then continued a north-northeastern path and made another landfall on 28 August at 0935 UTC near Atlantic City, New Jersey. Continuing the same path, Irene then passed over Coney Island, New York at 1300 UTC on 28 August and a hour later passed over Manhattan, New York. By 0000 UTC on 29 August, while passing over the New Hampshire/Vermont border, Irene became extratropical and then was absorbed by 0600 UTC on August 30 in Canada. Irene caused an estimated \$15.8 billion in total damages. (Avila and Cangialosi 2013)

Due to Irene's path over NC (Figure 2.2), the area experienced high winds and storm surge. As the storm progressed through NC, wind speeds up to 38 m/s were observed (Avila and Cangialosi 2013). During the storm, the highest storm surge reported by a tide gauge was 2.16 m at Oregon Inlet Marina, though post-storm surveys suggest there was a storm surge of 2.4 to 3.3 m in areas of the Pamlico Sound. Along the Atlantic coast of the U.S., Irene produced a large swath of 12.7 to 25.4 cm rainfall from inland NC northward. The largest amount of rainfall, approximately 39.9 cm, was reported at Bayboro, NC (Figure 2.1) (Avila and Cangialosi 2013).

Irene disrupted the ecosystem in the APES. Its strong winds pushed fresh and saline waters away from their typical locations in the system, and its large rainfall led to large freshwater inputs along the four rivers. According to the NC Department of Environmental Quality, there were 12 reports of fish kills from the hurricane, with 10 being in the area of study (Figure 2.3) (North Carolina Department of Environmental Quality 2011). These fish kills occurred due to low amounts of dissolved oxygen after the storm. Several of these events were located on the Chowan and Roanoke Rivers, which empty into the Albemarle Sound. The last report was on the Roanoke River on 13 September, more than 17 days after the storm exited the area (North Carolina Department of Environmental Quality 2011).

2.2 Technologies to Describe Circulation in APES

The dynamic circulation in APES due to storms and density stratification are described by multiple sources. Point observations of salinities, temperatures, and other water quality data

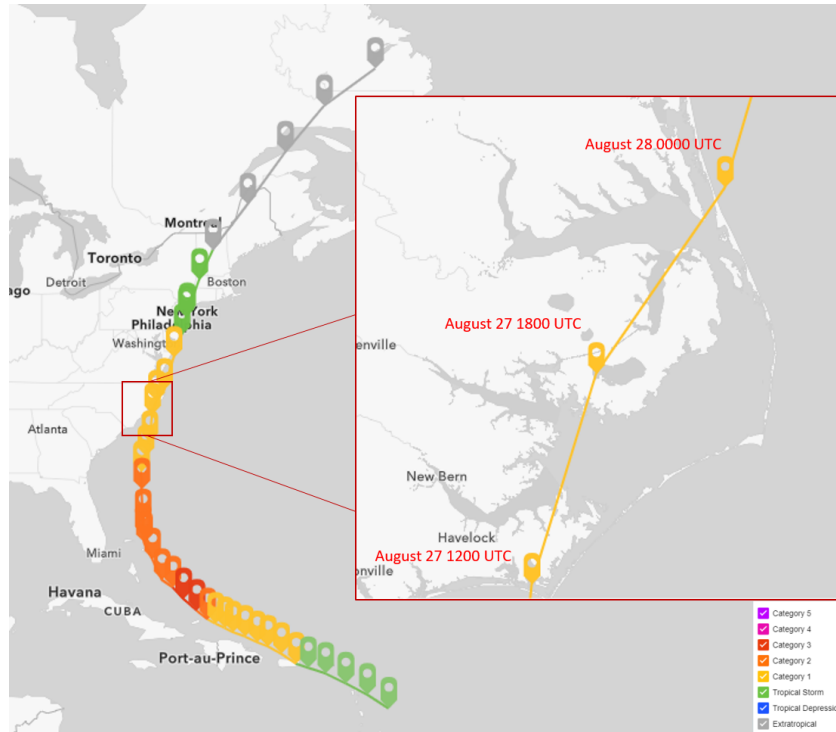


Figure 2.2: The path of Irene through the area of study from the National Hurricane Center best-track file, which records the location of the eye at 6-hr intervals. It made landfall at 1200 UTC 27 August and left the area by 28 August. During this time, it was a Category-1 hurricane.

have been compiled into a database spanning decades, thus allowing for understanding of how the salinity and temperature vary in the area of study as well as information for the development of inputs for the model. ADCIRC has been applied to APES to understand various aspects of its circulation, from storm surge to the transport of oyster larvae. These existing technologies will be leveraged in the research in this study.

2.2.1 SalWise

APES is described by observations collected by numerous researchers over many years. These observations were collected recently into SalWise, which was developed as a comprehensive, state-wide salinity database (Lindquist and Fegley 2016). The database development was supported by NC's Coastal Recreational Fishing License Grant program and NC Sea Grant, and it was led by Dr. Niels Lindquist and Dr. Stephen Fegley of the University of NC at Chapel Hill. Major contributors included the NC Department of Environment

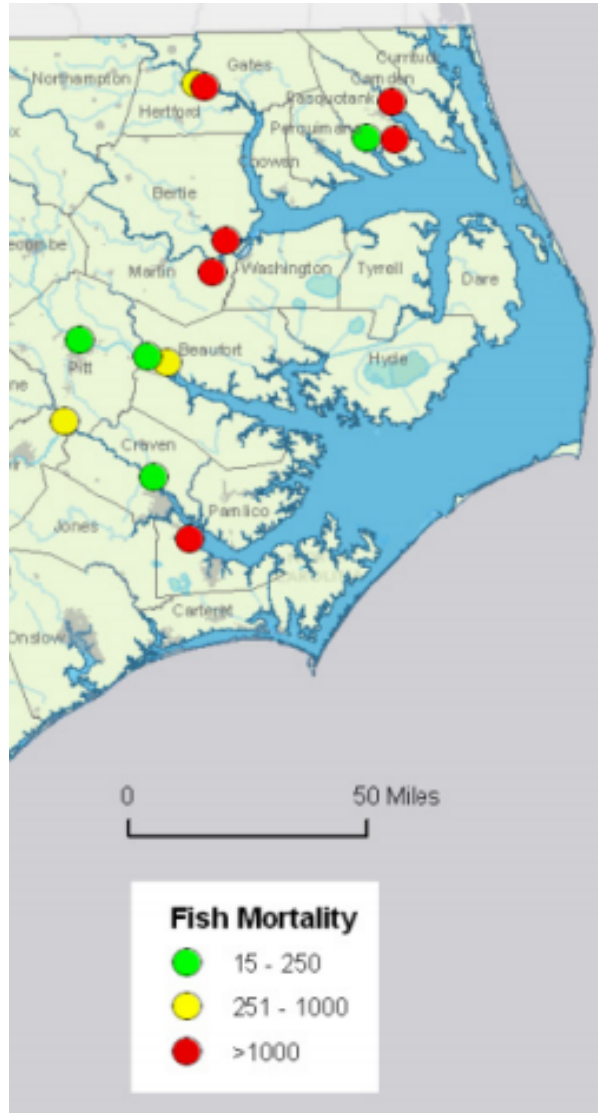


Figure 2.3: Fish kill locations during Irene (2011), as reported by the North Carolina Department of Environmental Quality. The color of marker indicates the amount of fish killed, with red being greater than 1000 kills.

Quality, University of NC at Chapel Hill, NC Division of Marine Fisheries, and United States Department of Defense's Defense Coastal / Estuarine Research Program.

The database includes observations of salinity, temperature, and other water characteristics. For most observations, the location, date and time, and depth of the observation were noted. This allows for the data to be sorted in a variety of ways, including by water body or date. There are more than 1,980,000 records from 1945 to 2015. The highest number of these records are found in the Pamlico Sound, with more than 822,000 records over the time period (Lindquist and Fegley 2016).

Although the database contains a large number of observations, it becomes sparse, both temporally and spatially, for the specific study area and time frame for this research. For instance, while there are observations taken throughout the water column in many spots, the sampling methods are not consistent between observational points and might only occur once at a given depth throughout the entire time range of data. It is much more typical to have observations at the surface and bottom of the water column. For the month of August across all years, there are more than 70,000 observations (Figure 2.4). The number of observations taken at the surface is nearly 42 times greater than the number taken at the bottom. The observation locations are also skewed throughout the study area. There are significantly more observations in the Pamlico Sound compared to the Albemarle Sound, with about 16 points in the Albemarle and about 70,230 in the Pamlico.

Due to this sparseness of the data, it must be processed and averaged to create spatial fields for use in models. In this study, this was accomplished by a process called binning, details of which can be found in Chapter 3. Even though the SalWise data are sparse, they still provide a detailed description of salinity and temperature variations through the system.

2.2.2 ADCIRC applied to APES

ADCIRC is a high-resolution, finite-element-based, hydrodynamic model. It uses unstructured meshes, which allow for predictions of complex coastal circulation with a fine resolution. With input physical forcings and topography/bathymetry specified correctly, ADCIRC can accurately create water levels, currents, and changes due to forcings (Blain et al. 2009). ADCIRC has versions for two-dimensional and three-dimensional circulation. Both versions solve the vertically-integrated Generalized Wave Continuity Equation to predict the water surface elevations (Luettich and Westerink 2004). The two-dimensional version of ADCIRC solves vertically-integrated momentum equations to predict depth-averaged velocities (Luettich and Westerink 2004). It is assumed that momentum dispersion terms are

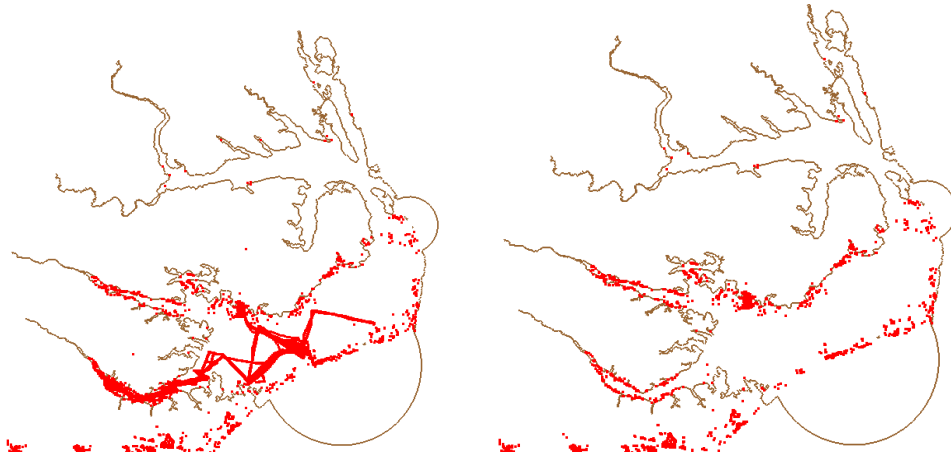


Figure 2.4: Distributions of observations collected in the month of August in any year, as reported in the SalWise database, for (left) surface and (right) bottom.

negligible and density is depth-averaged.

For the three-dimensional version of ADCIRC, the velocities are predicted by solving the three-dimensional, shallow water momentum equations. These were derived from the Navier-Stokes equations after applying the Boussinesq and hydrostatic approximation (Luettich and Westerink 2004; Cyriac et al. 2020). This allows for momentum diffusion and baroclinic pressure terms to be included in the calculations. Also, ADCIRC uses a terrain-following, generalized sigma-coordinate system in the vertical direction (Cyriac et al. 2020). This sigma-coordinate system is applied to all terms, except the baroclinic pressure gradients and the horizontal diffusion terms to reduce instabilities in areas with steep bathymetry changes. In the baroclinic version, salinities and temperatures evolve as predicted by a scalar transport equation (Cyriac et al. 2020).

In APES, ADCIRC has been applied for a variety of studies, including storm surge and the transport of fluid and biological quantities. Many of these studies used the two-dimensional, depth-averaged version of ADCIRC. For this section, we examine three examples of ADCIRC usage in APES.

To investigate a semi-diurnal signal found within the Neuse River, Luettich et al. (2002) used the barotropic, depth-integrated, two-dimensional version of ADCIRC. While primary forcing for circulation in the Neuse River was wind stress, there was also influence from the barrier islands, large surface area of the APES, and the alignment of the long axis of the Pamlico Sound with the prevailing wind direction. The semi-diurnal tidal signal investigation is key in understanding the position and strength of the Neuse River salt wedge.

The mesh utilized in this study encompassed the APES and contained more than 5,000 vertices. Wind forcings were applied, and the velocity output compared with observations. It was determined that seiches were excited by significant shifts in either the magnitude or direction of the wind field. With simulations using idealized wind forcing, it was determined that the APES has a natural mode oscillation period of 13.2 hr (Luettich et al. 2002).

Dresback et al. (2013) developed a total water forecast system based on ADCIRC. This system included multiple model couplings, including for atmospheric forcing and waves. This forecast system, known as ADCIRC Surge Guidance System Scalable, Terrestrial, Ocean, River, Meteorology (ASGS-STORM), was tested using Irene (2011) with the study area located in APES. For this simulation, the two-dimensional, depth-averaged version of ADCIRC was used. The physical forcings included tidal, atmospheric, riverine, and waves, with initial conditions and boundary forcing for temperature and salinity from a coupled model. The model was able to predict the water levels, had an overprediction for wind speeds but good predictions for wind directions, and a consistent overprediction of the significant wave heights due to the wind fields. It was determined that no conclusive statements could be developed for the river discharges, as Irene did not produced significant discharges compared to storms such as Floyd (1999), but ASGS-STORM provided a good test for the storm (Dresback et al. 2013).

Haase et al. (2012) used ADCIRC to predict oyster larvae dispersion in APES. Two-dimensional and three-dimensional models were developed. Results from the two models were compared with each other, as well as to observations, to determine the most suitable method for the predictions. The mesh used covered the Croatan-Albemarle-Pamlico Estuarine System (CAPES) and had more than 22,000 vertices. For areas near ocean inlets and in the estuaries, the resolution was about 300 m, and in the main body of the Pamlico Sound, the resolution was about 1 km. In the three-dimensional ADCIRC model, seven vertical layers were used. Both models were forced with hourly wind observations from the National Weather Service. After fine tuning some of the parameters in ADCIRC, it was determined that the three-dimensional model's velocities were a better fit to the observational values compared to the two-dimensional. It was also noted that in both the two-dimensional and three-dimensional models the velocities were correlated with the wind forcing (Haase et al. 2012).

Each of these studies determined that the application of ADCIRC in APES produced good results for each of the studies and that winds were the primary forcing within APES. In Luettich et al. (2002), ADCIRC was used to determine physical characteristics of the seiching that occurs in the Neuse River and it was concluded that these were heavily dependent on

the wind magnitude and direction. Dresback et al. (2013) was able to use APES to test the forecasting system, with ADCIRC as the base, with good results. Haase et al. (2012) found that the model was validated for studying the larval dispersal and that velocities correlated with the wind forcing. For each of the studies, it was also noted that more understanding of the density-driven circulation is needed. Luettich et al. (2002) noted that determining the physical attributes of the seiche will allow for better investigation into the Neuse River saltwedge. Dresback et al. (2013) notes that a storm simulation with more freshwater discharge is needed to understand the impact that the freshwater discharges would have. Haase et al. (2012) did not analyze the vertical behavior of oyster larval vertical because the water columns were generally well-mixed. The inclusion of the density-driven circulation is necessary for a full understanding of the circulation in APES.

2.3 Motivation

There are remaining questions about how the APES horizontal salinity stratification reacts to storm events. These questions will motivate the research objectives in this thesis.

2.3.1 Remaining Questions

The first set of questions are about how to investigate the estuarine horizontal salinity distribution during storm events. Previous studies have focused on only one effect, such as seiches in the Neuse River (Luettich et al. 2002) or oyster larvae dispersion in APES (Haase et al. 2012). To fully understand the impacts of storm events, it is necessary to incorporate density-driven circulation into predictive model simulations, and then explore the variations of surface salinities in a typical estuarine system.

By simulating the density driven circulation during a storm, we can answer questions about the system response. How does the horizontal salinity distribution in estuaries change during storm events? And how do these changes vary spatially through the system? It is expected that the surface salinities will be transported quickly by strong winds during the storm, and that their spatial distributions will be influenced heavily by the geometries and connectivities through the estuary.

The second set of questions are about how the system recovers after the storm. It is expected that the estuary will recover to typical conditions over some time period, possibly with help from elevated river discharges in the days and weeks after the storm. However, previous studies have shown a range of recovery rates depending on the location, model

used, and physical forcings. There is a need for a detailed, systematic exploration of how an estuary will recover during a storm. For this research, all physical forcings of density circulation, tidal, atmospheric, and river flows are included. This also allows for the simulation to be continued after the storm event has left the area. Not only will the length of time be examined but also the varying density locations will be known. For marine fisheries, this is key as many marine species depend on specific ranges of salinity and temperature. By examining the disruption and recovery of surface salinities during a typical storm, we can gain insight on how the salinities can vary at fishery locations.

2.3.2 Objectives

By developing a three-dimensional model to include density driven circulation and applying hurricane force winds, tides, and river flows based on Irene (2011), this research will examine alterations to the horizontal salinity stratification due to the storm event and afterward. To investigate the hypotheses of this study, this research will have the following objectives:

1. *Identify and develop data to describe the typical conditions in APES.* An ADCIRC mesh will be tailored for APES, and initial density conditions will be developed from the SalWise database by using average August conditions.
2. *Develop simulations with and without Irene (2011).* These simulations will include a spin-up to allow the model to achieve a dynamic equilibrium, the duration of the storm, and then several weeks after the storm. One simulation will include the storm winds and elevated post-storm river discharges, and another control simulation will reflect the typical non-storm conditions. Not included are dominant wind forcing for sections of the simulation before the storm and after.
3. *Quantify the storm effects on horizontal salinity distributions throughout APES.* A detailed synoptic history will show how the changing winds affected surface salinities during different stages of the storm. Then the analyses will focus on sub-regions of APES like the estuaries, the inlets, and the connecting region near Roanoke Island.
4. *Analyze how salinity zones are transported spatially and vary temporally.* The results will be analyzed by using biologically-based salinity zones, thus allowing an understanding of how salinities varied through the system. At known oyster habitats, time series of salinities will allow an understanding of the duration and magnitude of the local system response.

By the end of this research, we will have a better understanding of the surface salinity distribution in APES, as well as the changes due to a storm event. This will include how the system mixes during the storm, the impact of the increased freshwater discharges after the storm, and how the system attempts to regulate following the storm.

CHAPTER

3

METHODS

Simulations of three-dimensional, density-driven circulation are among the most challenging applications of ADCIRC, because they require additional efforts to generate inputs for the density forcings, and to ensure the coastal system is represented consistently. In this chapter, we describe how the mesh for the study area was developed, which physical forcings were included, and how the input values were developed for use by ADCIRC.

3.1 Mesh Development

ADCIRC represents the coastal system with unstructured, finite-element meshes, which allow resolution to vary over several orders of magnitude to improve accuracy near critical regions of interest. For this research, a mesh was developed from an existing, forecast-grade mesh with high resolution in North Carolina. This mesh was trimmed to describe only the Albemarle-Pamlico estuarine system (APES). By removing the offshore, open-water regions and the onshore, overland regions, we focus on the density-driven circulation in the sounds and estuaries, and we reduce the computational requirements. By smoothing the bathymetry in this new mesh, we improved the numerical stability of the simulations.

In this section, we describe how the mesh was trimmed, and how the bathymetry was smoothed.

3.1.1 NC9 Mesh

For this research, the unstructured, finite-element ADCIRC mesh referred to as NC v9.98 (NC9) was used as a starting point (Figure 3.1). This mesh was developed for floodplain mapping and risk assessment for the Federal Emergency Management Agency (Blanton and Luettich 2008), and it is now used for real-time forecasting as storms approach the coast (Renaissance Computing Institute 2016). The NC9 mesh spans a large domain of the western North Atlantic Ocean, the Gulf of Mexico, and the Caribbean Sea. This large domain is to allow for storms to be simulated within the mesh, instead of bringing them across a mesh boundary. However, most of the mesh resolution is concentrated in coastal North Carolina. NC9 has 624,782 vertices with spacings as small as 50 m coastal North Carolina. In areas like Oregon Inlet, the spacings are smaller than 50 m to allow for finer details to be accounted for. In the open ocean, the resolution is coarser, with vertex spacings as large as 4 km (Blanton and Luettich 2008).

The NC9 mesh is well-validated for simulations of storm surge and coastal flooding (Blanton and Luettich 2010; Blanton et al. 2012a; Cyriac et al. 2018), but it was not designed for simulations of density-driven circulation. With the application of the three-dimensional version of ADCIRC that includes baroclinic simulations, there is a significant increase in computational demand (Dresback et al. 2010). Due to this increase it is necessary to restrict the model domain to smaller regions with the open boundaries outside of the areas of dense computations. Cyriac et al. (2020) used a shelf-scale mesh, trimmed from a regional mesh. Blain et al. (2009) limited the ADCIRC mesh to the Dardanelles Strait, while one HYCOM model spanned the Mediterranean, Aegean, Marmara, and Black Seas and the regional model was expanded to outside the Aegean Sea. Dresback et al. (2010) also used a higher resolution ADCIRC mesh coupled to the lower resolution HYCOM model. Another common instability is due to steep bathymetry changes. Haney (1991) found that, in conjunction with the use of sigma coordinate systems, insufficient resolution in areas of steep bathymetry can cause inaccuracies in ocean numerical modeling. In order to circumvent these instabilities, models can smooth out the bathymetry (Cyriac et al. 2020; Adcroft et al. 2016; Marshall et al. 1997). Thus, to adjust the NC9 mesh for the research in this study, it was trimmed and smoothed, with a focus on the APES.

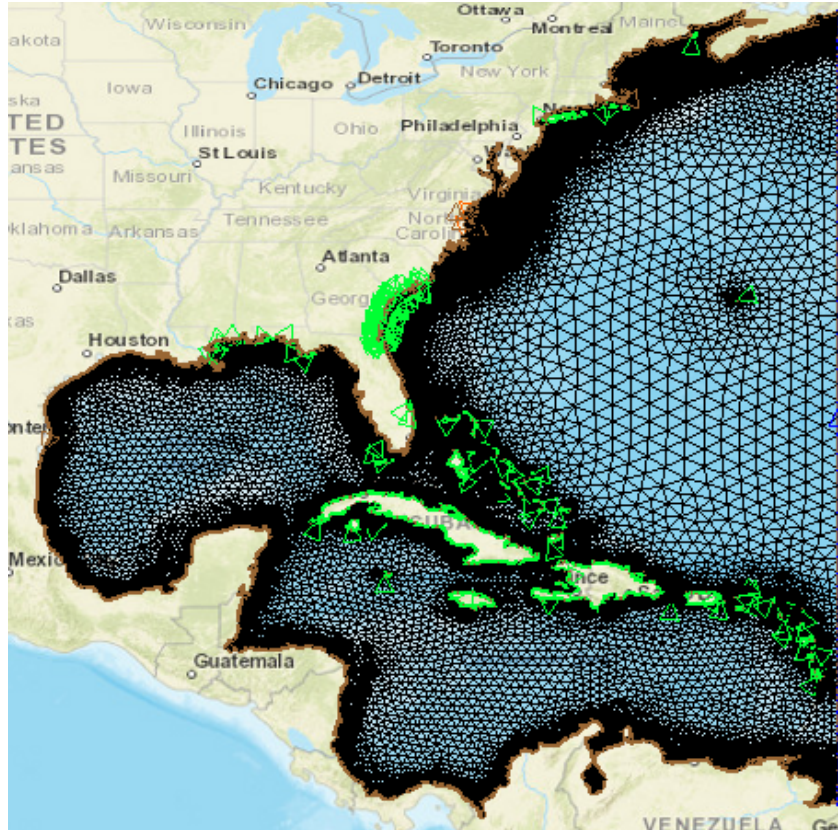


Figure 3.1: The NC9 mesh encompasses a large domain, which includes the entire Atlantic coast of the United States.

3.1.2 Trimmed Mesh for APES

The NC9 mesh was trimmed to describe only the APES, including the upstream river boundaries, the estuaries and sounds, and the inlet connections to the continental shelf. This was completed through multiple steps. First, the study area was trimmed out of the NC9 mesh by using the zero elevation contour. By doing this, the floodplains were removed, but the river boundaries were kept. Following the guidance found in Dresback et al. (2010), the ocean boundaries were extended into semi-circles outside of the study area. This would allow for the elimination of complexities in dynamics at the boundaries. The bathymetry from NC9 was interpolated onto the trimmed mesh. To ensure the stability, a few other modifications were necessary. For the rivers, the heads were artificially deepened. Some man-made channels, one located by Oregon Inlet and another between estuary rivers, were either smoothed out or removed.

The new mesh describes the APES (Figure 3.2). It includes four major rivers: Chowan,

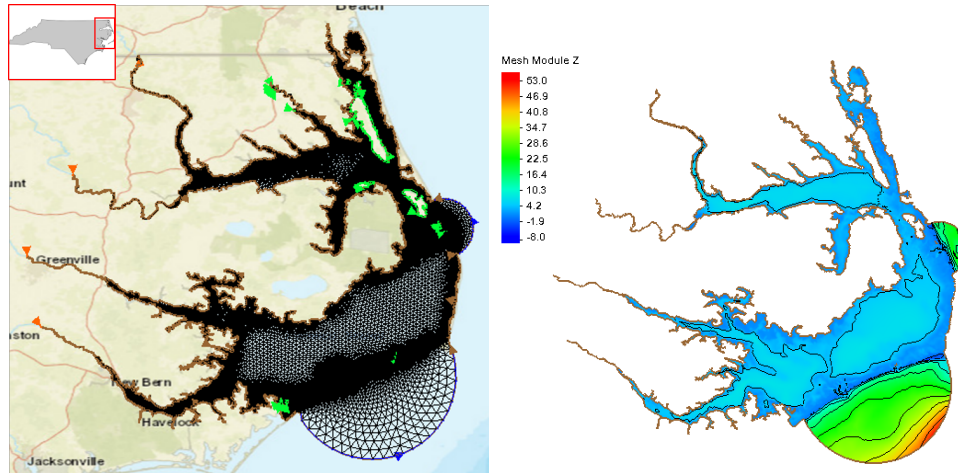


Figure 3.2: The NC9-APES mesh (left) was cut from NC9 and encompasses the Albemarle and Pamlico Sounds and the four key river estuaries. Bathymetry (m, positive downward, right) was interpolated from NC9.

Roanoke, Tar-Pamlico, and Neuse. At each of these four rivers, flow rates were applied as incoming flux boundary conditions. It also includes three key ocean inlets: Oregon, Hatteras, and Ocracoke. Outside these inlets, the mesh is extended onto the continental shelf, where tides and density information are specified at ocean boundaries. Oregon Inlet has one ocean boundary, while the Hatteras and Ocracoke Inlets share an ocean boundary. The sounds are shallow with an average depth of approximately 4 to 5 m. The deepest portions of the mesh are located at the ocean boundaries, with depths as large as 52 m. Since the mesh was trimmed by using the zero elevation contour, and before the semi-circular ocean boundaries were added, the eastern mesh boundary was along the sound sides of the Outer Banks. This removed the land masses of the Outer Banks from the mesh. With the addition of the ocean boundaries, select portions of the land masses of the Outer Banks near the inlets were necessary to include inside of the mesh and not part of the boundary. We designate this mesh as NC9-APES.

3.1.3 Bathymetry Smoothing

The bathymetry in the NC9-APES mesh was smoothed to improve the performance of the ADCIRC simulations. In certain areas of the mesh, like Oregon Inlet, steep bathymetry gradients can cause numerical instabilities. An example of these steep bathymetry changes can be seen in Figure 3.3. Looking on the northern side of the inlet, as shown by the red

arrow, there is a change of 3.5 m over 78.64 m. Slightly east of the arrow, there is a change of 3.74 m over 137.93 m. To circumvent the instabilities caused by this, the bathymetry was smoothed selectively (Cyriac et al. 2020). In order to develop the mesh for the study, two different steps were needed. First, the bathymetry smoothing method is applied to the entire mesh. Then, the unsmoothed and smoothed meshes are combined, by selecting bathymetries in depth ranges from each mesh to develop the final mesh.

First, a smoothed mesh is developed. The smoothing method limits the relative variation of the depth over a mesh element and thus limits the hydrostatic inconsistency number. The hydrostatic inconsistency number, also known as Haney number, is a metric used to measure error in the horizontal pressure gradient by using the bathymetry at adjacent vertices (Sikiric et al. 2009). Cyriac et al. (2020) enforced limits, 0.2 for relative variation and 3–6 for the hydrostatic inconsistency number. This was applied to regions deeper than the 15 m contour. For the NC9-APES mesh, the limits for the relative variation and hydrostatic inconsistency number were increased, 100,000 for relative variation and the hydrostatic inconsistency number. This increase was to make the resulting mesh bathymetry resemble the original mesh bathymetry as close as possible, ensuring the depths in the ocean boundaries remained. In doing this, an entirely separate mesh was developed, which is referred to as the smoothed mesh.

Then, after the smoothed mesh was developed, a new mesh was created by combining the bathymetry of the original mesh and that of the smoothed mesh. For different depth ranges, including areas above sea level, different combinations of the bathymetry were used. Depending on the bathymetric depth, the combined mesh may select bathymetries from only the original mesh, only the smoothed mesh, or a weighted linear combination of the two. The ranges for each of these options can be seen in Table 3.1, with the variable h indicating below mean sea level and d for above. When choosing these ranges, the main goal was to keep as much of the original bathymetry as possible. To keep the large depths in the ocean boundaries, the lower limit for the completely original bathymetry was based on the areas around the inlets. This was due to the majority of the areas with steep bathymetry being located in the inlets. Since inlets had depths of 15 m or less, this lower limit allowed for the retention of the original bathymetry in the ocean boundaries. For the deepest linear weighted combination limit, this was to allow for a transition section between the full original bathymetry and the smoothed bathymetry. Since the steepest bathymetry gradients were located inside the inlets, the shallower depths were set to be the smoothed bathymetry. To allow for a smooth transition to the original bathymetry, another linear weighted combination was needed above mean sea level. After the transition section

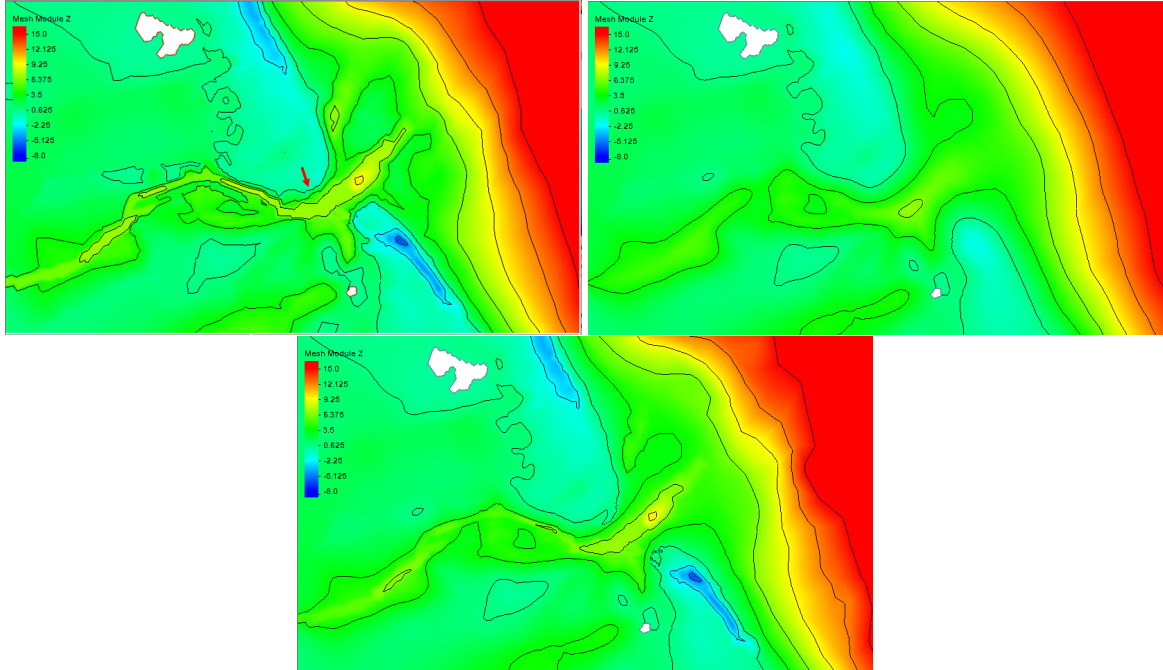


Figure 3.3: Bathymetry (m, positive downward) near the Oregon Inlet, as represented in the original mesh (top left), smoothed mesh (top right), and final mesh (bottom). Notice the steep gradients near either side of the inlet in the original mesh. In the smoothed mesh, these are removed. The final mesh is a combination of both.

above mean sea level, an effort was made to keep the original dune crests to decrease the probability of over wash during the simulation.

The final mesh (Figure 3.4) has a combination of both the original bathymetry and the smoothed bathymetry. Oregon Inlet has been smoothed, resulting in a shallower but wider inlet. The same can be said of the Hatteras and Ocracoke Inlets. At Oregon Inlet, looking at the northern side, over a distance of 73.9 m, there is a difference of about 0.9 m. Further east on the northern side, over a distance of 156.7 m, there is a difference of about 3.7 m. Ocean boundaries near the Outer Banks have been smoothed and made a little shallower, but retained the deepest portions. The rivers remained the same, ensuring the channel details were not lost. For the sounds, they are still shallow with the same average depth. This final mesh is used from here on in the research.

There are a few exceptions to this combination method. One exception is the rivers, where the bathymetries are maintained from the original mesh, so as not to lose key channel details. Another exception is the dune crests on the Outer Banks. If combined or smoothed bathymetries are applied to the dune crests of the islands, then dune height is lost and

Table 3.1: Bathymetric depth ranges for which bathymetry was utilized to develop the combined mesh.

Range (m)	Source for Bathymetry in Combined Mesh
$h > 15$	Original
$5 < h \leq 15$	Linear Weighted Combination
$0 < h \leq 5$	Smoothed
$-3.5 < h \leq 0$	Linear Weighted Combination
$d < -3.5$	Original

inundation becomes prevalent throughout the entire simulation, with or without a storm event. To prevent this inaccurate inundation, the dune crests were selected via mesh vertex number and required to keep their original bathymetry depths (negative, above sea level).

3.2 Physical Forcings

In this section, each forcing used in the simulations is described. These physical forcing are the physical processes that drive the circulation within the study area. Examples include tides and winds. The sources of the input data are described, as well as how those input data were manipulated to be compatible with ADCIRC simulations.

ADCIRC can accept inputs via a larger number of files. The Grid and Boundary Information File (`fort. 14`), described in the previous section, contains information about the vertex and element numbering and connectivity, bathymetric depths, and boundary locations and conditions. Physical forcings are implemented in other input files. The main input file for ADCIRC, beside the mesh file, is the Model Parameter and Periodic Boundary Condition File (`fort. 15`). This file includes information about what type of simulation will be run, what key physical attributes are used, and what forcings will be applied. Some of the forcings require additional files for input. In each of the following sections, what is changed in the `fort. 15` file for each forcing will be highlighted and, if necessary, explanation of other input files needed. For exact file formats for each of these, see Appendix A.

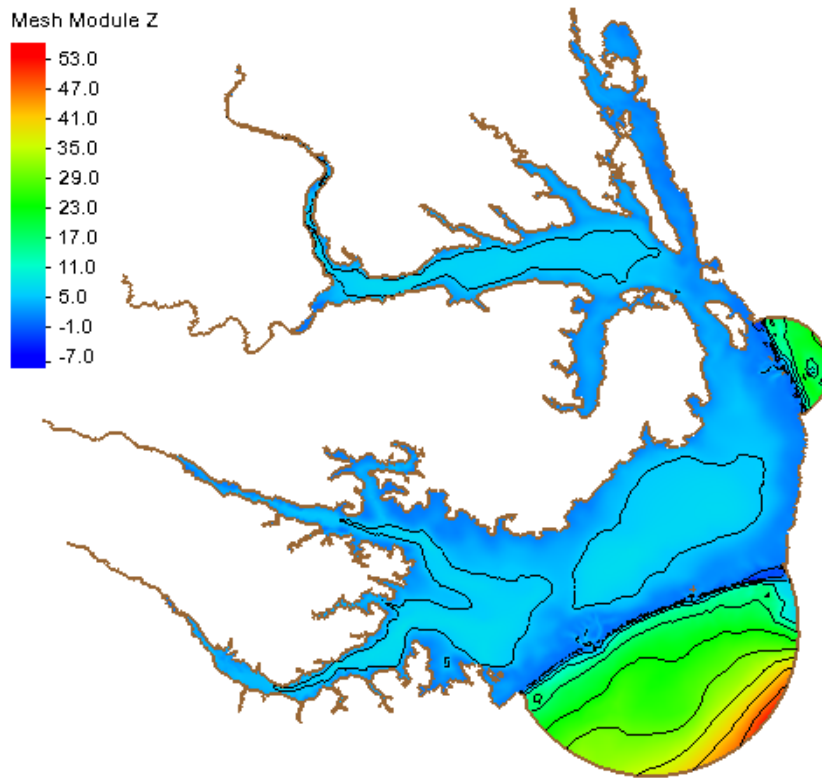


Figure 3.4: The final bathymetry (m, positive downward), after the smoothing, was used for simulation.

3.2.1 Tides

Tides are forced in the model in two ways: at the ocean boundaries, and with tidal potentials within the domain. The ocean boundary locations are specified within the `fort . 14` file, whereas the amplitudes and phases for each tidal constituent are specified within the `fort . 15` file. For each of the vertices at the ocean boundary, a tidal signal is applied. To develop this signal, tidal constituents and their respective location and time specific information is provided. In this research, the tides are developed using eight tidal constituents. These are M_2 , S_2 , N_2 , K_2 , K_1 , O_1 , P_1 , and the Q_1 constituent. The M_2 constituent is the largest lunar tidal constituent and is related to the gravitational effect of the Moon. The S_2 is the largest solar constituent and is related to gravitational effect of the Sun. The N_2 is the largest lunar elliptic and K_2 is the lunisolar constituent. Each of these constituents are semi-diurnal, indicating they occur twice a day. Constituents K_1 , O_1 , and Q_1 are lunar constituents, with Q_1 being larger lunar elliptic. P_1 is a solar constituent. These constituents are diurnal, indicating

they occur once a day (National Oceanic and Atmospheric Administration 2021b).

In ADCIRC, for each of these constituents, location-specific and time-specific data must be supplied. For the location-specific information, ADCIRC uses the amplitudes and phases for each constituent at each ocean boundary vertex. These are determined by interpolating values from a tidal database, (EC2015). This database was developed for the Western North Atlantic, Caribbean, and the Gulf of Mexico region and includes information for 37 constituents (Szpilka et al. 2016). It was developed using the two-dimensional version of ADCIRC and used harmonic data from the National Oceanic and Atmospheric Administration (NOAA) Center for Operational Oceanographic Products and Services. For the time-specific information, the node factors and equilibrium arguments for each of the tidal constituents were calculated for the time period of the simulation used. This information is listed in the `fort.15` file, including the desired tidal constituents, the time-specific information for each constituent, and the location-specific for each constituent at each ocean boundary vertex. With this information, ADCIRC develops the tidal signals at each vertex in the ocean boundaries, and it develops the tidal potentials at each interior vertex.

3.2.2 Atmospheric

ADCIRC can apply atmospheric forcing as surface pressures and stresses at each vertex in the domain. For this study, we are interested in the effects of Irene (2011), which must be represented as atmospheric forcing via additional input files. The storm is represented with the Generalized Asymmetric Holland Model (GAHM), which uses tropical cyclone storm parameters to develop pressure and wind fields to represent the storm event (Gao 2018; Dietrich et al. 2018). GAHM was developed from the Holland model (Holland 1980), which used a rectangular hyperbola with two scaling parameters to approximate the surface pressure profile and solve the gradient wind equation. These scaling parameters were determined by setting the wind speed to the maximum and the change in wind speed with respect to the radius set to zero at the maximum radius, and assuming the Coriolis acceleration is negligible compared to the centrifugal acceleration. GAHM uses the Holland model as its base, but has some additional changes. These changes include the removal of the assumption that the Coriolis acceleration is negligible and inclusion of a piecewise continuous radial wind profile to allow for the multiple wind isotachs in each storm quadrants. This allows for the GAHM to include the two scaling parameters from the original Holland model, but is able to do so without the assumption of the negligible Coriolis acceleration. Whereas the Holland model uses a spatially constant value for the

maximum radius, thus creating a symmetric vortex, the GAHM model includes spatially varying maximum radius allowing for the development of an asymmetric vortex. Due to these alterations, the GAHM is able to represent the storm asymmetrically, develop a radial wind profile to match the isotachs in each quadrant, and is able to better represent of the storm described (Gao 2018; Dietrich et al. 2018). GAHM reads information about the winds in quadrants, and then constructs an asymmetric wind field, which allows for different quadrants to be stronger or weaker.

GAHM is included within ADCIRC, so that the surface pressure and wind fields can be developed during the simulation. To apply this type of forcing, the data needed is the best track file for the storm. This file is developed by NOAA. It includes information about the pressures, different isotachs for winds, path location, and times of observation. Each data entry is for every six hours. For Irene, the best track file begins on 0000 UTC August 21 and ends 0000 UTC August 30. To use in ADCIRC, the best track file is written into a Meteorological Forcing Data file (`fort . 22`) to be read into the simulation. In order to do this, the best track file needed to be prepared. First, the lines with missing information were removed from the file. This changed the time frame of usable information to 0000 UTC August 21 till 0000 UTC August 29. Next, the time increment in hours added. Since the observations are taken every six hours, the time increments are multiples of six. Once these edits have been made, the name of the file was changed to `fort . 22`. The file layout was then reformatted to be compatible with ADCIRC.

In the `fort.15` file, it is specified that the GAHM will be used by setting the atmospheric forcing parameter and including additional information about the storm. Additional information includes the start day and time, the storm number, and the boundary-layer adjustment. For this research, the atmospheric forcing parameter was set to 19 (indicating GAHM), start day and time were 0000 UTC August 21, the storm number is set to 1, and the boundary-layer adjustment is set to 0.9. The boundary-layer adjustment is the adjustment factor between wind speed at 10 m and the wind speed at the top of the atmospheric boundary layer and 0.9 is the maximum of the reasonable range. Once this information is added, ADCIRC will use this combined with the best track (transformed to the `fort . 22`) to simulate Irene using the GAHM.

Also included in the model is the vertex attribute of the surface canopy coefficient (Figure 3.5). This attribute is able to turn off the wind stress in heavily forested areas that have been flooded, essentially shielding the water from the effect of the wind. For this model, the canopy coefficient is turned off in the majority of the study area has the full wind stress applied as it is open water. If more landmasses were included inside of the study

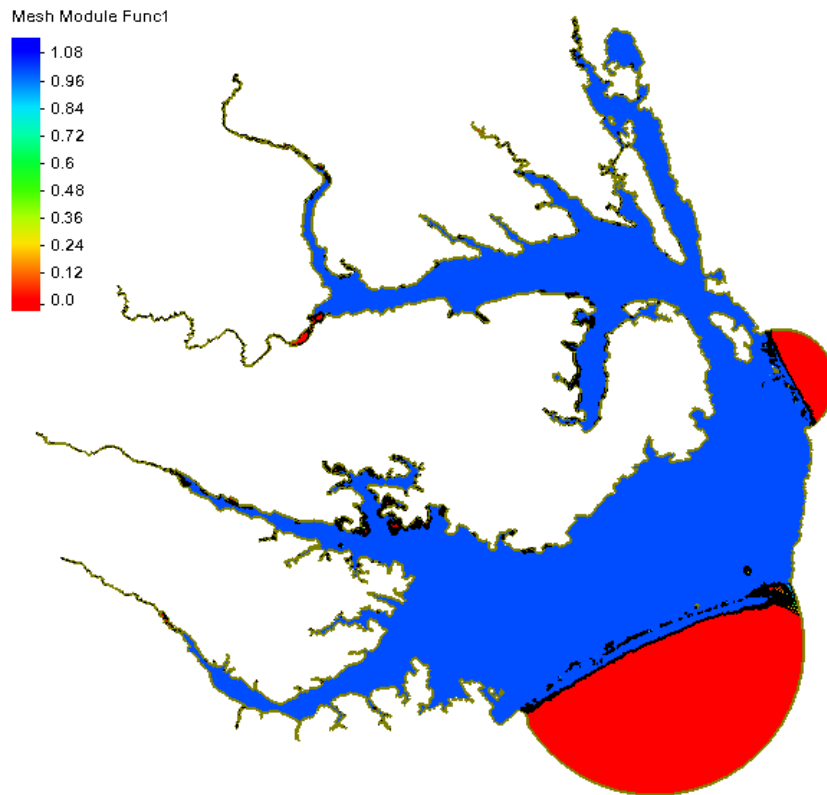


Figure 3.5: Surface canopy coefficient values for the area of study. Blue indicates a value of 1, showing wind stress is applied, while red indicates a value of 0, with no applied wind stress.

area, there would be more instances in which the wind stress would be turned off due to the forested regions. In the ocean boundaries, it was necessary to turn off the wind stress. This was due to when the hurricane-strength winds progressed through the area, water was pushed against the ocean boundaries, going against the previously defined water levels via the tides. Due to this, instabilities began to occur. To stop these, the wind stress was turned off inside the ocean boundaries.

3.2.3 Rivers

In ADCIRC, riverine flows are applied at non-zero normal flow boundaries, with locations specified in the `fort . 14` file. There can be two different types of flows: steady flow specified in the `fort . 15` file, or unsteady flows applied by using the Non-periodic Normal Flow Boundary Condition File (`fort . 20`). In this file, the input increment and variable flow rates

Table 3.2: USGS stream gauges selected at the four river boundaries for the NC9-APES mesh. The flow rates are the average values of the simulation before the storm segment, 0000 UTC 6 August to 0000 UTC 21 August. These values will be used during the no-storm simulation.

River	USGS Gauge	Flow Rate (m ³ /s)
Chowan	02050000	2.4
Roanoke	02080500	63.9
Tar-Pamlico	020840000	9.6
Neuse	02091814	39.2

are specified.

At each boundary vertex, the incoming flux is calculated by dividing the flow rate by the length of the river boundary. This results in a flux with units for the normal flow per width. With this flux determined, the next step is to assign values to the vertices located on the boundary. To do this, each vertex will have a portion of the flux assigned. This portion is determined by the tributary length of the boundary that the vertex is responsible for. For example, the Chowan River boundary has four vertices. This indicates that the two end vertices will only be responsible for an sixth of the boundary length while the interior two vertices will be responsible for a third of the boundary length. The process is completed for each river boundary and flow rate.

To develop these river fluxes, observational data from the United States Geological Survey (USGS) stream gauges were used. For each of the four rivers, USGS stream gauges that were closest to the river boundaries in the mesh were selected. These stations are listed in Table 3.2. At each of these stations, the flow rates for the time span of the simulation were retrieved. For the constant flow rates, an average for the time period before the storm segment of the simulation began, was used. These are also listed in Table 3.2. The other type of river forcing was developed from the flow rate time series at each station. These values can be seen in Figure 3.6.

3.2.4 Density

The baroclinic version of ADCIRC also requires that salinities and/or temperatures be specified. These parameters must be specified spatially throughout the mesh as initial conditions in the `fort.11` file, as well as temporally as boundary conditions in the `fort.36`,

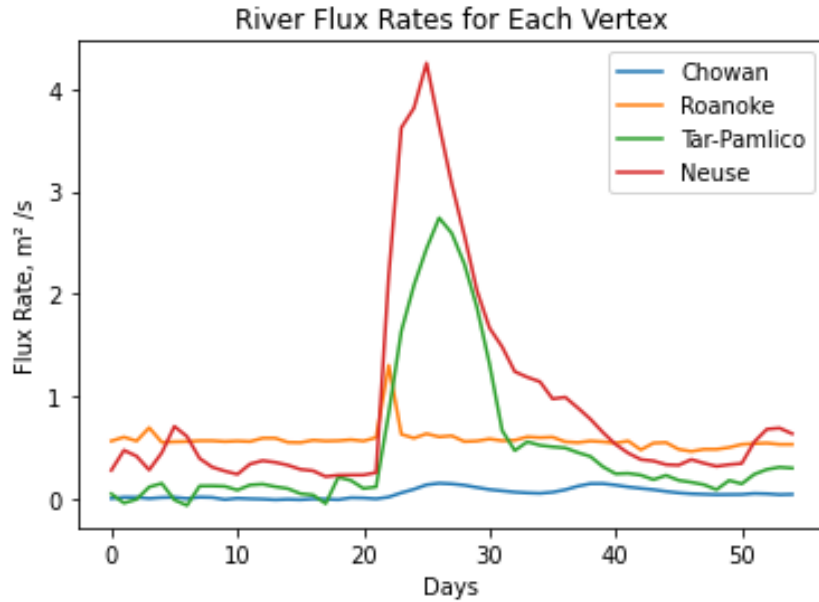


Figure 3.6: Flux rates ($\text{m}^3/\text{s}/\text{m}$) applied to each river boundary internal vertex. The largest flux is on the Neuse River, while the smallest is on the Chowan River.

fort .37, fort .39 files. ADCIRC uses the salinity and temperature, along with pressure, to develop the density field. This is completed by using the equation of state described in McDougall et al. (2003).

To create these input files for this study, observational data from SalWise were used. Although the database provided values for salinities and temperatures, the observations were not consistent in time or space. Due to the sparseness of the data, an alternative method to develop the density field inputs was created. This method consists of identifying monthly data from the database, using the Geographic Resources Analysis Support System (GRASS) geospatial software (GRASS Development Team 2017) to develop surfaces for salinity and temperature, and then interpolating the values from the surfaces onto the mesh vertices. The beginning steps rely heavily on the use of Python to develop codes to achieve the necessary calculations and data management. The following paragraphs detail this process.

The first step in developing the salinity and temperature surfaces was to select the data from SalWise. For every available year in SalWise, all available data for the month of August were extracted. These data was then separated by measurement depth. As stated in Chapter 2, only the surface and bottom measurements were used in this research.

Then the selected data were analyzed to reduce the spatial sparseness of the observa-

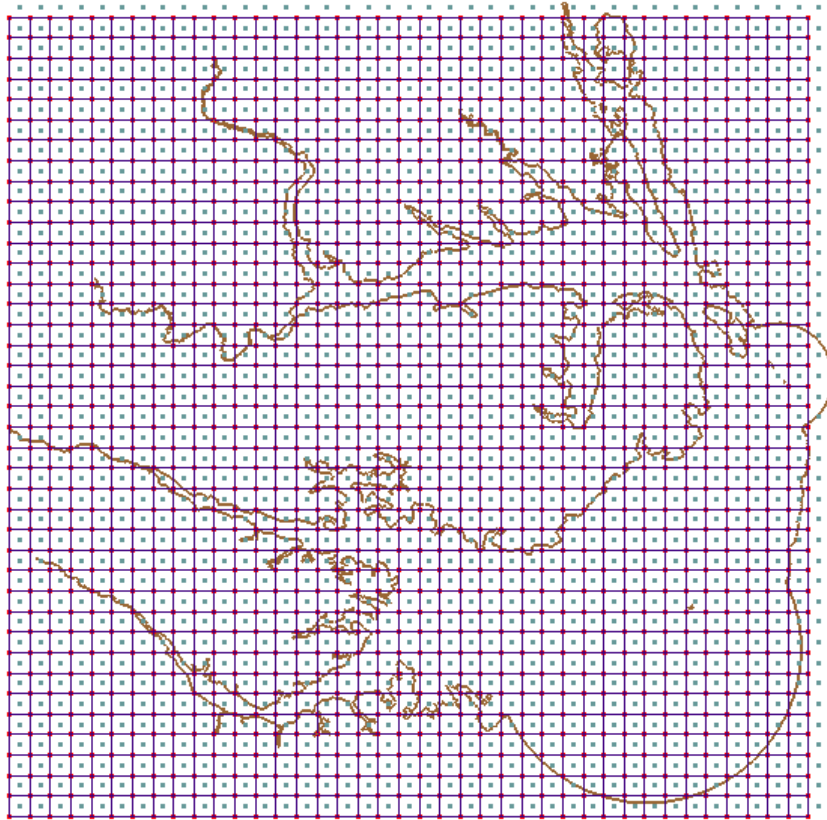


Figure 3.7: Square grid used for binning of the SalWise observational data. The blue lines are the 0.05-degree bins, with blue dots at the center of each bin. Within each bin, SalWise observations from August in any year were averaged.

tions. The data were binned spatially. A regular square grid was developed to span the area of study and to have a resolution of 0.05 degrees (Figure 3.7). These bins are arbitrary and were only used to group the observational points together. With these bins defined, each observational point from SalWise was placed into a bin based on its latitude and longitude. To assist in developing a smoother surface, artificial values were added into the bins located at the beginning of the rivers and in the ocean boundaries, to represent fresh and saline waters, respectively. In the observational data, no points were located in these areas, which would have resulted in large discrepancies in the surfaces. After all observational points were binned, they were used to compute key attributes of each bin: the number of points in each bin, and the maximum, minimum, medium, and mean for salinities and temperatures.

To create the surface, only bins with observational points were used. The center of each bin was imported into GRASS as a point vector file. To develop the salinity and temperature fields over the entire study area, the ADCIRC mesh was also imported as a point vector file.

This allows for GRASS to perform interpolation methods on these data sets. To develop the surfaces, the GRASS tool `v. surf . rst` was used (Mitas et al. 2021). This tool applies interpolation from vector points to develop a raster surface by using splines. There were two key parameters that could alter how the surface was developed: the tension parameter and the smoothing parameter. The tension parameter defines how rigid the resulting surface is compared to the original points. This means the higher the value of tension, the more flexible the surface is, resembling the original points more. The smoothing parameter controls the allowable deviation from the original values. Essentially, the higher the smoothing parameter, the less the surface resembles the original data.

To examine the impact of each of these parameters, surfaces were developed using varied values for each. First, the tension parameter was explored. This parameter was varied from 0 to 100, with the smoothing parameter being set to 0. By doing this, just the impact of the tension parameter was examined. This was accomplished by comparing the observational value at a bin to the surface value at that bin's location. To keep the surface values close to the original values as possible, a one-to-one line was plotted as well. The best value was selected based on how close to the one-to-one line the majority of the points were located. It was determined that a tension parameter of 100 would be best. Next, the smoothing parameter was investigated. This was completed by using the same method as outlined for the tension parameter, with the tension being held at a value of 100. The smoothing parameter was varied from 0 to 40. It was determined a smoothing parameter of 0 would be best in this application. These resulting plots can be seen in Figure 3.8.

With the parameters for the GRASS tool determined, surfaces were then developed for the surface salinity, bottom salinity, surface temperature, and bottom temperature. These can be seen in Figure 3.9. Using the vector point file of the ADCIRC mesh, each of these raster surfaces were sampled to assign values to each point. This step utilized the GRASS tool `v. what . rast` (Blazek and Bowman 2021). This tool uploads raster values from the position of the vector points. After this was completed for all four surfaces, the resulting file with the values at each mesh vertex was exported as comma-separated-value files.

The comma separated value files were then used to develop the input files for the simulation. There are four key files ADCIRC requires for the implementation of the density circulation. The first of these files is the Density Initial Condition File (`fort . 11`), which specified the initial values for salinities and temperatures at every mesh vertex. Because only the surface and bottom values were usable from the SalWise database, for the remaining vertical layers, a linear interpolation for the salinity and temperature values was computed.

The next input files are the Salinity Boundary Condition Input (`fort . 36`) and Tempera-

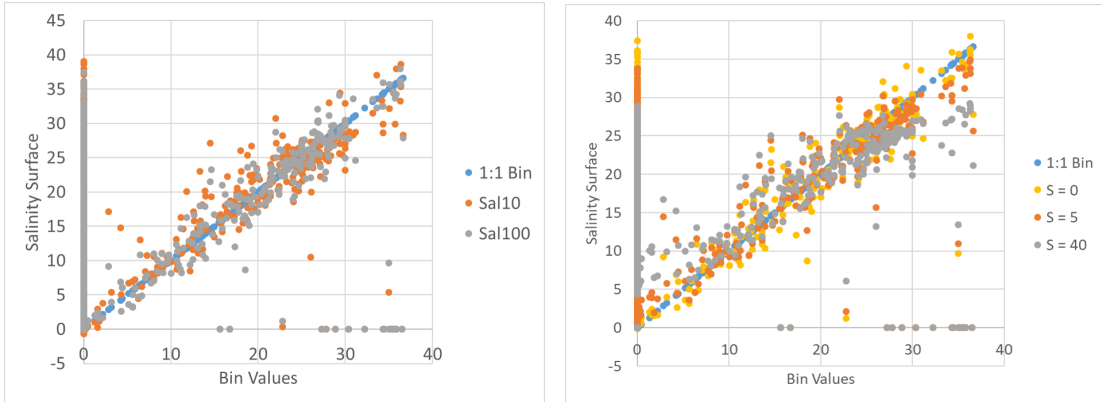


Figure 3.8: Sensitivity of interpolated surface to tension and smoothing parameters. The x -axis in both graphs represents the salinity values for each bin. The y -axis is the value taken from the developed salinity surface at the bin location. For both graphs, if the surface was a perfect match to the observational values, the points would fall on the one-to-one line. The left graph depicts variations within the tension parameter between values of 0 and 100. The right graph shows variations with the smoothing parameter, with a tension parameter set to 100. This is due to higher tension value more closely resembling the observational values, the blue dots.

ture Boundary Condition Input (`fort . 37`). In these files, the forcing values for the salinities and temperatures are defined at every ocean boundary vertex for every vertical layer. These files are also a time series, meaning if desired these salinity and temperature values can change over the course of the simulation.

The last input file is the Salinity and Temperature River Boundary Values (`fort . 39`). This file also allows for unsteady inputs and has values for each river boundary vertex and for each vertical layer. The `fort . 39` contains both the salinity and temperature values. However, for this study, the boundary conditions were steady at the monthly mean values. The ocean boundary files are activated through the `fort . 15` file by specifying the type of simulation to be developed and the time steps for the files. The river boundary file is called into the simulation through the boundary type specified in the `fort . 14` and one of parameter changes for the `fort . 36` and `fort . 37`. For each of the salinity and temperature boundary forcing files, these values were kept constant with time. With these files developed and the changes in the `fort . 15` and `fort . 14`, the simulation can now be three-dimensional with tide, atmospheric, riverine, and density forcings.

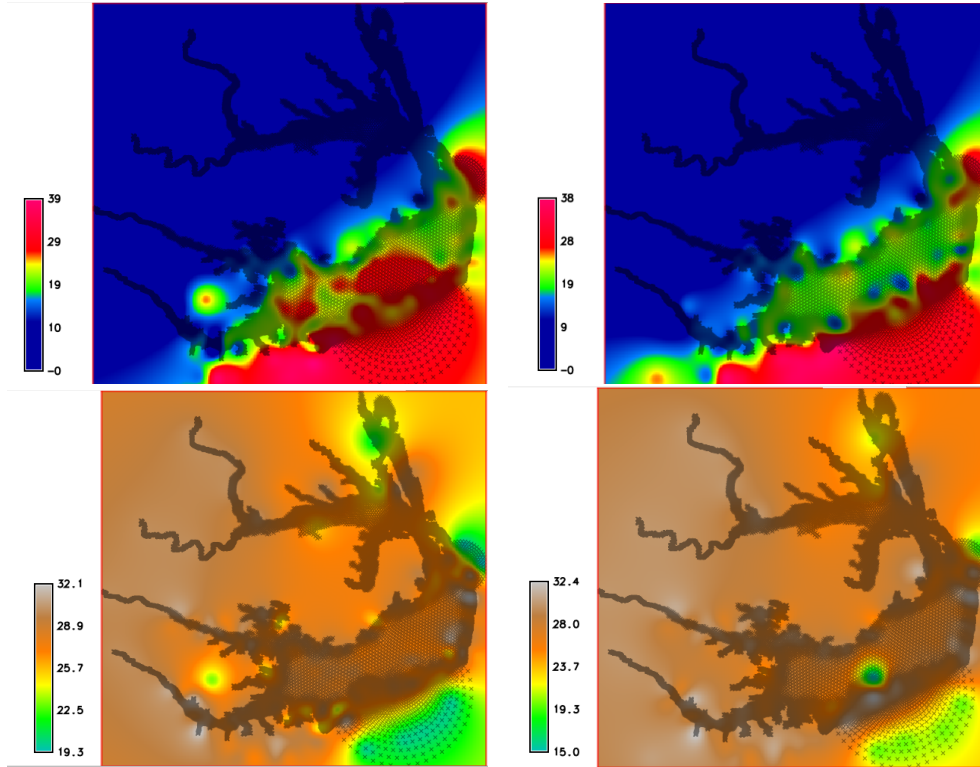


Figure 3.9: Initial conditions for (top) salinities and (bottom) temperatures, shown at both the (left) surface and (right) bottom. The salinities have dimensions of ppt, and the temperatures have units of degrees Celsius.

3.3 Simulation Setup

To investigate Irene’s effects on water levels and density transport in APES, simulations with and without were developed. This allows for a comparison between a typical month of August without any storms and then an August that includes Irene. Both simulations have a total duration of 37 days spanning: tidal spin-up, density spin-up, storm duration, and two weeks after (Figure 3.10). Also, with the vertical water column having been noted previously as well-mixed (Jia and Li 2012; Luettich et al. 2002), eleven equally spaced sigma layers were chosen to represent the vertical water column. The first two sections, tidal and density spin-up, are included to allow for model stability and regulation of forcings.

Both simulations (storm and non-storm) start with a tidal spin-up at 0000 UTC 6 August 2011. This section includes only tidal and river forcings. For the density, initial values for salinities and temperatures are read from the `fort.11` file, but they are used in a diagnostic model: the density fields are fixed, and no mixing or transport is allowed to occur. Instead,



Figure 3.10: Timeline of simulation with corresponding dates, types, and forcings. The storm simulation (top) includes the atmospheric forcing and changing river discharges. The no-storm simulation (bottom) does not include atmospheric forcing and constant discharges.

the tides and river flows are allowed to acclimate to the initial density field. The tidal spin-up segment extends for 10 days, ending on 16 August. Between the storm simulation and the no-storm simulation, the only difference at this stage is the riverine forcing. For the storm simulation, a time series of river flows is applied, while the no-storm simulation has a constant river flow.

Then, starting on 16 August, the density spin-up segment is started. This segment includes tidal, river, and density forcings. The initial salinities and temperatures, which remain fixed during the tidal spin-up, are now allowed to evolve during the density spin-up. This allows for the density to change both horizontally and vertically. The density spin-up segment extends for 5 days. In this segment, again the only difference between the storm and no-storm simulations is the different river flows.

The storm segment of the simulation extends from 21 August until 29 August, a total length of 8 days. For the storm simulation, physical forcings included tidal, river, density, and atmospheric. As stated above, the atmospheric forcing is developed using the best-track file to create the wind and pressure fields. The density forcing is again set to prognostic to allow for the salinity and temperature fields to evolve. In the simulation without the storm, the atmospheric forcing is not applied; instead, only the tidal, river, and density forcings are applied. The river, again, is the constant averaged value from before the storm occurs.

Beginning on 29 August and lasting until 12 September, the after storm segment lasted 14 days. During this segment, the physical forcings included tidal, river, and density. Between the two simulation types, with storm and without, the only difference was the river forcing.

This portion was divided into two different weeks to allow for analysis of weeks after the storm.

3.4 Analyses

A key question of this research is how did the storm affect the surface salinities throughout APES. These effects will be quantified by identifying salinity contours and measuring their spatial variabilities during and after the storm, as well as by examining time series of salinities at specific locations and measuring the temporal variabilities.

3.4.1 Salinity Contours

The APES has a full range of possible salinities, from fully fresh waters in the upper rivers, to fully saline waters at the inlets and offshore, and everything in-between. To quantify the variations in surface salinities during Irene, we focus on salinity ranges that are tied to wildlife preferences.

To examine how changes in salinity can affect the various types of wildlife, estuaries can be classified into zones. One example is the Venice System. It was developed in 1959, and was based upon observations, the judgement, and experience of that time (Caspers 1959). While the Venice System was a good starting point, it lacks the objective criteria for the zone boundaries and has fixed zones. Another example of salinity zones was developed by NOAA National Estuarine Inventory. It defined three zones, tidal fresh, mixing, and seawater, but it is based only on hydrographic characteristics (National Ocean Service 1985).

For this research, we use the biologically based estuary salinity zones presented by Bulger et al. (1993). These zones have overlapping boundaries and were developed by using multivariate statistical analysis on salinity data for more than 300 species found in the Chesapeake and Delaware Bays (Bulger et al. 1993). The overlapping of these zones were due to the grouping of these various species. These zones were developed by exploring the species distribution across the estuarine salinity gradients. To develop these zones, first a salinity gradient ranging from 0 percent to 30 percent was divided into 34 increments. The species were then placed into the increments, and, after applying the multivariate statistical analysis, it was determined that the salinity structure can be defined into five zones. The five zones consist of the limnetic, oligohaline, mesohaline, polyhaline, and the euhaline (Table 3.3).

Table 3.3: Biologically based estuarine salinity zones from Bulger et al. (1993). The salinities shown are in ppt and are the lower and upper limits of each zone.

Zone	Lower	Upper
Limnetic	0	4
Oligohaline	2	14
Mesohaline	11	18
Polyhaline	16	27
Euhaline	24	>24

Using these zones, sorting key aquatic wildlife can occur. Looking at the 2019 commercial fishing report, shellfish were the main sources of revenue (North Carolina Division of Marine Fisheries 2020). This includes blue crabs, listing first with a net revenue of \$22.1 million, and oysters, listing third with \$4.8 million (North Carolina Division of Marine Fisheries 2020). Salinity is vital to each of these shellfish species. While blue crabs can survive a range of salinities, for reproduction to occur females need salinity of 22 ppt or higher. If the salinity is below 22 ppt their eggs and larvae are not able to survive (Albemarle-Pamlico National Estuary Partnership 2019). Oysters are the third highest revenue and require a salinity in the range 12 ppt to 25 ppt (North Carolina Division of Marine Fisheries 2010). Due to the important role that oysters play in APES, like filtration and food sources, NCDMF has placed oyster sanctuaries within the Pamlico Sound. These can be seen in Figure 3.12 and the locations used as synthetic stations for analysis in Chapter 4. Based off of the requirements each of these species need, to focus in the results will be on the mesohaline, polyhaline, and euhaline zones.

While the selected salinity zones are based off of wildlife needs, the behaviors of stated wildlife are not analyzed in this study. Instead, these salinity zones will be the basis on how the results of the simulation will be examined. In Figure 3.11, the average August surface salinities for the study area. The bluer hues are the fresher zones (dark blue 0 ppt to 11 ppt; light blue is mesohaline zone), the yellow hues are the moderately saline (green is polyhaline mixed zone; yellow is polyhaline), and the redder hues are the most saline (red is euhaline mixed; pink is euhaline). This distribution is solely based on the observational data from SalWise; there has been no simulation to allow for regulation. The Albemarle Sound is in the fresher zone. Roanoke Island is in the mesohaline/polyhaline mixed zone at the northern end, southern end, and western side. The eastern side is in the polyhaline

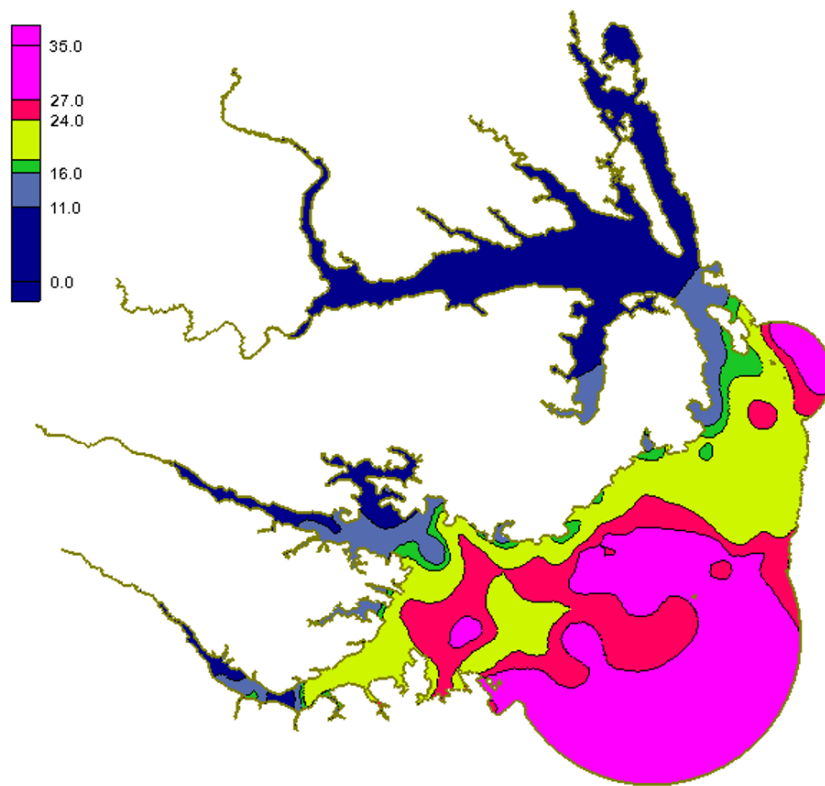


Figure 3.11: Average surface salinities for the month of August, developed using the method in Section 3.2.4, with contour values to show the selected salinity zones.

zone. Pamlico Sound is mostly in the polyhaline, with euhaline mixed and euhaline near the ocean inlets. In the Tar-Pamlico River, the fresher zone extends about 18 km and the mesohaline about 43 km from the downstream of the constriction. The lower Neuse River, downstream of the constriction, is polyhaline. The downstream of the constriction in the Neuse, there a pocket of fresher zone. Upstream of the constriction, there is a pocket of mesohaline about 13 km long.

For the analysis of the results, we will rely heavily on these zones and their locations. Measurements of the extents of intrusions, as well as any formed pockets of different zones, will be taken from contour plots. Comparisons of the no-storm simulation to the storm simulation will also be used. These comparisons will be done by using difference plots of the surface salinities. Synthetic stations will also be used to examine time series of the surfaces at select locations. This will allow for an in-depth analysis of the locations of the the salinity zones and how they change during and after the storm.

3.4.2 Analysis Methods

While the movements of the salinity zones will be examined through physical processes, the values and extents will be examined using multiple different analysis tools. To develop time series of the surface salinity values, synthetic stations will be used. The location of these synthetic stations is shown in Figure 3.12. Details for each station are shown in Table 3.4. These synthetic stations are placed in areas to monitor the surface salinity changes, like the mouths of the Tar-Pamlico and Neuse Rivers. They are also placed at the oyster sanctuaries locations, to establish the range of salinities these sanctuaries would experience. Details of these stations are shown in Table 3.5. Another tool that will be utilized are the surface salinity contours. This will allow for dimensions of the salinity zones to be taken. These dimensions will be taken by using the synthetic station locations as bases for the measurements. Another metric that will be examined, is the differences between the no-storm simulation surface salinities and those of the storm simulation. These differences will be developed by subtracting the surface salinities of the storm simulation by the no-storm simulation.

Table 3.4: Coordinates and geographic regions for the synthetic stations to be used in later analyses.

Number	Longitude	Latitude	Area
1	-76.458	35.346	Tar-Pamlico River
2	-76.850	35.437	Tar-Pamlico River
3	-76.500	35.100	Neuse River
4	-76.813	34.956	Neuse River
5	-75.720	35.940	Roanoke Island
6	-75.640	35.920	Roanoke Island
7	-75.620	35.810	Roanoke Island
8	-75.710	35.870	Roanoke Island
9	-76.019	35.069	Ocracoke Inlet
10	-75.762	35.190	Hatteras Inlet
11	-75.530	35.773	Oregon Inlet
12	-76.387	35.243	Pamlico Sound
13	-76.079	35.229	Pamlico Sound
14	-75.754	35.425	Pamlico Sound
15	-75.593	35.593	Pamlico Sound
16	-76.63596	35.99005	Albemarle Sound
17	-76.365641	36.02812	Albemarle Sound
18	-75.99971	36.063231	Albemarle Sound
19	-75.818977	36.02639	Albemarle Sound
20	-75.770302	36.098209	Albemarle Sound
21	-75.821327	36.219761	Albemarle Sound

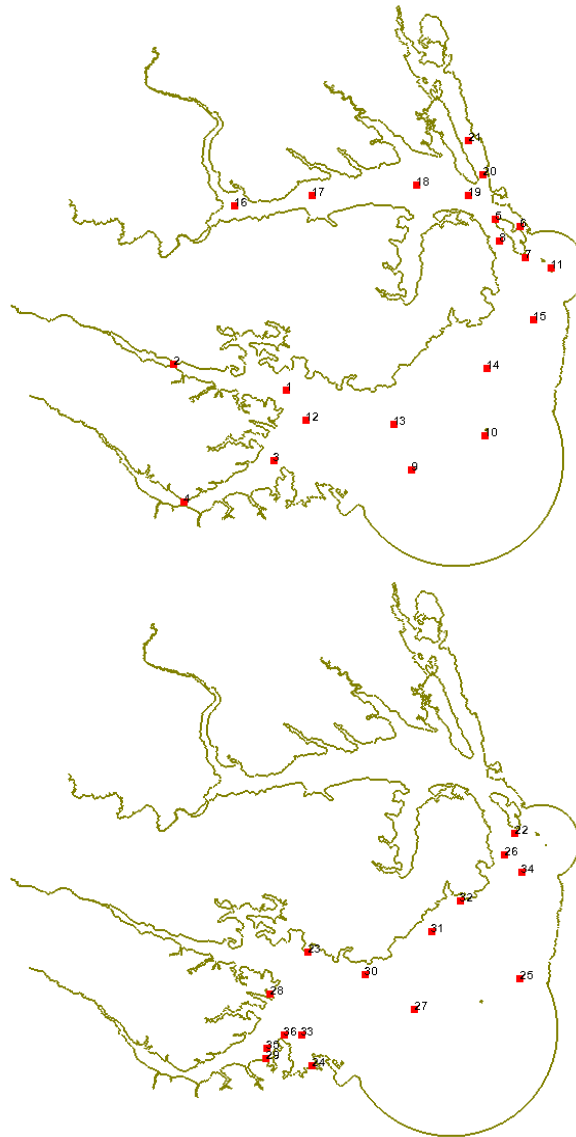


Figure 3.12: Locations of synthetic stations (top) and oyster sanctuaries (bottom) to be used to analyze time series of surface salinities.

Table 3.5: Coordinates and geographic regions for the oyster sanctuary stations to be used in later analyses.

Number	Longitude	Latitude	Sanctuary
22	-75.638933333	35.80473667	Croatan Sound
23	-76.369353333	35.38187667	Deep Bay
24	-76.356053333	34.98086167	West Bay
25	-75.619666667	35.29133333	Clam Shoal
26	-75.675138333	35.728055	Crab Hole
27	-75.993866667	35.18025	Ocracoke
28	-76.502966667	35.23596667	Middle Bay
29	-76.518150000	35.00790333	Neuse River
30	-76.168150000	35.305	West Bluff
31	-76.930723333	35.45592833	Gibbs Shoal
32	-75.830600000	35.56345	Long Shoal
33	-76.391233333	35.09036667	Raccoon Island
34	-75.615666667	35.666	Pea Island
35	-76.514816667	35.0436	Little Creek
36	-76.452233333	35.09251667	Swan Island

CHAPTER

4

RESULTS AND DISCUSSION

Irene's effects on the Albemarle-Pamlico Estuarine System varied spatially and temporally. As the storm approached, its easterly winds pushed saline waters across the sounds and brackish waters far into the estuaries. As the storm moved over the system, its winds changed direction and pushed fresh waters farther down the estuaries and sounds. In the weeks following the storm, its large rainfalls led to large river flows, which further affected the density distributions. The magnitudes of these responses varied significantly through the system.

This chapter is divided into two sections. First, a synoptic history of Irene in APES is presented, with a qualitative focus on the storm forcing and the overall system response, including surface salinity variations. Then, the storm's effects are quantified via comparisons with a no-storm simulation, and the responses are investigated for specific sub-regions with APES. Finally, time series of surface salinities are examined at the oyster habitats in APES, to understand the magnitude and duration of the variations at these locations. The methods of analysis are described in Chapter 3.

4.1 Synoptic History of Irene in APES

Irene's effects on APES can be separated into two stages: in the 8 days during the storm, when the surface pressures and winds were included in the ADCIRC simulation to drive water levels and density transport; and in the 14 days after the storm, after the atmospheric forcing but when the large river flows helped to regulate the system.

The results of this simulation will indicate how the atmospheric forcing of Irene would affect the typical August salinity distribution. This distribution was developed in Chapter 3. We will focus on the surface salinity distribution from our storm simulation and comparing it to the surface salinities of the typical August. This will allow for the analysis of deviations due to the storm forcings.

4.1.1 During Irene

To understand Irene's effects on APES, it is necessary to examine the evolution of the hydrodynamics and transport as the storm approached, moved over the system, departed, and then as the system regulated afterward. The storm timeline is shown in Figure 4.1. First, as the storm approached (Figure 4.2), its easterly winds pushed waters across the sounds and into the estuaries, thus pushing brackish saline waters beyond their typical ranges in APES. Then, as the storm moved over the system (Figure 4.3), the southeasterly winds on the eastern side of Irene pushed more saline waters into the sounds, while the northwesterly winds on the western side of Irene pushed fresher waters into the sounds. Next, as the storm departed the system (Figure 4.4), the remaining westerly winds pushed waters out of the estuaries and into the sounds. As the wind magnitudes tapered off, the extents of the intrusions were also slowed. Last, in the weeks after the storm (Figure 4.5), the increased river discharges due to rainfall, propagated the fresher zones into the sounds. These storm stages are described in the following subsections.

4.1.2 Before Landfall

The storm simulation started at 0000 UTC 21 August, about 6.5 days before Irene's landfall, and thus the system was not yet experiencing the effects of the storm (Figure 4.2, top row). Water levels were within their typical ranges due to river discharges and tidal inflows. The maximum water level was 1.0 m above mean sea level at the head of Roanoke River. Surface salinities were distributed in zones with typical locations. Fresh waters (darkest blue in the figures) were located in the estuaries and across most of the Albemarle Sound.

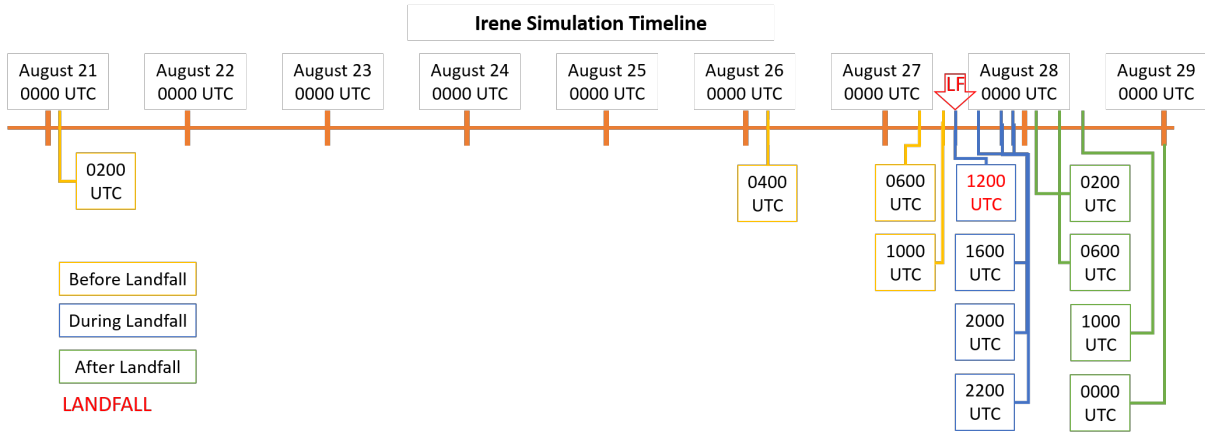


Figure 4.1: Timeline for Irene (2011) to indicate timesnaps shown in later figures.

The mesohaline zone (relatively fresh, light blue in the figures) was located near Roanoke Island and at the mouths of the Tar-Pamlico and Neuse River estuaries. The polyhaline zone (relatively brackish, yellow) was located across the Pamlico Sound. The euhaline zone (relatively saline, pink) was located mostly offshore, but also in plumes from the inlets into the sounds due to the tides.

More than five days later, at 0400 UTC 26 August (Figure 4.2, second row), the storm effects were significant in the system. Wind speeds had an average of 9.0 m/s and were west-northwesterly. At this time, water levels had not changed much, but the salinity zones had shifted. The polyhaline zone expanded in the Pamlico Sound, pushing to its northern edge. This zone was also being pushed into the Neuse River, with only a small boundary zone before the mesohaline zone. In the Tar-Pamlico River, the boundary zone between mesohaline and polyhaline zones was pushed further into the river. The same was true for the mesohaline zone in the river. Around Roanoke Island, the mesohaline zone shrunk, being replaced by a mixed zone and the polyhaline zone.

At 0600 UTC 27 August (Figure 4.2, third row), about 6 hours before landfall, the winds were westerly over most of the study area; however, in the estuaries, they were northeasterly. The average wind speed was 22.0 m/s. These strong winds began to push water from the Outer Banks toward the estuaries. This caused the maximum water level to be 3.34 m in the Neuse River. Both in the Neuse and Tar-Pamlico, the water levels were elevated. These winds pushed the salinity zones westward. In the Neuse and Tar-Pamlico Rivers, the mesohaline zone extended into the upper portions. The polyhaline zone began to extend into the rivers. The euhaline zone extended further from the inlets. Oregon Inlet's euhaline zone reached

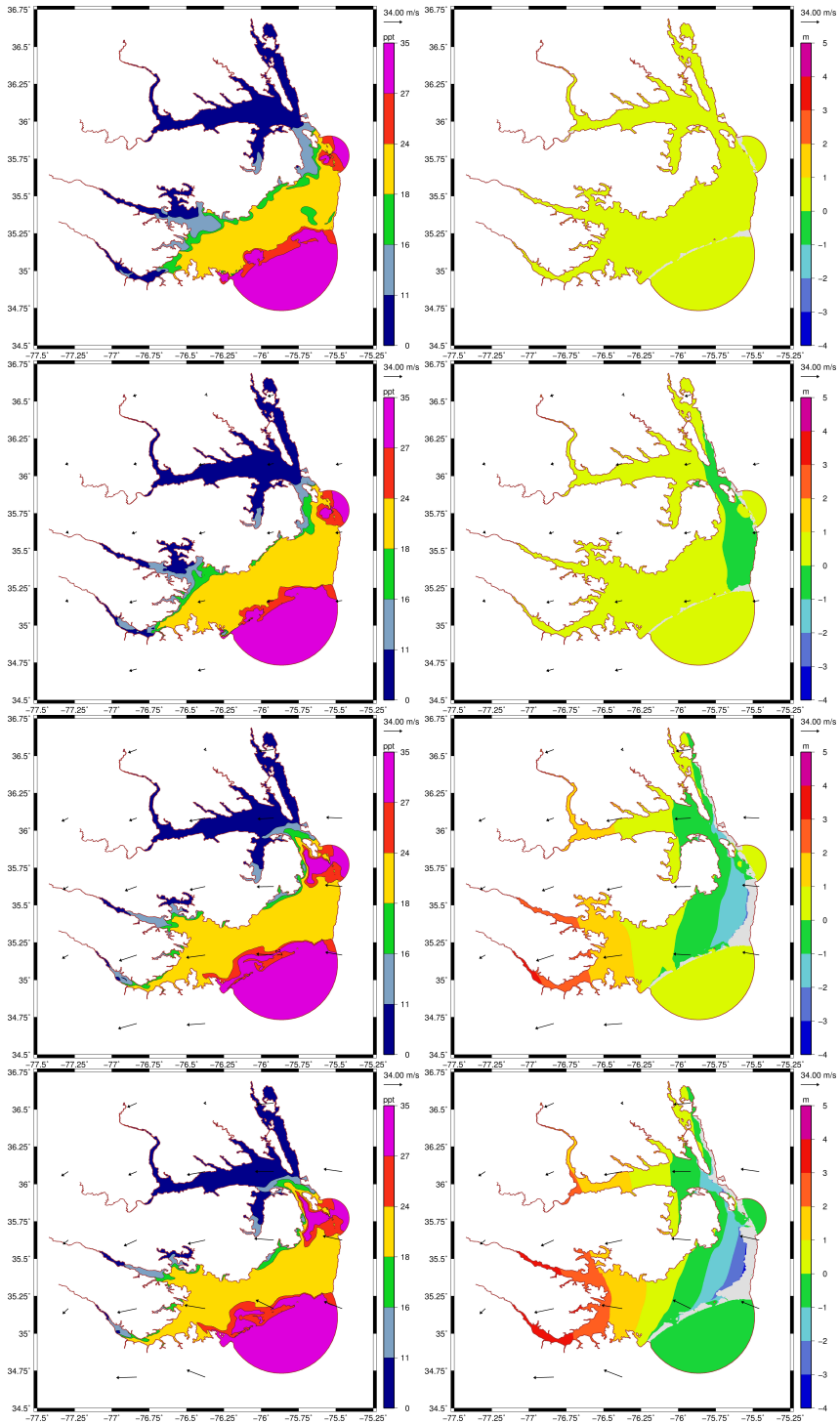


Figure 4.2: Irene's effects on (left) surface salinities (ppt) and (right) water levels (m relative to mean sea level), with time snaps of (top row) 0200 UTC 21 August, (second row) 0400 UTC 26 August, (third row) 0600 UTC 27 August, and (bottom row) 1000 UTC 27 August. For the surface salinities, the colors indicate zones of (light blue) mesohaline, (yellow) polyhaline, and (purple) euhaline.

the southern end of Roanoke Island.

By 1000 UTC August 27 (Figure 4.2, bottom row), the winds increased to 32.4 m/s and changed directions to westerly. At this time, Irene was two hours from landfall just south of the area. These large winds caused dramatic gradients in the water levels in the Pamlico Sound. Water continued to be pushed away from the Outer Banks and into the rivers and west sides of the area. These water levels in the rivers were up to about 4.0 m. Also due to these winds, the salinity zones pushed further westward. The polyhaline zone extended into the Albemarle Sound. The euhaline zone extended around the western side of Roanoke Island. More of the polyhaline zone was pushed into the Tar-Pamlico and Neuse Rivers.

4.1.3 During Landfall

At 1200 UTC 27 August (Figure 4.3, top row), Irene made landfall just south of the study area. The cyclone's rotating winds were located over APES, with the eastern portion blowing southeasterly and the western portion blowing northeasterly. Wind speeds were as large as 33.4 m/s. At this time, the east-to-west water-level gradient was extreme, with extensive dry portions on the east side of Pamlico Sound, and water levels in the estuaries up to 4.4 m. Saline waters in the euhaline zone were pushed from Oregon Inlet into the west sides of the Albemarle and Pamlico Sounds, as well as from Hatteras and Ocracoke Inlets into the south side of the Pamlico Sound. In the Neuse and Tar-Pamlico river estuaries, the fresh and mesohaline zones were overwhelmed, with relatively brackish waters from the polyhaline zone extending far westward.

At 1600 UTC 27 August (Figure 4.3, second row), Irene's eye was located near the Tar-Pamlico River. In the eastern half of APES, the winds were southeasterly, while in the western half, the winds were northeasterly. South of the eye of Irene, the winds were northwesterly. The maximum wind speed was 28.2 m/s. Water levels were being pushed northward in the Pamlico Sound, westward in the Albemarle, and southward in the Neuse and Tar-Pamlico Rivers. The maximum water level was 3.9 m, located in the estuaries. The changing wind directions also had a fast effect on the surface salinities. The polyhaline intrusion in the Neuse River was reduced, and euhaline zones in the Pamlico Sound were pushed eastward. However, the euhaline zone continued to push into the west side of the Albemarle Sound.

By 2000 UTC 27 August (Figure 4.3, third row), Irene's eye was located over the Albemarle Sound. Over most of the area, the water levels were being pushed eastward. The maximum water level was 3.7 m in Roanoke River. The maximum wind speed was 27.05 m/s. In the Pamlico Sound, the winds were westerly, with a southerly influence near Roanoke Island.

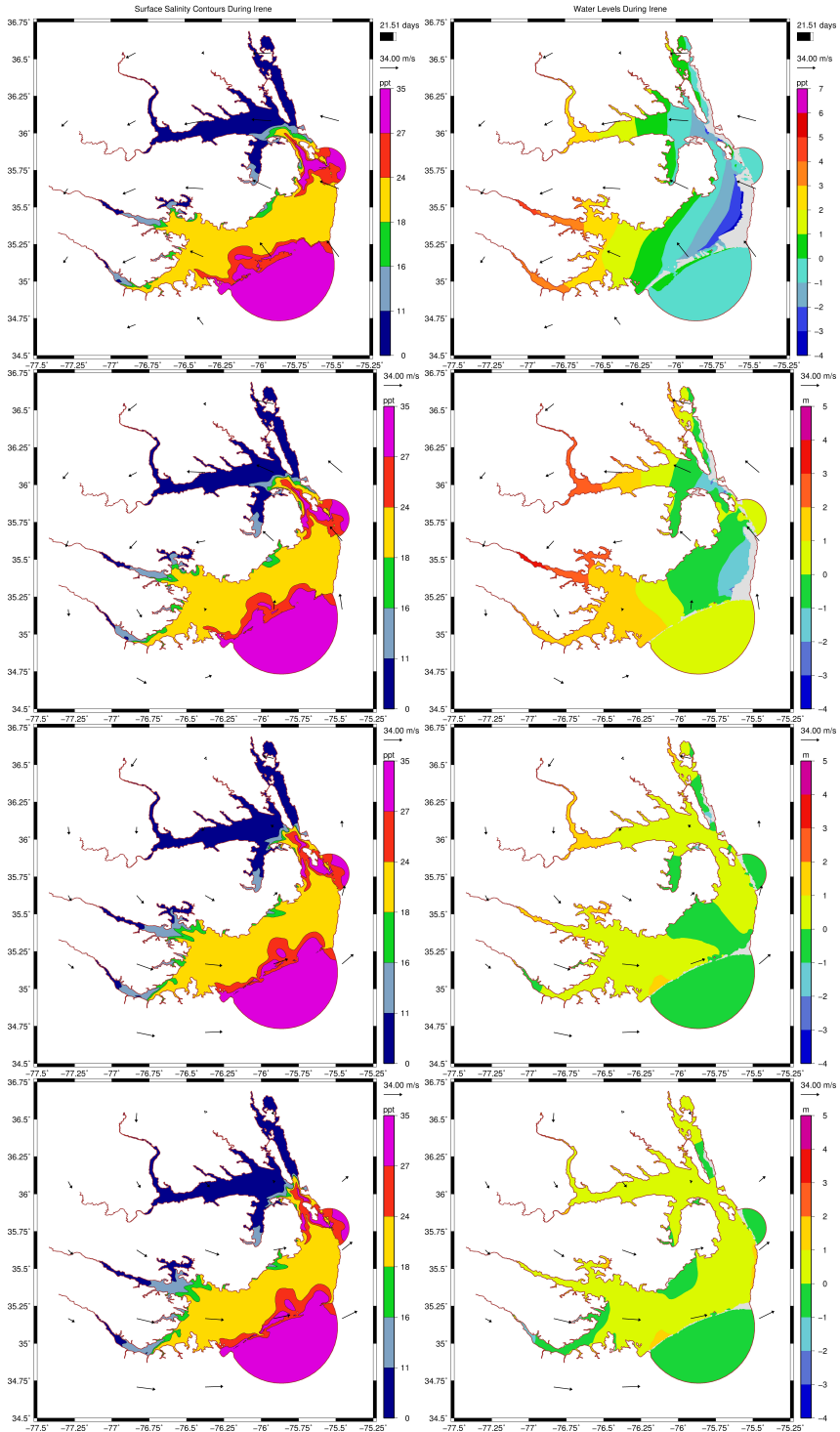


Figure 4.3: Irene's effects on (left) surface salinities (ppt) and (right) water levels (m relative to mean sea level), with time snaps of (top row) 1200 UTC 27 August, (second row) 1600 UTC 27 August, (third row) 2000 UTC 27 August, and (bottom row) 2200 UTC 27 August. For the surface salinities, the colors indicate zones of (light blue) mesohaline, (yellow) polyhaline, and (purple) euhaline.

Roanoke Island was surrounded by an euhaline zone, and an euhaline zone was pushed into the Currituck Sound. The euhaline zones from the southern two inlets were pushed northeastern, as was the polyhaline intrusion on the southern two rivers.

Two hours later, at 2200 UTC 27 August (Figure 4.3, bottom row), Irene's eye was located over Currituck Sound. The maximum wind speed was westerly and 28.05 m/s. The water levels continued to push eastward, with a maximum of 3.48 m by the Outer Banks. With the eye over the Currituck Sound, the winds over the sound pushed the salinity zones northeastward. The polyhaline mixed and euhaline zones extended into the sound. At Roanoke Island, the euhaline zone was surrounding the southern end. In the Neuse and Tar-Pamlico Rivers, the fresher zones were pushed eastward, down the rivers towards the mouths. At this point, ten hours had passed since landfall.

4.1.4 After Landfall

At 0200 UTC 28 August (Figure 4.4, top row), Irene's eye had left the study area, but the winds continued in strength. The maximum wind speed was 28.65 m/s, blowing west-southwesterly. Water levels reach to 2.99 m in the Roanoke River. Along the northern Outer Banks, the water levels were 1.7 m on average. The winds pushed the euhaline mixed and euhaline zones away from the Hatteras and Ocracoke Inlets, forming pockets in the Pamlico Sound. In the Neuse and Tar-Pamlico Rivers, the fresher and mesohaline zones extended to the mouths of the rivers. The Albemarle Sound's fresher and mesohalting zones extended towards Roanoke Island.

By 0600 UTC 28 August (Figure 4.4, second row), the movements were amplified. This was due to the wind southwesterly with a maximum of 25.21 m/s. Up the Neuse River, the maximum water level was 3.18 m. From the Neuse and Tar-Pamlico Rivers, the mesohaline zone extended into the Pamlico Sound. The fresher and mesohaline zones from the Albemarle Sound extended to the northern end of Roanoke Island. In the Currituck Sound there was a pocket of polyhaline and mesohaline zones that were separated as Irene passed over. At the Oregon Inlet, a larger intrusion of polyhaline zone into the ocean boundary occurred.

The wind speeds tapered off by 1000 UTC 28 August (Figure 4.4, third row). The average wind speed was about 12.3 m/s and southwesterly. The pocket of mesohaline and polyhaline zones in the Currituck Sound was mixed as time progressed. A large portion of the euhaline zone being pushed from the Albemarle Sound was forced to the eastern side of Roanoke Island. The intrusion of polyhaline into the Oregon Inlet ocean boundary was

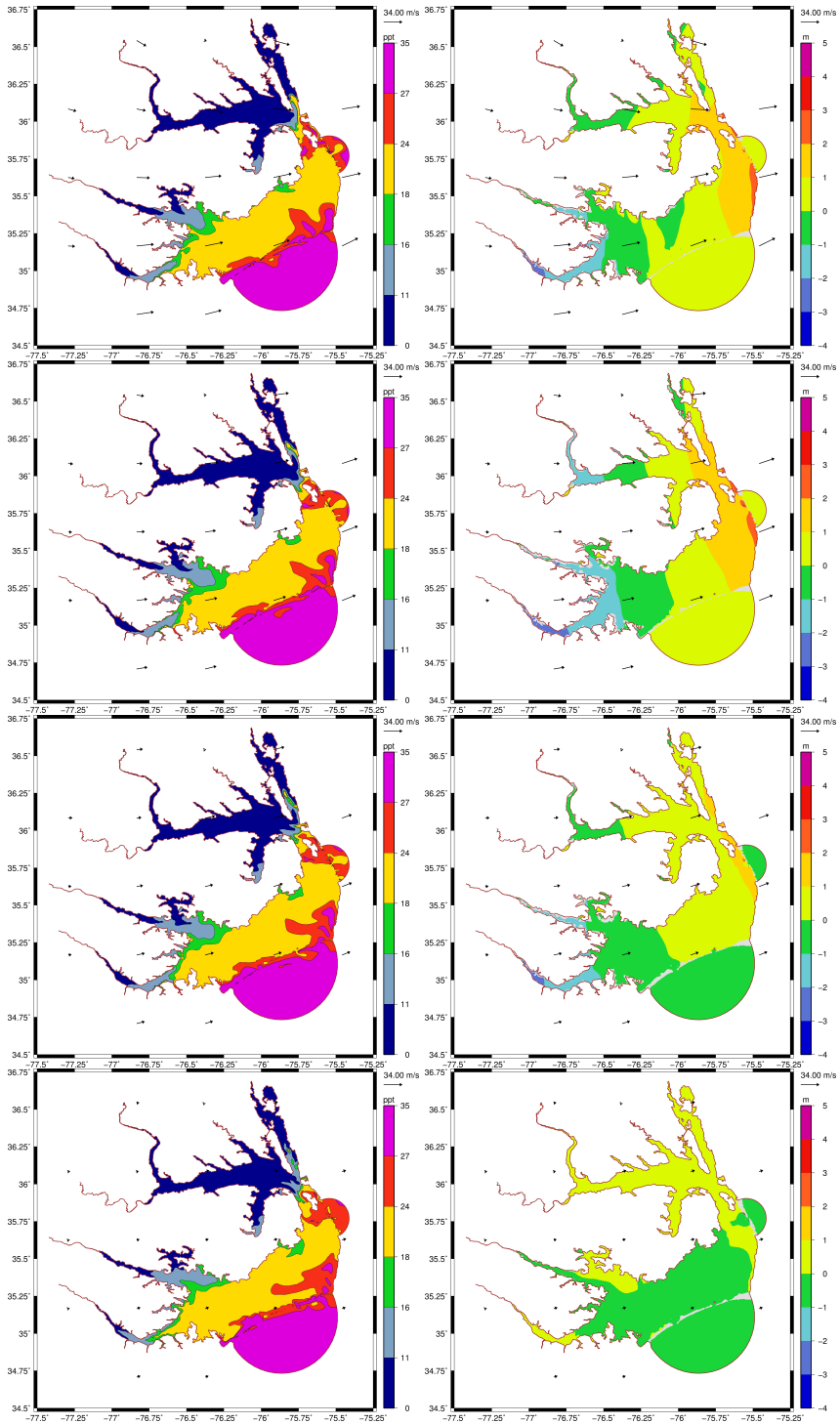


Figure 4.4: Irene's effects on (left) surface salinities (ppt) and (right) water levels (m relative to mean sea level), with time snaps of (top row) 0200 UTC 28 August, (second row) 0600 UTC 28 August, (third row) 1000 UTC 28 August, and (bottom row) 0000 UTC 29 August. For the surface salinities, the colors indicate zone of (light blue) mesohaline, (yellow) polyhaline, and (purple) euhaline.

larger. Euhaline zones from the Hatteras and Ocracoke Inlets progressed northward against the Outer Banks. At Hatteras Inlet, there was a polyhaline intrusion.

On 0000 UTC 19 August (Figure 4.4, bottom row), the storm section of the simulation ended. Wind speeds had an average of 5.36 m/s, with higher speeds near the Outer Banks. Maximum water levels were 4.09 m. The salinity zones followed the same patterns as noted previously. The pockets noted became more mixed. This includes the pocket of euhaline in the Pamlico Sound that originated at the southern two inlets. At the Tar-Pamlico and Neuse Rivers, the fresher and mesohaline zones were pushed further down. In the Albemarle Sound, the fresher zone pushed the other zones around Roanoke Island.

4.1.5 After Irene

By 1200 UTC 31 August (Figure 4.5, top row), large changes in salinities had occurred. The polyhaline zone had mixed in Currituck Sound, and most of the mesohaline zone had been pushed out of the area. Albemarle Sound was full of the fresher water zone, which had pushed by Roanoke Island. Around the island, the entire western side was the fresher water zones with some mesohaline. The eastern side was largely the mixed zone between the polyhaline and euhaline. Looking in the main body of the Pamlico Sound, the pockets of mixed zone (between mesohaline and polyhaline) were appearing. The pocket of euhaline has been mostly mixed, leaving a large area of the mixed zone, between the polyhaline and euhaline. In the Neuse and Tar-Pamlico Rivers, the fresher zone continued to expand with increase of discharge due to rainfall. This pushed the mesohaline zone further into the sound. The maximum water level, 6.16 m, was located in the Neuse River.

By the end of the first week after the storm, on 0000 UTC 5 September (Figure 4.5, second row), these patterns of transport had intensified. The fresh water zone from the Albemarle Sound encompassed the southern and northern ends of Roanoke Island. The eastern side had some of the mixed zone between polyhaline and euhaline. From the Neuse and Tar-Pamlico Rivers, the mesohaline zone progressed into the main body of the Pamlico Sound. Also in the main body of the Pamlico Sound, the mixed zone between mesohaline and polyhaline had expanded, while the pocket of euhaline and mixed zones had nearly dissipated. The maximum water level was 3.95 m, located in the Neuse River.

By a week and a half from the end of the storm, on 1200 UTC 7 September (Figure 4.5, third row), the salinity zone movements noted at the end of the first week had continued. The southern rivers pushed the mesohaline zone further into the Pamlico Sound. With respect to the mixed zone found in the main body of the Pamlico Sound, it had grown.

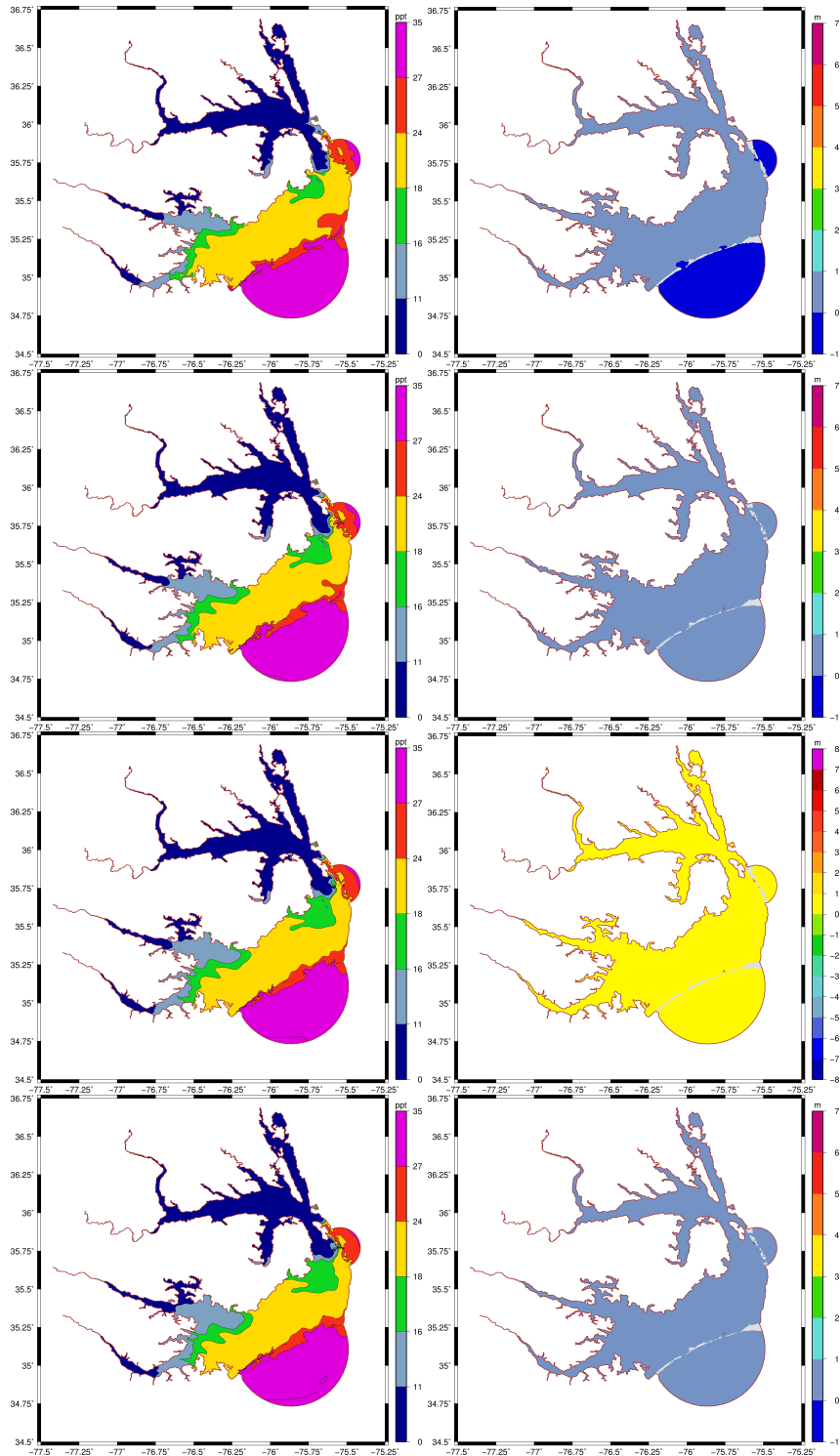


Figure 4.5: Irene’s effects on (left) surface salinities (ppt) and (right) water levels (m relative to mean sea level), with time snaps of (top row) 1200 UTC 31 August, (second row) 0000 UTC 5 September, (third row) 1200 UTC 7 September, and (bottom row) 0000 UTC 12 September. For the surface salinities, the colors indicate zones of (light blue) mesohaline, (yellow) polyhaline, and (purple) euhaline.

Around Roanoke Island the southern and northern ends were encompassed by the fresher water zone, while the eastern side was seeing the euhaline mixed zone. Water levels reached a maximum of 2.05 m in the Neuse River.

At the end of the second week, 0000 UTC 12 September (Figure 4.5, bottom row), water levels had decreased, as the maximum was 1.73 m in the Neuse River. The salinity zones followed the same trends. Roanoke Island was surrounded by the fresher zone at the northern end, western side, southern end, and partially the eastern side. The middle area of the eastern side was in euhaline mixed zone. From the intrusions around Roanoke Island, the fresher, mesohaline, and polyhaline mixed zones had expanded into the northern Pamlico Sound. At the Neuse and Tar-Pamlico Rivers, the mesohaline and polyhaline mixed zones extended further into the southern Pamlico Sound.

4.2 Irene's Effects on Surface Salinities

As shown in the synoptic history, Irene had significant and varied effects on surface salinity transport in APES. In this section, we quantify those effects by using the methods described in Chapter 3. Difference plots will quantify the spatial extents of Irene's effects on the surface salinities, and time series at synthetic stations will quantify the duration of these effects. We focus on specific sub-regions: Albemarle Sound, Pamlico Sound and the Hatteras and Ocracoke Inlets, Roanoke Island and Oregon Inlet, and the Neuse and Tar-Pamlico Rivers. By focusing on these sub-regions, we can explore and quantify the storm's effects on mixing and transport through the entire system.

4.2.1 Albemarle Sound

Irene affected the surface salinities in the Albemarle Sound by pushing brackish waters into its east side during the storm. These brackish waters extended into Currituck Sound, but then were pushed back southward as the winds changed after the storm. These brackish water intrusions have the potential to affect ecosystems in the east side of Albemarle Sound.

At 0200 UTC 21 August (Figure 4.6, top row), near the start of the storm simulation, the Albemarle Sound was fresh, with salinities below 11 ppt throughout the region. The mesohaline zone started about 2 to 5 km north of Roanoke Island, but it did not extend into the Albemarle Sound. At the western side of the sound, station 16 had a salinity of 0.6 ppt while the eastern side, station 19, had a salinity of 2.3 ppt. At this time, there were no significant differences from the non-storm simulation. However, as the storm approached

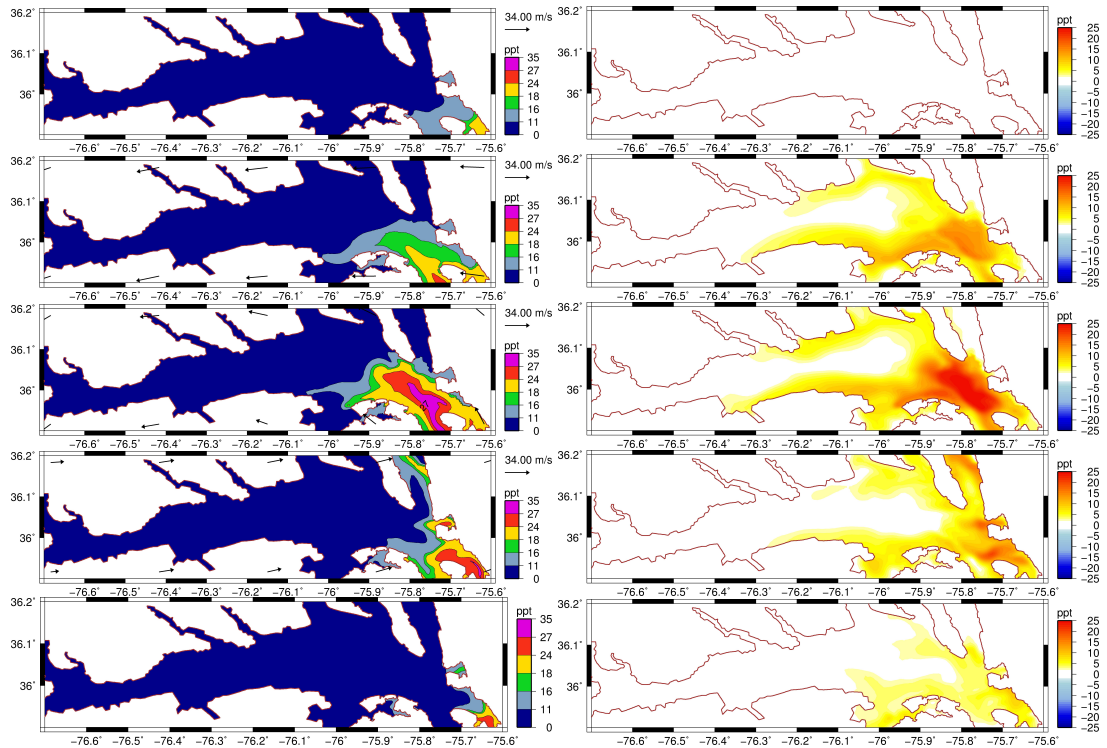


Figure 4.6: Irene's effects on the Albemarle Sound: (left) surface salinities (ppt) and (right) differences (ppt) from a non-storm simulation. Rows correspond to: (top row) 0200 UTC 21 August, (second row) 0800 UTC 27 August, (third row) 1800 UTC 27 August, (fourth row) 0800 UTC 28 August, and (last row) 0000 UTC 5 September.

over the next several days, its easterly winds pushed currents westward, and brackish waters moved into the east side of the sound.

By 0800 UTC 27 August (Figure 4.6, second row), the easterly winds pushed currents westward. Due to this, an intrusion of brackish waters into the east side of the sound occurred. At this time, the mesohaline zone extended up to 25.9 km into the sound, and the polyhaline zone was about 8.8 km from the edge of Roanoke Island. At station 19, the surface salinity was 15.6 ppt. In the western side of the Albemarle, station 16, the surface salinity was at 0.9 ppt. Higher salinities compared to the no-storm simulation were present. Along the northern and southern edges, differences ranged to 5 ppt. In some areas along these edges, the difference was larger, up to 10 ppt. The highest differences were seen at the eastern side of the sound, due to the intrusion of the polyhaline zone. These differences ranged from 15 to over 20 ppt.

As Irene moved over the Albemarle Sound, at 1800 UTC 27 August (Figure 4.6, third row), the shape of these intrusions changed. Instead of being pushed westward into the

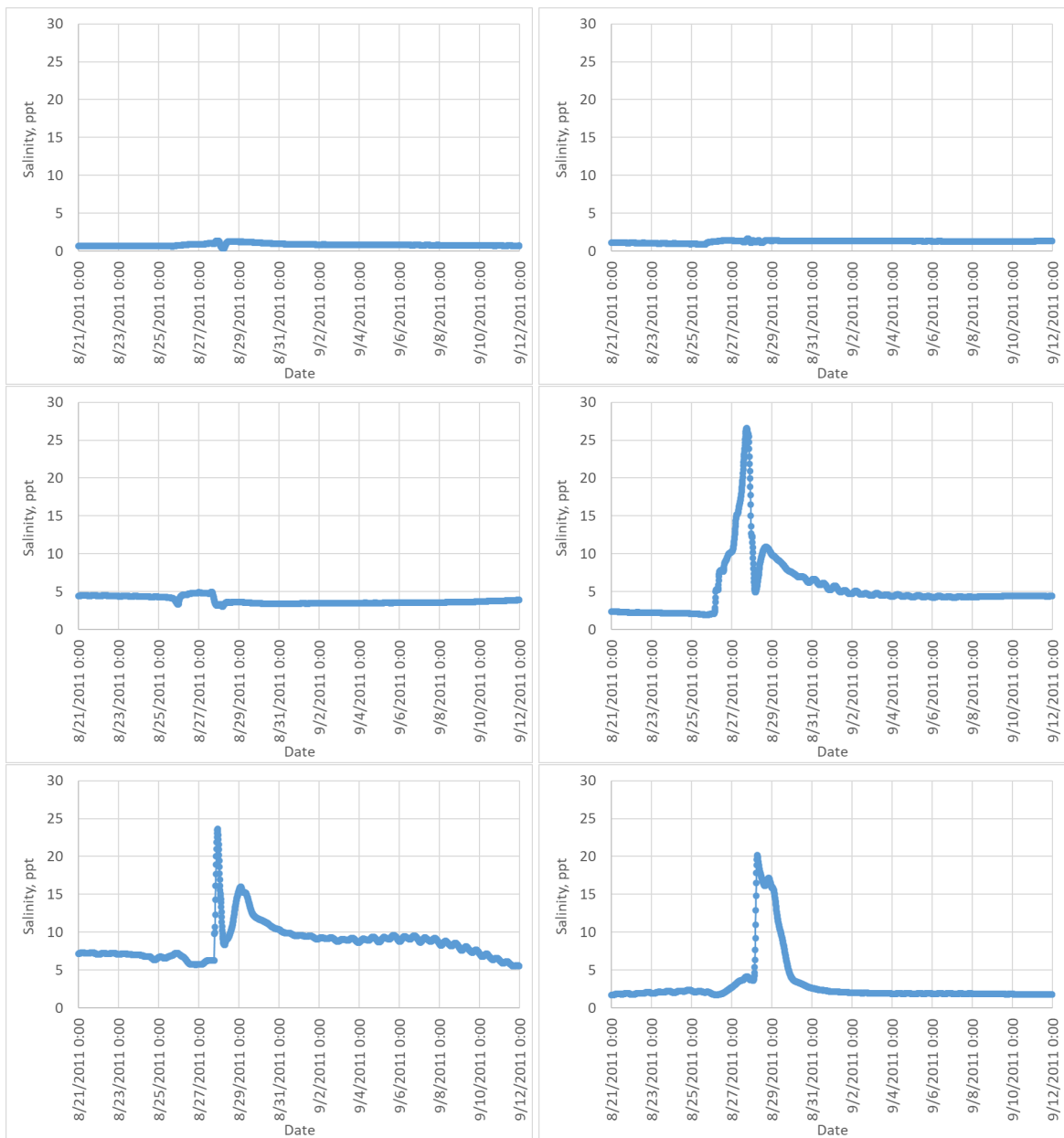


Figure 4.7: Time series of surface salinities (ppt) in Albemarle Sound at synthetic stations: 16 (top left), 17 (top right), 18 (middle left), 19 (middle right), 20 (bottom left), and 21 (bottom right). Details listed in Table 3.4 and shown in Figure 3.12.

Albemarle, they were pushed northwestward. This motion was due to the winds blowing southeasterly, and forcing the currents northwestward. These currents caused some of the intrusion to move into the Currituck Sound. The mesohaline zone extended 30.0 km on the southern side and 20.0 km on the northern side into the sound. The polyhaline zone reached 18.1 km on the southern side and 16.3 km on the northern side. The euhaline zone extended 10.6 km. Looking at station 16 on the western side of the Albemarle, the surface salinity has stayed around 0.9 ppt, while the eastern side, at station 19, the surface salinity is 26.5 ppt. This is placing the station 19 on the edge of the euhaline zone. Along the northern and southern edges of the sound, differences between the storm simulation and the no-storm simulation had spread. These differences extended to station 17 and were mostly in the range up to 5 ppt. Few areas had differences ranging into 10 to 15 ppt. The largest differences were in the eastern Albemarle Sound, with differences more than 25 ppt. This was the farthest extent of the salinity intrusions into the Albemarle Sound; after this time, the winds shifted, changed the direction of the currents, and push waters eastward.

By 0800 UTC 28 August (Figure 4.6, fourth row), these zones had shifted completely. Due to the winds shifting to the opposite direction, the currents were now flowing eastward. These currents caused the removal of the euhaline and polyhaline zones from the Albemarle Sound. It should be noted that a pocket of polyhaline and mesohaline zones remained inside the Currituck Sound. This pocket was largely mesohaline, with two spots of polyhaline (about 5-km-long northern and about 7.6-km-long southern). The mesohaline portion of the pocket was still connected to the part in the Albemarle. This can also be seen at stations 20 and 21. At this point, these stations had surface salinities of 8.6 ppt and 19.2 ppt. The mesohaline in the Albemarle extended to 13.0 km. The differences along the outer edges of the Albemarle have decreased in size and magnitude. These mostly range up to 5 ppt, while in the Currituck Sound the differences were up to 20 to 25 ppt. The large differences in the eastern sound had reduced in size and spread. Pockets of differences of 20 to 25 ppt had shifted southward. Over the next few hours, the winds continued to drive the brackish waters out of the Albemarle Sound.

By 0000 UTC 5 September (Figure 4.6, bottom row), about a week after the storm moved over the system, the larger river discharges caused currents to be push eastward throughout the sound. Closer to the eastern side of the sound, the currents were being forced southward. Due to these currents, the mesohaline intrusion in the sound had dissipated. This can also be seen in the difference plot. While the salinity values are still higher near Currituck Sound, a difference of up to 5 ppt near the mouth, the storm effects had reduced. Along the edges, the differences decreased in size and magnitude. Pockets of the higher differences had

dissipated, with the eastern sound differences ranging up to 20 ppt. The fresher zone from the Albemarle had now extended along the western side of Roanoke Island, about 10.8 km from station 7. At the western side of the sound, station 16, the surface salinity was 0.8 ppt, while at the eastern side, station 19 had a salinity of 4.3 ppt. These smaller salinity values were due to the influence of larger fresh water discharges.

During the full simulation, the time series show key salinity changes. Station 19 had a large increase in salinities during landfall, showing that the westward currents pushed the higher saline zones into the eastern Albemarle. It also included a slight increase more than a day after landfall. On the west side of the Albemarle, Station 16 had surface salinities that stayed relatively constant, with only a slight increase during landfall. In the Currituck Sound, stations 20 and 21 show the intrusion of the polyhaline zone from when the storm eye was located over the Albemarle.

By the end of the entire simulation, eastern Albemarle Sound had multiple changes in salinity zones. Station 19 had the largest range (24.63 ppt) between the maximum (26.57 ppt) and the minimum (1.93 ppt) compared to the other stations. The minimum occurred almost a day before landfall, and the maximum occurred after Irene's landfall. In Currituck Sound stations 20 (lower) and 21 (upper), had ranges of about 18 ppt. Of these two stations, the upper station experienced the largest range with a maximum of 20.15 ppt and a minimum of 1.71 ppt. These occurred almost three-quarters of a day after landfall and at the start of the simulation. Stations 16, 17, and 18 experienced the smallest ranges throughout the simulation, with the maximum difference being 1.89 ppt at station 18.

4.2.2 Pamlico Sound and Hatteras and Ocracoke Inlets

This section examines the Pamlico Sound, Hatteras Inlet, and Ocracoke Inlet, where saline waters entered the south part of the sound and then were pushed over large distances during the storm. At 0200 UTC 21 August (Figure 4.8, top row), there were intrusions of mesohaline zone near the mouth of the Tar-Pamlico River. The mesohaline zone reached 17.7 km into the sound. It should be noted that the tides have some influence on this plume from the Tar-Pamlico River. The timing of this influence was delayed, but following the ebbing tide, the plume extended about 19.1 km from the inlet. The station at the mouth of the Neuse River was encompassed by the polyhaline zone. At the western boundary of the Pamlico, there were pockets of the polyhaline mixed zone. Near the Outer Banks, on the eastern side, there were two pockets of the mixed zone as well. The larger pocket was approximately 15 km in length and the smaller 10.5 km. Comparing the widths of the two

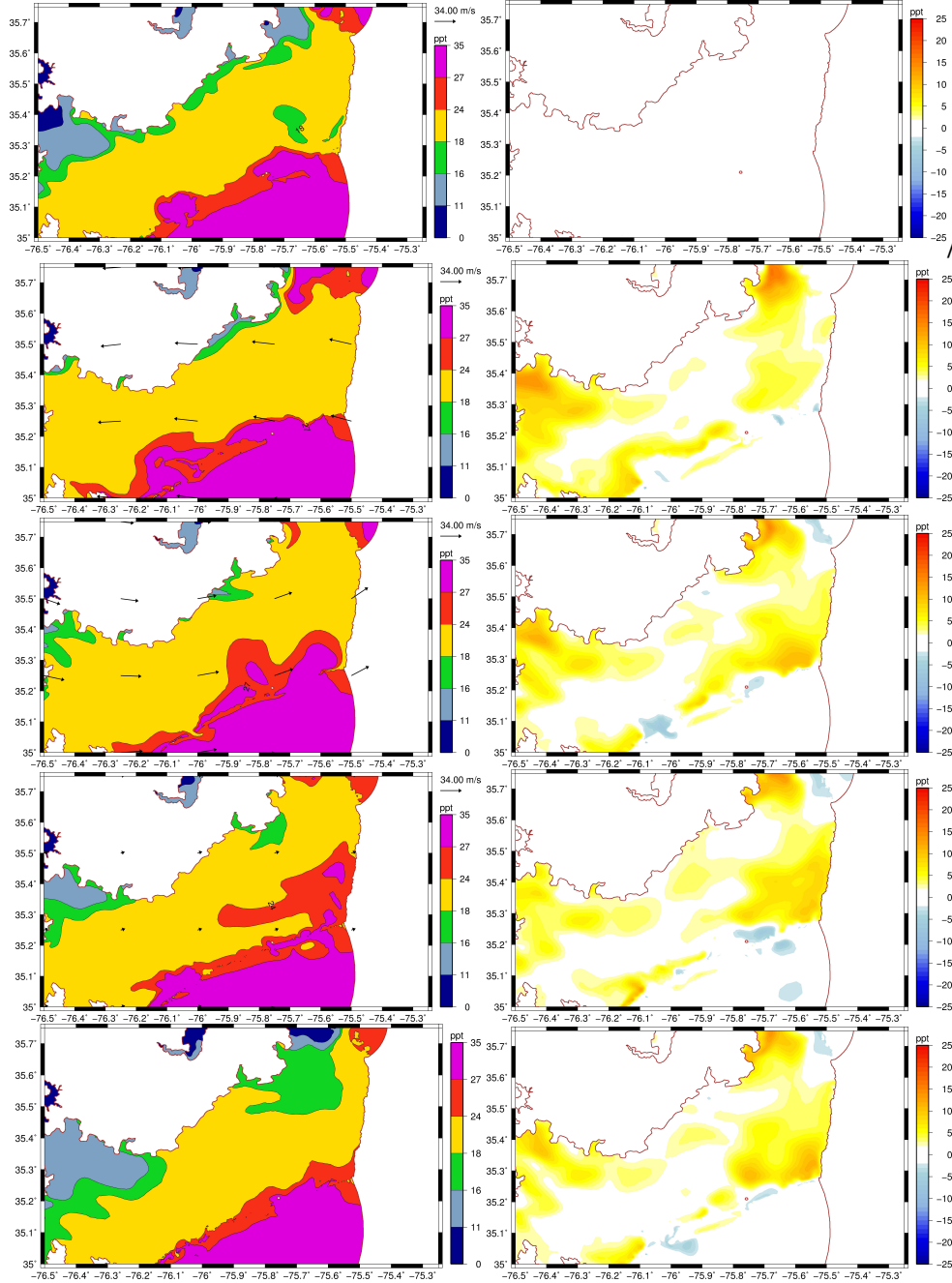


Figure 4.8: Irene forced effects on the Pamlico Sound, Hatteras Inlet, and Ocracoke Inlet: (left) surface salinities (ppt) and (right) differences (ppt) from a non-storm simulation. Rows correspond to: (top row) 0200 UTC 21 August, (second row) 0800 UTC 27 August, (third row) 2200 UTC 27 August, (fourth row) 0000 UTC 29 August, and (last row) 0000 UTC 12 September.

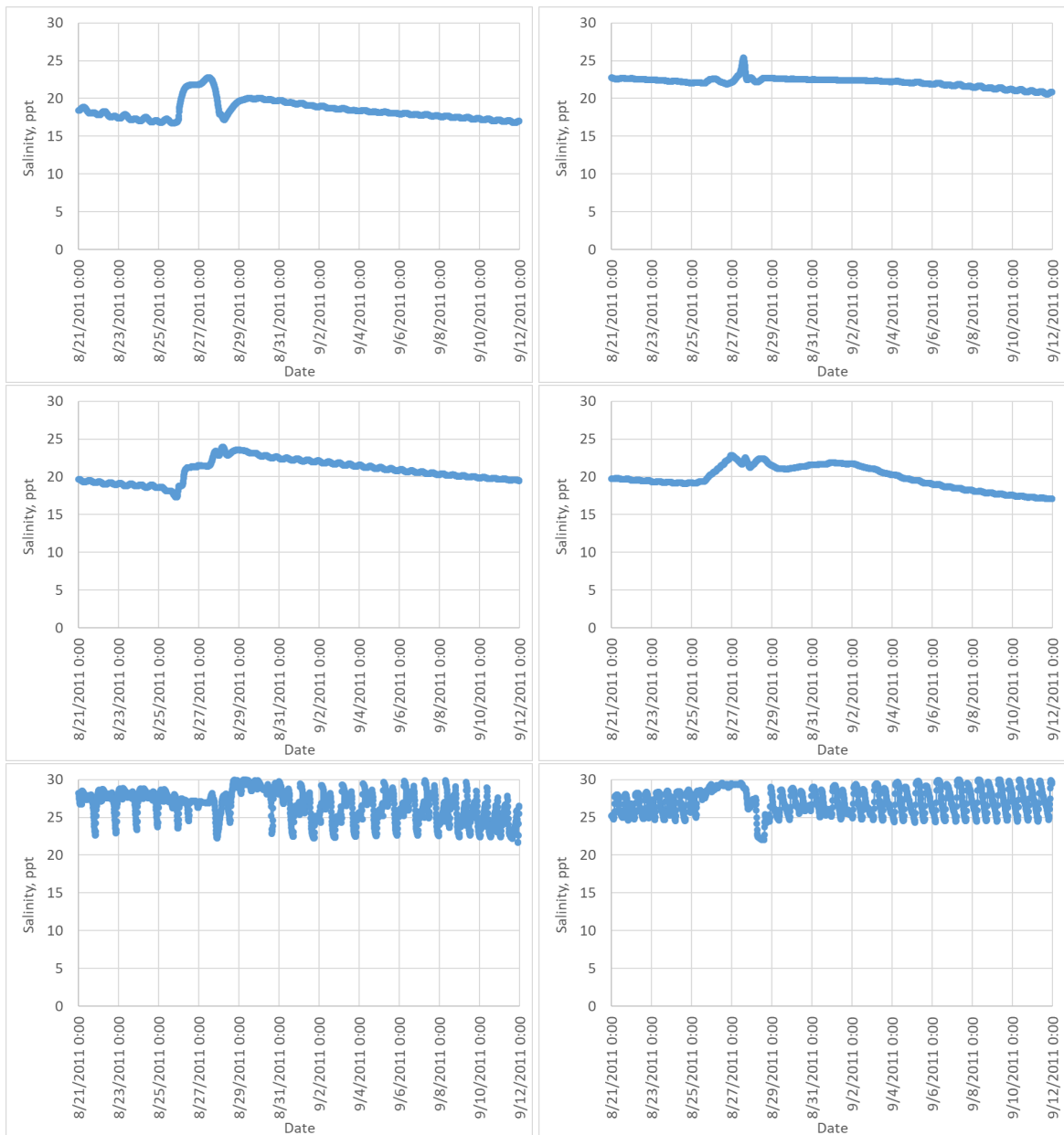


Figure 4.9: Time series of surface salinities (ppt) near Pamlico Sound and Hatteras and Ocracoke Inlets at synthetic stations: 12 (top left), 13 (top right), 14 (middle left), 15 (middle right), 9 (bottom left), and 10 (bottom right). Details listed in Table 3.4 and shown in Figure 3.12.

pockets at the widest points, the larger was about 5 times wider at 9.6 km compared to the smaller at 1.7 km. At this point, the differences between the storm and no-storm simulation were negligible.

By 0800 UTC 27 August (Figure 4.8, second row), the euhaline zones from the inlets had separated into two parts. The zone from Hatteras Inlet reached about 13.7 km. The portion of the large plume closest to Ocracoke Inlet had expanded into the sound by approximately 17.1 km. At western side of the sound, station 12, had a salinity value of 22.5 ppt placing it in the polyhaline zone. The northern intrusion of mesohaline had moved southward and became mixed into the polyhaline zone of the Pamlico. In this area, station 15 had a value of 22.1 ppt, in the polyhaline zone. Compared to the surface salinities from the no-storm simulation, the salinities of the storm simulation were generally larger. At this point, from the northern portion of the study area, there were differences ranging from about 5 ppt to 10 ppt, with some areas in the 15 ppt to 20 ppt range. From the Tar-Pamlico and Neuse Rivers, there were differences in the 10 ppt to 15 ppt range, extending along the southern Outer Banks and around the inlets.

At 2200 UTC 27 August (Figure 4.8, third row), the pocket of euhaline zone had disconnected from Ocracoke Inlet. Instead, Ocracoke Inlet experienced a intrusion of polyhaline zone, by about 3.8 km, and the polyhaline mixed zone, by about 6.6 km, toward the ocean boundary. The euhaline pocket had moved closer to station 14, about 6.7 km to the closest mixed zone. It was still connected to the Hatteras Inlet. Station 14 had a value of 23.3 ppt, closer to the edge of the euhaline zone. The euhaline pocket caused differences between the no-storm simulation mostly in the 10 ppt range. The differences stemming from the rivers had decreased in size but ranged mostly from 10 to 15 ppt. The northern intrusion had differences that were in the 15 to 20 ppt range.

By the end of the storm simulation, 0000 UTC 29 August (Figure 4.8, fourth row), the extrusion from the more saline pocket was 20 km in length and its leading edge was 22.6 km from station 14. From station 12, the polyhaline mixed zone was 6.8 km (farthest point) and closer to the Tar-Pamlico River. Station 14 had a value of 23.5 ppt and station 12 had a value of 19.6 ppt, placing both in the polyhaline zone. At Ocracoke Inlet, there was an euhaline mixed intrusion into the sound 9.2 km, resembling the tides. Around Ocracoke Inlet, the differences between the no-storm simulation were mostly in the 5 to 10 ppt range, with select areas in the 10 to 15 ppt range. From the rivers, the differences ranged from 5 to 10 ppt. The euhaline pocket caused differences of 10 to 15 ppt. At the northern intrusion, the size of the differences had decreased, but remained at 10 to 20 ppt.

After two weeks, 0000 UTC 12 September (Figure 4.8, bottom row), the polyhaline

mixed zones from the Tar-Pamlico and from the Neuse Rivers had combined. These zones measured 25.5 km into the sound from station 12. At station 12 there was a value of 16.9 ppt, indicating it was in the polyhaline mixed zone. The mesohaline zone reached 20.6 km. The polyhaline mixed zone from the northern portion had expanded, now surrounding station 15, with a value of 17 ppt, and 6.4 km from station 14, a value of 19.4 ppt. Near the inlets, the differences were in the range of -5 to -10 ppt, indicating less saline waters were in the storm simulation. The euhaline pocket, while smaller, had higher salinities than the no-storm simulation of 10 to 15 ppt. At the northern intrusion, the differences were higher at about 10 to 20 ppt. The size of the river differences had decreased, but was in the range of 5 to 10 ppt.

The stations located in the Pamlico Sound, Hatteras Inlet, and Ocracoke Inlet (Figure 4.9) experienced surface salinity ranges less than 9 ppt. The inlets had the largest ranges, with Ocracoke at 8.43 ppt and Hatteras at 8.05 ppt. Ocracoke Inlet experienced the smallest salinity, 21.66 ppt, nearly two weeks after the storm simulation. Hatteras Inlet's smallest salinity, 22.0 ppt, occurred a day after landfall. The stations located near the center of the sound experienced ranges less than 7 ppt, indicating that the Pamlico Sound's main body stayed in the polyhaline zone throughout the simulation. The jumps, outside of the tidal influences, are located near landfall of Irene.

4.2.3 Roanoke Island and Oregon Inlet

Roanoke Island and Oregon Inlet experienced the largest range of surface salinities during Irene. At the start of the simulation, 0200 UTC 21 August (Figure 4.10, top row), the northern end of the island was in the mesohaline zone, with station 5 having a value of 13.46 ppt. This zone extended 2.4 km, northward from station 5, at the closest edge of the zone. The eastern side was mostly in the polyhaline zone, with station 6 having a measurement of 18.7 ppt. Northward from this station, the polyhaline zone extended 1.5 km. The southern end is surrounded by a polyhaline mixed zone, with station 7 having a salinity of 17.37 ppt. Station 8, located on the western side, had a salinity of 13.83 ppt, putting it in the mesohaline zone. This zone extended 25.9 km from station 8 southward. There were no differences between the no-storm simulation and the storm simulation. At Oregon Inlet, the salinity fluctuated with the tides in the euhaline mixed and euhaline zones.

Six hours before landfall, at 0600 UTC 27 August (Figure 4.10, second row), the differences had propagated along the western side of the island and increased. This propagation was due to the currents flowing northward, stronger on the western side compared to the eastern

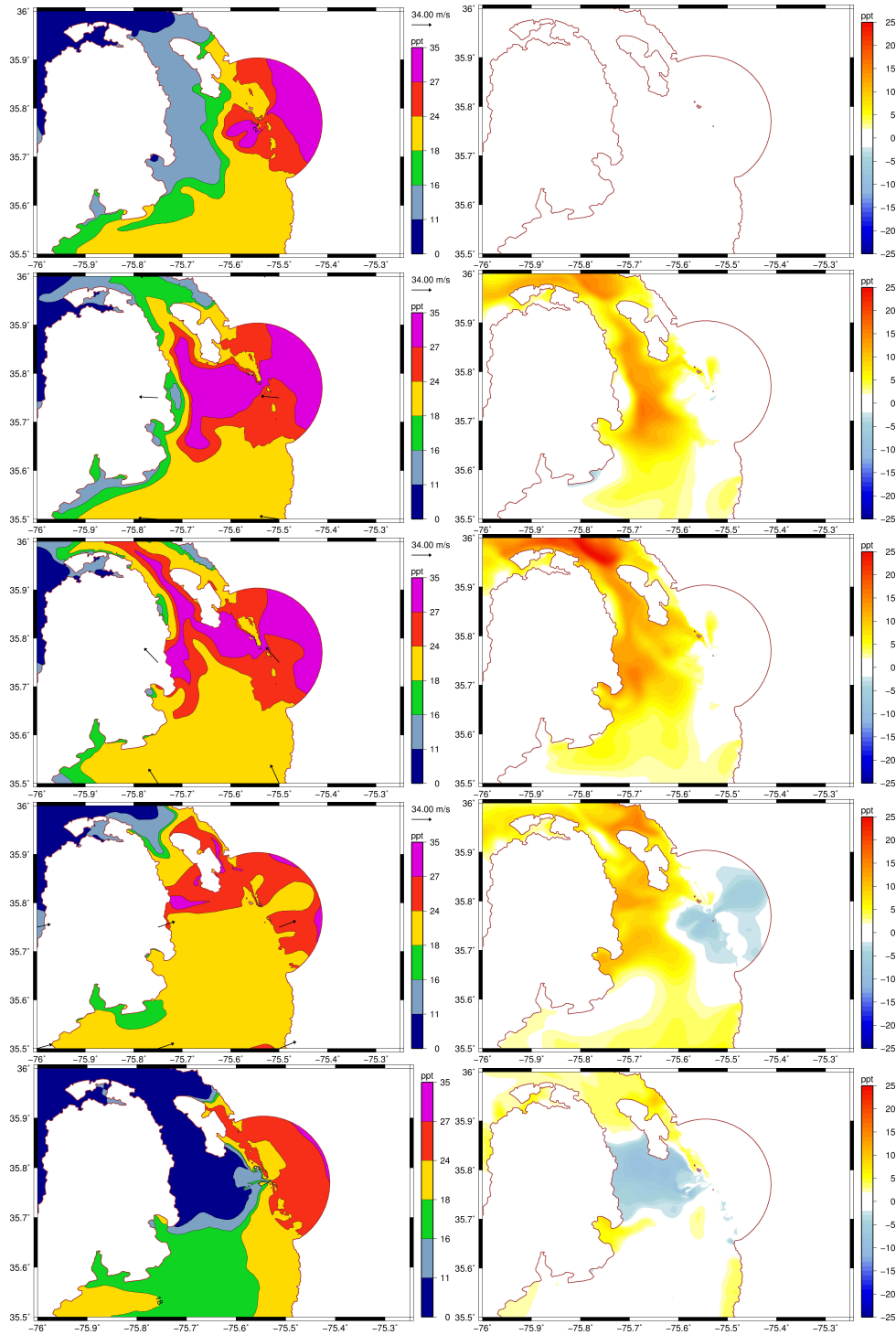


Figure 4.10: Irene forced effects on the Roanoke Island and Oregon Inlet: (left) surface salinities (ppt) and (right) differences (ppt) from a non-storm simulation. Rows correspond to: (top row) 0200 UTC 21 August, (second row) 0600 UTC 27 August, (third row) 1600 UTC 27 August, (fourth row) 0600 UTC 28 August, and (last row) 0000 UTC 12 September.

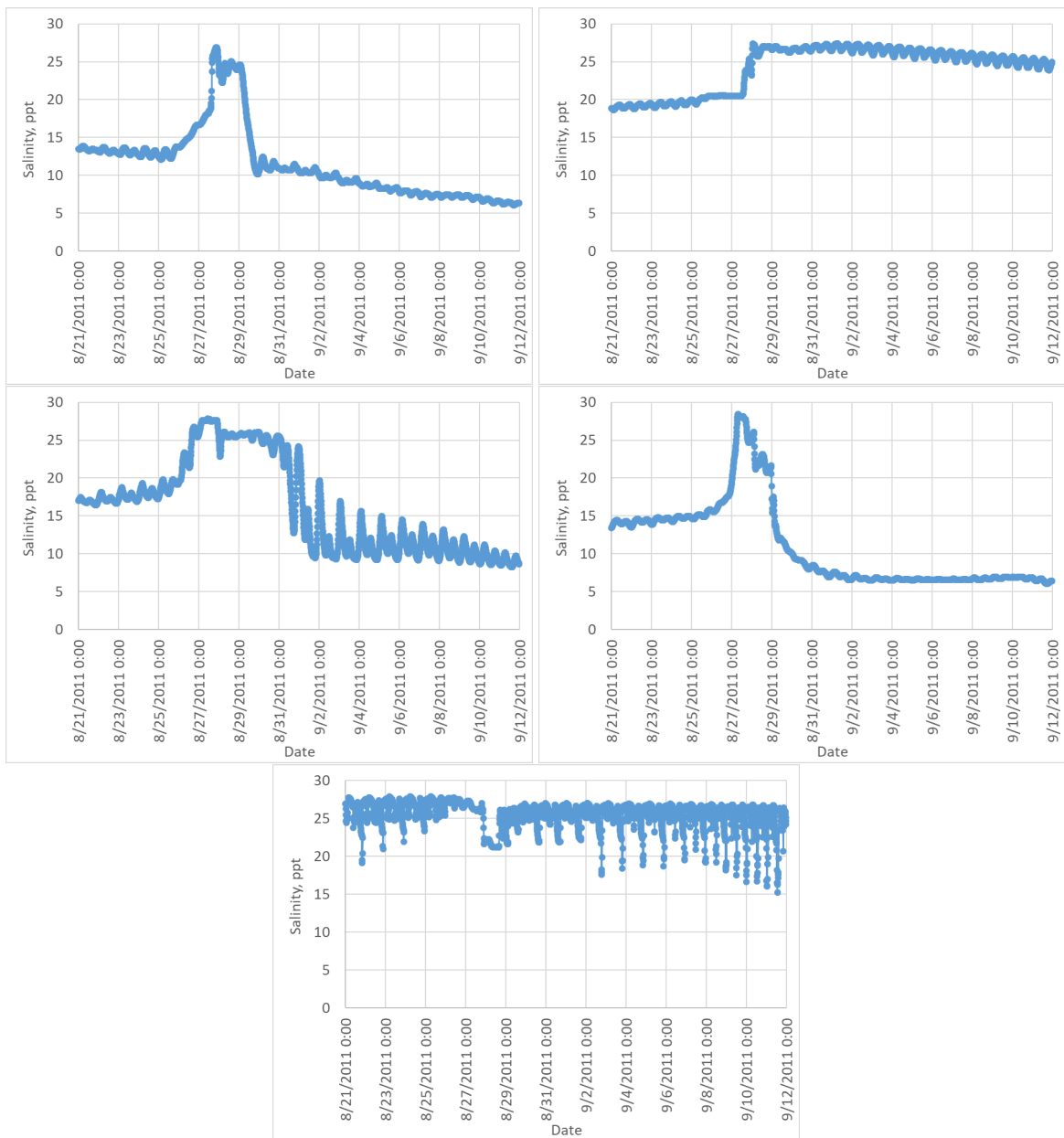


Figure 4.11: Time series of surface salinities (ppt) near Roanoke Island and Oregon Inlet at synthetic stations: 5 (top left), 6 (top right), 7 (middle left), 8 (middle right), and 11 (bottom). Details listed in Table 3.4 and shown in Figure 3.12.

side. These differences progressed to encompass the entire western side, northern end, and southern end of Roanoke Island. There was a small section on the eastern side that still resembles the no-storm simulation. These differences were about 20 ppt. On the western side, the surface salinities at the station were in the euhaline mixed zone, with a value of 26.07 ppt. From this station, the polyhaline zone extended 11.3 km northward. Surface salinities at the northern end were in polyhaline mixed zone, having a value of 17.46 ppt. For the southern end, surface salinities were 27.62 ppt and in the euhaline zone. This zone extended 18.7 km southward from station 7 and was connected to the Oregon Inlet. Near the Oregon Inlet, the surface salinities were relatively unchanged, have values of about 26.95 ppt and in the euhaline mixed zone.

At 1600 27 August (Figure 4.10, third row), the currents were moving northwestward, carrying the more saline zones. Surface salinities near the northern end of Roanoke Island were in the euhaline mixed zone, with values of about 24.9 ppt. From station 5, the euhaline zone extended 8.4 km northward. The southern and western sides of Roanoke Island had surface salinities in the euhaline zone, with values of about 27.50 ppt and 27.71 ppt, respectively. From the station on the western side, the euhaline zone extended 17.9 km southward. At the eastern side, the surface salinities started to show differences due to the storm. The station had values of about 23.54 ppt, placing it near the boundary of the polyhaline zone. Higher differences were located on at the northern end and western side, ranged from 15 to 25 ppt.

By 0600 UTC 28 August (Figure 4.10, fourth row), the currents had shifted directions, now flowing southward. These currents pushed back the more saline zones and brought the fresher zones southward. At the northern end of Roanoke Island, the surface salinities at the station were in the polyhaline zone, with values of about 23.54 ppt. From station 5, the mesohaline zone was 1.6 km to the north. The eastern side of Roanoke Island saw increased differences due to the storm. Its station had surface salinities in the euhaline mixed zone with values of about 26.02 ppt. A pocket of euhaline zone near station 6 was about 8 km in length. The western side of Roanoke Island had surface salinities in the polyhaline zone with values of about 21.71 ppt. A small pocket of euhaline zone was located about 4 km from station 8 and had a length of 2.6 km. The southern end of Roanoke Island had surface salinities in the euhaline mixed zone with values of about 26.04 ppt. Another pocket of euhaline waters was located 2.4 km away and had a length of about 7.3 km. Near the inlet and into the ocean, lower salinities persisted. At the inlet station, the surface salinities had values of about 21.64 ppt, placing it in the polyhaline zone, which extended 10.7 km into the ocean. This can be seen in the differences, with a range of about -5 to -10 ppt.

At 0000 UTC 12 September (Figure 4.10, bottom row), a fresher zone intrusion extended past Roanoke Island. From station 7, this zone extended 11.8 km southward. The mesohaline zone also extended 14.5 km southward. On the eastern side of Roanoke Island, there was a pocket of polyhaline zone with a length of 5.1 km. At Oregon Inlet, there was a polyhaline intrusion with a length of 9.1 km. The fresh water intrusion can also be seen in the difference plot. Around part of the western side and southern end of Roanoke Island, the differences ranged from -5 to -10 ppt. On the northwest side, northern end, and east side of Roanoke Island, the salinities are higher, with a differences of about 5 to 10 ppt.

Over the course of the simulation, the eastern side of Roanoke Island, stayed above 18.5 ppt. This is due to the currents flowing more around the western, larger, side of Roanoke Island. Following the highest value experienced, 27.4 ppt, the salinity stayed above 20 ppt but was decreasing. At Oregon Inlet, with the shifting wind and corresponding current direction to the east, the intrusion of the polyhaline zone can be seen in the time series at the station. This lasted about three quarters of a day. By the end of the entire simulation, each side of Roanoke Island experienced differences outside of the regular August distribution, as seen at the synthetic stations (Figure 4.11). At the northern end of Roanoke Island, station 5 had a maximum of 26.88 ppt (after landfall) and a minimum of 6.08 ppt (near two weeks after), a range of 20.8 ppt. The southern end experienced a maximum of 27.80 ppt (right before landfall) and a minimum of 8.24 ppt (near two weeks), having a range of 19.56 ppt. At the western side, the station had a maximum of 28.42 ppt (before landfall) and a minimum of 6.07 ppt (near two weeks), a difference of 22.34 ppt. The eastern side had the smallest range at 8.76 ppt, with a maximum of 27.42 ppt (after landfall) and a minimum of 18.66 ppt (near start of storm simulation). Oregon Inlet had a maximum of 27.86 ppt (about 3 days before landfall) and a minimum of 15.26 ppt (near two weeks).

4.2.4 Neuse and Tar-Pamlico Rivers

At the west side of Pamlico Sound, the Tar-Pamlico and Neuse Rivers had saline intrusions and fresh extrusions during Irene. Near the beginning of the simulation, 0200 UTC 21 August (Figure 4.12, top row), the upper portions of both rivers were in the fresher zone, and the lower parts were more saline. This distribution was developed from the river discharges, pushing the currents towards the mouths of the rivers. The Tar-Pamlico River had a mesohaline zone intrusion 23.9 km from the station located at the mouth, on the south side of the river. On the north side, the fresher zone extended 40.1 km down the river, from the upper station. This fresher zone passed the station located at the mouth of the

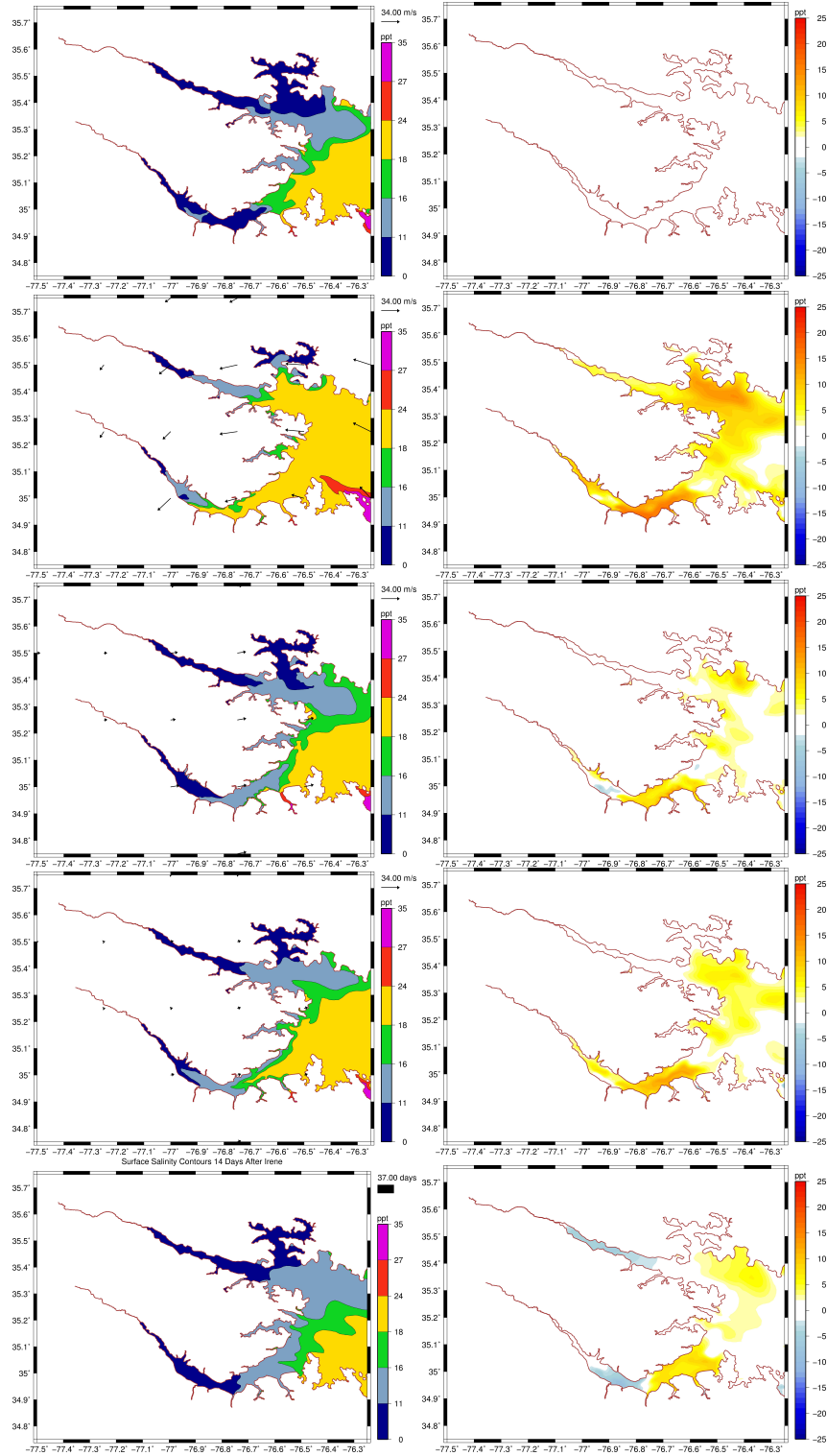


Figure 4.12: Irene forced effects on the Neuse and Tar-Pamlico Rivers: (left) surface salinities (ppt) and (right) differences (ppt) from a non-storm simulation. Rows correspond to: (top row) 0200 UTC 21 August, (second row) 1200 UTC 27 August, (third row) 0800 UTC 28 August, (fourth row) 0000 UTC 29 August, and (last row) 0000 UTC 12 September.

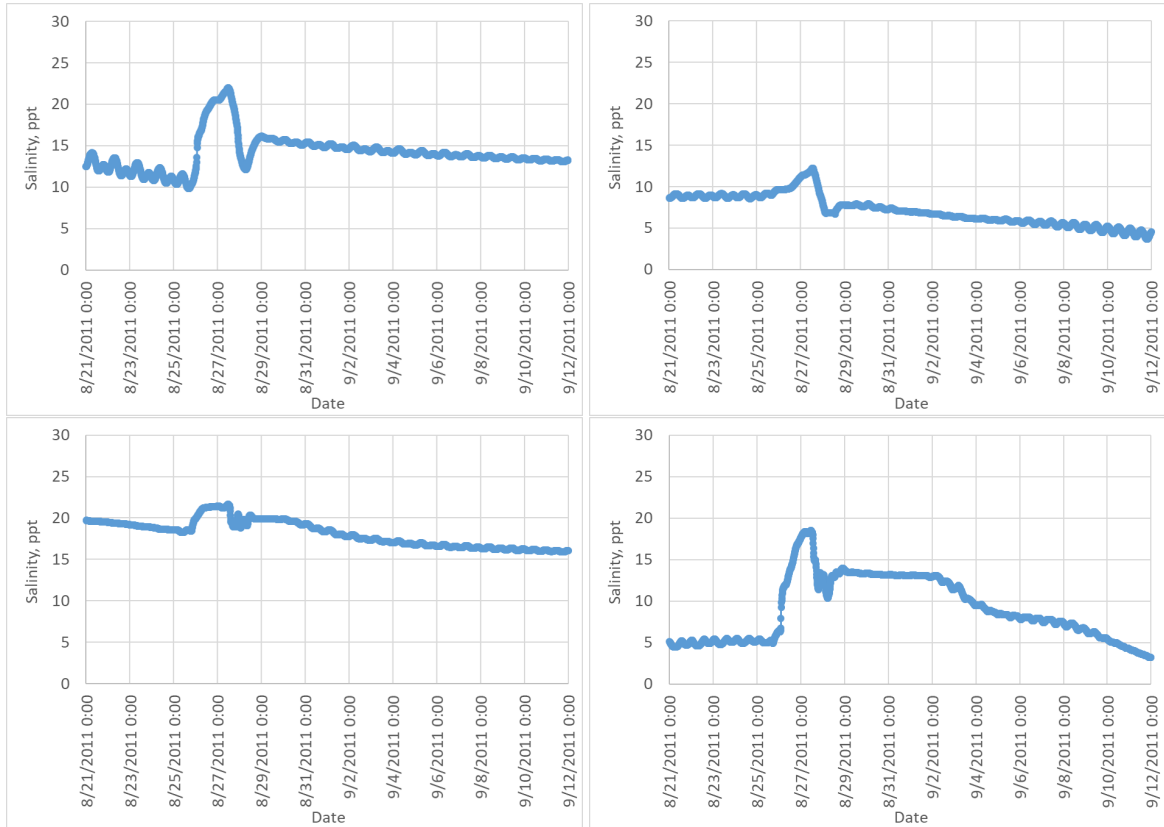


Figure 4.13: Time series of surface salinities (ppt) in the Neuse and Tar-Pamlico Rivers at synthetic stations: 1 (top left), 2 (top right), 3 (bottom left), and 4 (bottom right). Details listed in Table 3.4 and shown in Figure 3.12.

Tar-Pamlico. At the upper station the salinity was 8.6 ppt and the lower 12.8 ppt, indicating the upper is in the fresher zone and the lower in the mesohaline zone. In the Neuse, before the large bend in the river, there was a small pocket of mesohaline zone with length of 8.3 km and with of 1.8 km, with a thin protrusion across the width of the river. The fresher zone extended 17.1 km past the upper Neuse station. After the fresher zone, there was a band of mesohaline zone, approximately 1.3 km wide, about 2.9 km at the widest portion. At the mouth of the river, a polyhaline intrusion occurred about 10.6 km from the mouth station. Between the mesohaline zone and the polyhaline intrusion, there was a wide zone of polyhaline mixed across the river, and had a maximum length of 17.2 km. In this river, the upper station had a value of 4.7 ppt and the lower of 19.6 ppt. Both rivers had small (ranging approximately 0.4 km to 1.1 km) oscillations that correspond to the tides. The differences from the no-storm simulation were negligible.

At landfall, 1200 UTC 27 August (Figure 4.12, second row), the currents in the rivers were still moving toward the heads of the rivers. These currents were flowing against the river discharges, moving westward. This movement was also evident in the salinity zones. At the upper Tar-Pamlico River, the mesohaline zone extended 8.1 km toward the head of the river, and the station had a value of 12.07 ppt. At the upper Neuse, the polyhaline zone extended 10.8 km and the station had a value of 18.34 ppt. The mesohaline reached 24.5 km up the Neuse. Differences between surface salinities for the storm simulation were in the range of 10 to 15 ppt.

By 0800 UTC 28 August (Figure 4.12, third row), the mesohaline and fresher zones had migrated down the rivers. This is due to the winds blowing westerly. The wind direction is pushing the currents in the direction of the river discharges, thus creating a large current eastward. The Tar-Pamlico upper station was in the fresher zone with a value of 6.81 ppt, and it extended 18.4 km down the river. The lower station was in the mesohaline zone with a value of 12.20 ppt. This zone extended 15.4 km past the lower station into the sound. In the Neuse River, the upper station was near the border of the mesohaline and fresher zones, with a value of 11.47 ppt. The lower station was in the polyhaline zone. Closer to the mouth of the river, there were extensions of the polyhaline mixed and mesohaline zones near the northern border. The mixed zone extended past the lower station by about 5.1 km, and the mesohaline zone was 5.7 km up the river from the station. The differences between the two simulations decreased in size and magnitude. In the lower Neuse, the differences were in the range of 5 to 10 ppt.

At the end of the storm simulation, 0000 UTC 29 August (Figure 4.12, fourth row), the currents switched directions and slowed. They moved westward in the mouths of the rivers,

thus pushing the currents back up the rivers. Following this movement, in the Tar-Pamlico River, the lower station was in the polyhaline mixed zone with a value of 16.08 km. This mixed zone extended 8.1 km closer to the southern edge of the river. The upper station was still in the fresher zone, which now extended 13.2 km. In the Neuse River, the upper station was in the mesohaline zone with a value of 13.76 ppt. This zone extended 15.6 km up the river. The lower station was in the polyhaline. From the lower station, there was a 29.1-km-long intrusion of polyhaline mixed and a 25.1-km-long intrusion of polyhaline zone. The differences between the storm simulation and the no-storm had increased. In the Tar-Pamlico, these differences ranged from 5 to 10 ppt, while in the Neuse, these differences ranged from 10 to 15 ppt.

Two weeks after the storm simulation, at 0000 UTC 12 September (Figure 4.12, bottom row), the fresher, mesohaline, and polyhaline mixed zones extended further. This is due to the large river discharges causing the currents to move eastward, towards the Pamlico Sound. From the upper Tar-Pamlico station, the fresher zone extended 31.8 km and from Greenville, NC, it stretched about 76 km. The mesohaline zone now extended 26.6 km from the lower station into the sound. Also, it had a value of 13.26 ppt. In the Neuse, the fresher zone extended 8.5 km from the upper station and about 36 km from New Bern, NC. The lower station was in the mesohaline zone with a value of 16.06 ppt. The mesohaline zones from both rivers had connected. In the upper portions of both rivers, differences from the no-storm simulation showed the influence of the larger river discharges. These differences range from -5 to -10 ppt. Closer to the mouths of the rivers, the storm simulation had higher salinities, on the range of 5 ppt in the Tar-Pamlico and 5 to 10 ppt in the Neuse.

Each of the stations (Figure 4.13) located in this area experienced ranges less than 16 ppt. The upper Tar-Pamlico station saw a salinity minimum of 3.66 ppt (two weeks after) and a maximum of 12.23 ppt (around landfall), having a range of 8.57 ppt. The lower station had a minimum of 9.83 ppt (less than a day before landfall) and a maximum of 21.97 ppt (around landfall), a range of 12.14 ppt. At the Neuse upper station, there was a maximum of 18.53 ppt (near landfall) and a minimum of 3.18 ppt (two weeks after), a difference of 15.35 ppt. This station held constantly above 11 ppt from about 0700 UTC 28 August to about 0900 UTC 3 September. The upper station stayed in the mesohaline zone about 6 days. The lower station had a maximum of 21.64 ppt (near landfall) and a minimum of 15.88 ppt (near two weeks after), a difference of 5.76 ppt. Over the course of the simulation, this station salinity values stayed above 15 ppt. The Neuse River had the highest range in the upper region, followed by the lower station in the Tar-Pamlico.

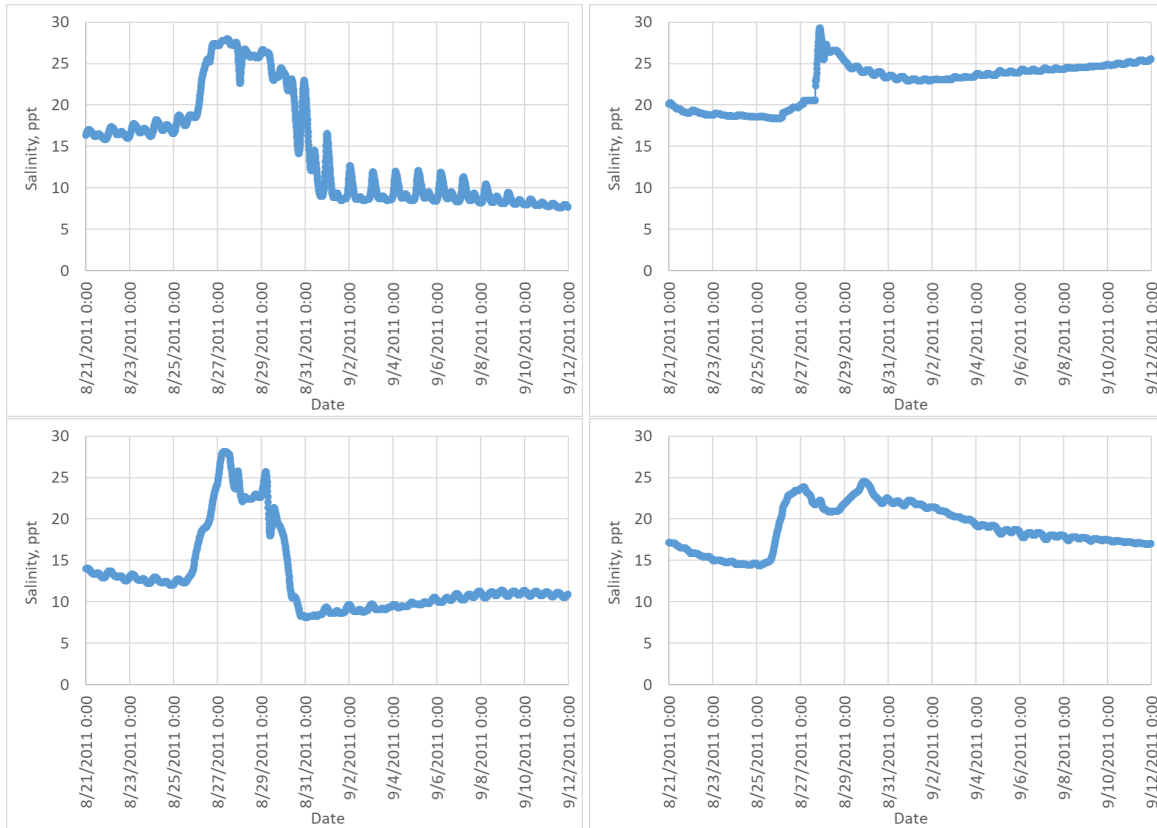


Figure 4.14: Time series of surface salinities (ppt) at the oyster sanctuaries stations: 22 (top left), 25 (top right), 26 (bottom left), and 34 (bottom right). Locations listed in Table 3.4 and shown in Figure 3.12.

4.3 Oyster Sanctuaries

There are a total of 15 oyster sanctuaries located in the study area (Figure 3.12). In this section, we examine the time series of the surface salinities at the sanctuaries with the largest ranges during the simulation. For the sanctuaries not discussed herein, the surface salinities had ranges less than 7.5 ppt during the storm.

The sanctuary with the largest change in salinity was station 22 in Croatan Sound, located near the southern end of Roanoke Island. This station experienced a range of about 20.37 ppt over the course of the simulation. The highest salinity, 27.9 ppt, occurred near the landfall of Irene. This higher salinity continued as the winds were pushing the euhaline zone westward, lasting about 4 days at these elevated levels. After the storm, there was a decrease in salinities corresponding to the increase of river discharges pushing the fresher zones from the Albemarle Sound. The lowest salinity, 7.5 ppt, occurred about two weeks

after the storm.

The next largest salinity range occurred at station 26 at Crab Hole, located near Oregon Inlet on the western side of the sound. This range was around 20 ppt during the storm. The highest salinity, 28.1 ppt, occurred before landfall, but earlier than the Croatan Sound sanctuary. These elevated levels of salinity lasted about 4 days. As currents moved northward with the progression of Irene's eye, the salinities began to decrease. This decrease continued even after the direction of the currents changed to southeastward. The eastward direction pushed the more saline waters away from the sanctuary. About two days after the storm, this sanctuary experienced the lowest salinity at 8.0 ppt. From then on, the salinity values increased gradually.

The remaining two sanctuaries, Clam Shoal (station 25) and Pea Island (station 34), experienced salinity ranges less than 11 ppt. Both were located in the Pamlico Sound. Clam Shoal is located near Hatteras Inlet and experienced a high of about 29 ppt right after landfall. These higher elevated levels lasted about 1 day, but through the rest of the simulation, the salinities remained elevated compared to the pre-storm values. The lowest salinity was 18.3 ppt and occurred about 1.5 days before landfall. Pea Island is located south of the Crab Hole sanctuary, but still near Oregon Inlet. This sanctuary experienced a maximum salinity of 24.4 ppt less than 1 day before landfall. These higher values lasted about 7 days. The lowest salinity was 14.3 ppt and occurred more than 2 days before landfall.

CHAPTER

5

CONCLUSIONS AND FUTURE WORK

To investigate the impact of storm events on circulation and transport in the Albemarle-Pamlico Estuarine System (APES), we developed a three-dimensional ADvanced CIRCulation (ADCIRC) model to include physical forcings of tides, river discharges, surface pressures and winds, and density differences via salinity and temperature. Irene (2011) was simulated using this model, and the resulting mixing and transport were examined.

The focus of this analysis was on the surface salinities, as it has been noted previously that the vertical stratification is minor (Luettich et al. 2002; Jia and Li 2012). Surface salinities were examined based on biologically based, salinity estuary zones. We selected zones that were relevant to two of the highest commercial revenue shellfish species: blue crab and oysters (North Carolina Division of Marine Fisheries 2020). This allowed for analyses of zones during and after Irene. For this research, the main takeaways are:

1. *In the eastern Albemarle Sound, surface salinities can increase by as much as three zones.* As the storm moved over the Albemarle, there was an intrusion of the euhaline zone by about 10 km into the sound. During the weeks after the storm had left the area, the fresher zone extended about 10.8 km on the western side of Roanoke Island. The largest salinity range, 24.63 ppt, was located near the mouth of the sound.

2. *Most of Pamlico Sound stayed within the polyhaline zone throughout Irene.* There were some intrusions from the inlets and rivers, but at locations near the middle of the sound, the surface salinity ranges were less than 7 ppt.
3. *Waters near Roanoke Island saw the largest changes in salinity.* Saline waters were pushed past the island during the storm, but then were pushed back by large freshwater runoff after the storm, thus leading to a large range of surface salinities during the storm. The west side of the island had the largest surface salinity range of 22.34 ppt, with similar ranges on the north and south sides.
4. *The Neuse and Tar-Pamlico Rivers experienced saline intrusions during the storm and fresh extrusions after the storm.* In the Tar-Pamlico, the fresher zone extended about 76 km down the river from Greenville, NC. In the Neuse, the fresher zone extended about 36 km past New Bern, NC.
5. *Most of the oyster sanctuary locations experienced changes in salinity less than 7.5 ppt.* Of the 15 sanctuaries located in the study areas, four had salinities that changed during the storm by ranges larger than 7.5 ppt. The sanctuaries with the largest salinity ranges of about 20 ppt were located in the northern Pamlico Sound by Roanoke Island. Two sanctuaries located near Hatteras Inlet and Roanoke Island experienced salinity ranges of about 10 ppt.

There are several ways that this Irene simulation can be improved in future work. Several improvements are related to model accuracy:

- *The inlets can be represented better in the mesh.* At the inlets in NC9-APES, the typical resolution is about 50 m, which is insufficient to represent the steep bathymetric gradients in these regions. The mesh was smoothed in these regions to improve numerical stability for the simulation in this thesis. By instead increasing resolution in the inlets and reinterpolating the bathymetries, the exchanges through the inlets would be better represented.
- *The rivers can be represented better in the mesh.* Four rivers are included in NC9-APES, but they are represented with relatively few elements across their width. In some places, the river width is represented by a single element. By increasing resolution in the rivers and reinterpolating the river bathymetries, the freshwater runoff would be better represented.

- *The river fluxes can be specified more accurately at the boundaries.* In the storm simulation in this thesis, the fluxes are specified evenly across the boundary. However, the fluxes can be specified by also including the bathymetric depths at the boundary vertices. This would allow larger fluxes to be specified in the deeper middle of each river.
- *Heat fluxes can be applied as a surface boundary condition.* These heat fluxes must be taken from another numerical model, and there was insufficient time to include them in the simulation in this thesis. The heat fluxes can be specified to vary spatially and temporally, thus allowing the surface temperatures to evolve more accurately.
- *The simulation can be extended.* Even 14 days after the storm, portions of APES had not returned to pre-storm conditions. By extending the simulation beyond that period, the recovery can be further investigated.

To assist in understanding the dynamics of how the horizontal salinity stratification can change due to a storm event, some additional investigation is necessary. For example, instead of looking at the resulting distribution from one type of storm, other types could also be considered and compared. Irene was a shore-parallel storm with a decent amount of rainfall. By examining the effects of a shore-perpendicular storm, like Florence (2018), or an excessive rainfall storm, like Floyd (1999), we could gain a better understanding of how different types of storm events alter the salinity distribution.

By including both storm and density-driven circulation, this and similar models have application outside the investigation of horizontal salinity distributions. For example, there are still uncertainties when it comes to the effect that density-driven circulation has on storm surge. These models could be used to investigate the effects. Another possibility is to examine how different types of storms can impact the system. This could include examining response of different nutrients, salinities, and/or temperature to varying storms. This could provide vital information for stakeholders, especially those relying on water quality for marine life development. These models could also be used to investigate which physical driver during a storm event has the greatest impact on density-circulation. This would allow for more understanding of the selected area's circulation.

REFERENCES

- Adcroft, A., Campin, J., Dutkiewicz, S., Evangelinos, C., Ferreira, D., Forget, G., Fox-Kemper, B., Heimbach, P., Hill, C., Hill, E., Hill, H., Jahn, O., Losch, M., Marshall, J., Maze, G., Menemenlis, D., and Molod, A. (2016). MITgcm user manual. Technical report, MIT Department of EPAS, Cambridge, MA.
- Albemarle-Pamlico National Estuary Partnership (2019). Blue Crab Unit. <https://apnep.nc.gov/media/475/open>. [Retrieved 18 October 2021].
- Albemarle-Pamlico National Estuary Partnership (2021). Our Estuary. <https://apnep.nc.gov/our-estuary>. [Retrieved 18 October 2021].
- Amein, M. and Airan, D. (1976). Mathematical modeling of circulation and hurricane surge in Pamlico Sound, North Carolina. Technical Report UNC-SG-76-12., NC Sea Grant.
- Avila, L. A. and Cangialosi, J. (2013). Tropical Cyclone Report, Hurricane Irene (AL092011), 21–28 August 2011. Technical report, National Hurricane Center.
- Black, W. and Dickey, T. (2008). Observations and analyses of upper ocean responses to tropical storms and hurricanes in the vicinity of Bermuda. *Journal of Geophysical Research-Oceans*, 113:C08009.
- Blain, C. A., Cambazoglu, M. K., and Kourafalou, V. H. (2009). Modeling the Dardanelles strait outflow plume using a coupled model system. In *OCEANS 2009*, pages 1–8.
- Blanton, B. O. and Luettich, R. A. (2008). North Carolina Coastal Flood Analysis System: Model Grid Generation. Technical Report TR-08-05, Renaissance Computing Institute.
- Blanton, B. O. and Luettich, R. A. (2010). North Carolina Floodplain Mapping Program, Coastal Flood Insurance Study: Water Level Validation Study. Technical Report TR-10-06, Renaissance Computing Institute.
- Blanton, B. O., Luettich, R. A., Hanson, J. L., Vickery, P., Slover, K., and Langan, T. (2012a). North Carolina Floodplain Mapping Program, Coastal Flood Insurance Study: Production Simulations and Statistical Analyses. Technical Report TR-12-03, Renaissance Computing Institute.
- Blanton, B. O., McGee, J., Fleming, J. G., Kaiser, C., Kaiser, H., Lander, H., Luettich, R. A., Dresback, K. M., and Kolar, R. L. (2012b). Urgent computing of storm surge for North Carolina's coast. In *Proceedings of the International Conference on Computational Science*, volume 9, pages 1677–1686.
- Blazek, R. and Bowman, H. (2021). *v.what.rast*. Open Source Geospatial Foundation. <https://grass.osgeo.org/grass78/manuals/v.what.rast.html>.

- Brown, M. M., Mulligan, R. P., and Miller, R. L. (2014). Modeling the transport of freshwater and dissolved organic carbon in the Neuse River Estuary, NC, USA following Hurricane Irene (2011). *Estuarine, Coastal and Shelf Science*, 139:148–158.
- Bulger, A. J., Monaco, M. E., and McCormick-Ray, M. G. (1993). Biologically-based estuarine salinity zones derived from a multivariate analysis. *Estuaries*, 16:311–322.
- Bunya, S., Dietrich, J. C., Westerink, J. J., Ebersole, B. A., Smith, J. M., Atkinson, J. H., Jensen, R. E., Resio, D. T., Luettich, R. A., Dawson, C. N., Cardone, V. J., Cox, A. T., Powell, M. D., Westerink, H. J., and Roberts, H. J. (2010). A high-resolution coupled riverine flow, tide, wind, wind wave and storm surge model for southern Louisiana and Mississippi: Part I – Model development and validation. *Monthly Weather Review*, 138:345–377.
- Caspers, H. (1959). Vorschläge einer Brackwassernomenklatur (The Venice System). *Int. Rev. Ges. Hydrbiol*, 44:313–316.
- Cheng, T., Hill, D., and Read, W. (2015). The Contributions to Storm Tides in Pacific Northwest Estuaries: Tillamook Bay, Oregon, and the December 2007 Storm. *Journal of Coastal Research*, 31(3):723–734.
- Cyriac, R., Dietrich, J. C., Blain, C. A., Dawson, C. N., Dresback, K. M., Fathi, A., Bilskie, M. V., Graber, H. C., Hagen, S. C., and Kolar, R. L. (2020). Wind and tide effects on the Choctawhatchee Bay plume and implications for surface transport at Destin Inlet. *Regional Studies in Marine Science*, 35:101131.
- Cyriac, R., Dietrich, J. C., Fleming, J. G., Blanton, B. O., Kaiser, C., Dawson, C. N., and Luettich, R. A. (2018). Variability in coastal flooding predictions due to forecast errors during Hurricane Arthur (2014). *Coastal Engineering*, 137:59–78.
- Davis, A. and Yan, X. (2004). Hurricane forcing on chlorophyll-a concentration off the northeast coast of the U.S. *Geophysical Research Letters*, 31.
- Dietrich, J. C., Muhammad, A., Curcic, M., Fathi, A., Dawson, C. N., Chen, S. S., and Luettich, R. A. (2018). Sensitivity of storm surge predictions to atmospheric forcing during Hurricane Isaac. *Journal of Waterway, Port, Coastal and Ocean Engineering*, 144.
- Dietrich, J. C., Trahan, C. J., Howard, M. T., Fleming, J. G., Weaver, R. J., Tanaka, S., Yu, L., Luettich, R. A., Dawson, C. N., Westerink, J. J., Wells, G., Lu, A., Vega, K., Kubach, A., Dresback, K. M., Kolar, R. L., Kaiser, C., and Twilley, R. R. (2012). Surface Trajectories of Oil Transport along the Northern Coastline of the Gulf of Mexico. *Continental Shelf Research*, 41:17–47.
- Dinápoli, M. G., Simionato, C. G., and Moreira, D. (2020). Development and validation of a storm surge forecasting/hindcasting modelling system for the extensive Rio de la Plata Estuary and its adjacent Continental Shelf. *Natural Hazards*, 103:2231–2259.

- Dolan, R. and Lins, H. (2000). The Outer Banks of North Carolina. Technical Report 1177-B, United States Geological Survey.
- Dresback, K. M., Fleming, J. G., Blanton, B. O., Kaiser, C., Gourley, J. J., Tromble, E. M., Luettich, R. A., Kolar, R. L., Hong, Y., Van Cooten, S., Vergara, H. J., Flamig, Z., Lander, H. M., Kelleher, K. E., and Nemunaitis-Monroe, K. L. (2013). Skill assessment of a real-time forecast system utilizing a coupled hydrologic and coastal hydrodynamic model during Hurricane Irene (2011). *Continental Shelf Research*, 71:78–94.
- Dresback, K. M., Kolar, R. L., Blain, C. A., Szpilka, C. M., Szpilka, A. M., Luettich, R. A., and Shay, T. (2010). Development and application of the coupled HYCOM and ADCIRC system. In *Proceedings of the 11th International Conference*, volume 388, pages 259–277. Estuarine and Coastal Modeling.
- D'Sa, E. J., Joshi, I. D., Liu, B., Ko, D. S., Osburn, C. L., and Bianchi, T. S. (2019). Biogeochemical Response of Apalachicola Bay and the Shelf Waters to Hurricane Michael Using Ocean Color Semi-Analytic/Inversion and Hydrodynamic Models. *Frontiers in Marine Science*, 6:523.
- Emanuel, K. (2013). Downscaling CMIP5 climate models shows increased tropical cyclone activity over the 21st century. *Proceedings of the National Academy of Science of the United States of America*, 110:12219–12224.
- Emanuel, K. (2017). Assessing the present and future probability of Hurricane Harvey's rainfall. *Proceedings of the National Academy of Science of the United States of America*, 114:12681–12684.
- Familkhalili, R. and Talke, S. A. (2016). The effect of channel deepening on tides and storm surge: A case study of Wilmington, NC. *Geophysical Research Letters*, 43:9138–9147.
- FEMA (2021). Flood risk study engineering library. <https://hazards.fema.gov/wps/portal/frisel>. [Retrieved 4 February 2021].
- Gao, J. (2018). *On the surface wind stress for storm surge modeling*. PhD thesis, University of North Carolina at Chapel Hill.
- GRASS Development Team (2017). *Geographic Resources Analysis Support System (GRASS GIS) Software, Version 7.2*. Open Source Geospatial Foundation.
- Haase, A., Eggleston, D., Luettich, R., Weaver, R., and Puckett, B. (2012). Estuarine circulation and predicted oyster larval dispersal among a network of reserves. *Estuarine Coastal and Shelf Science*, 101:33–43.
- Haney, R. L. (1991). On the Pressure Gradient Force over Steep Topography in Sigma Coordinate Ocean Models. *Journal of Physical Oceanography*, 21(4):610–619.

- Holland, R. W. (1980). An analytic model of the wind and pressure profiles in hurricanes. *Monthly Weather Review*, 108:1212–1218.
- Hu, K., Chen, Q., and Wang, H. (2015). A numerical study of vegetation impact on reducing storm surge by wetlands in a semi-enclosed estuary. *Coastal Engineering*, 95:66–76.
- Interagency Performance Evaluation Task Force (2008). Performance evaluation of the New Orleans and southeast Louisiana hurricane protection system. Technical report, US Army Corps of Engineers.
- Jelesnianski, C. P., Chen, J., and Shafer, W. A. (1992). SLOSH: Sea, Lake, and Overland Surges from Hurricanes. Technical report, U.S. Dep. of Commer., Natl. Oceanic and Atmos. Admin., Natl. Weather Serv., Silver Spring, Maryland.
- Jia, P. and Li, M. (2012). Circulation dynamics and salt balance in a lagoonal estuary. *Journal of Geophysical Research - Oceans*, 117:C01003.
- Kolar, R. L., Kibbey, T. C. G., Szpilka, C. M., Dresback, K. M., Tromble, E. M., Toohey, I. P., Hoggan, J. L., and Atkinson, J. H. (2009). Process-oriented tests for validation of baroclinic shallow water models: The lock-exchange problem. *Ocean Modelling*, 28:137–152.
- Lin, G. (1992). A numerical model of the hydrodynamics of Albemarle-Pamlico Sounds System, North Carolina. Master's thesis, North Carolina State University, Raleigh, North Carolina.
- Lin, J., Xie, L., Pietrafesa, L. J., Ramus, J. S., and Paerl, H. W. (2007). Water quality gradients across Albemarle-Pamlico Estuarine system: Seasonal variations and model applications. *Journal of Coastal Research*, 23:213–229.
- Lin, N., Emmanuel, K., Oppenheimer, M., and Vanmarcke, E. (2012). Physically based assessment of hurricane surge threat under climate change. *Nature Climate Change*, 2:462–467.
- Lindquist, N. and Fegley, S. (2016). Development of a Comprehensive North Carolina Salinity Database to Facilitate Management and Restoration of Critical Fish Habitats. Technical Report 2013-H-015, North Carolina Coastal Recreational Fishing License Final Report.
- Liu, Y., Weisberg, R., and Zheng, L. (2019). Impacts of Hurricane Irma on the Circulation and Transport in Florida Bay and the Charlotte Harbor Estuary. *Estuaries and Coasts*, 43(5):1194–1216.
- Luettich, R. A., Carr, S. D., Reynolds-Fleming, J. V., Fulcher, C. W., and McNinch, J. E. (2002). Semi-diurnal seiching in a shallow, micro-tidal lagoonal estuary. *Continental Shelf Research*, 22:1669–1681.

- Luettich, R. A. and Westerink, J. J. (2004). Formulation and numerical implementation of the 2D/3D ADCIRC finite element model version 44.XX. https://adcirc.org/files/2018/11/adcirc_theory_2004_12_08.pdf.
- Marshall, J., Adcroft, A., Hill, C., Perelman, L., and Heisey, C. (1997). A finite-volume, incompressible Navier Stokes model for studies of the ocean on parallel computers. *J. Geophysical Res.*, 102(C3):5753–5766.
- Maskell, J., Horsburgh, K., Lewis, M., and Bates, P. (2014). Investigating river–surge interaction in idealised estuaries. *Journal of Coastal Research*, 30(2):248–259.
- McDougall, T. J., Jackett, D. R., Wright, D. G., and Feistel, R. (2003). Accurate and Computationally Efficient Algorithms for Potential Temperature and Density of Seawater. *Journal of Atmospheric and Oceanic Technology*, 20(5):730–741.
- Mendelsohn, R., Emanuel, K., Chonabayashi, S., and Bakkensen, L. (2012). The impact of climate change on global tropical cyclone damage. *Nature Climate Change*, 2:205–209.
- Mitas, L., Mitasova, H., Kosinovsky, I., McCauley, D., Hofierka, J., Zubal, S., and Lacko, M. (2021). *u.surf.rst*. Open Source Geospatial Foundation. <https://grass.osgeo.org/grass79/manuals/v.surf.rst.html>.
- National Ocean Service (1985). National Estuarine Inventory, Data Atlas, Volume 1: Physical and Hydrologic Characteristics. Technical report, National Oceanic and Atmospheric Administration.
- National Oceanic and Atmospheric Administration (2021a). NOAA Hurricane Costs. <https://coast.noaa.gov/states/fast-facts/hurricane-costs.html>. [Retrieved 16 October 2021].
- National Oceanic and Atmospheric Administration (2021b). Tides & Currents: Duck NC Station. <https://tidesandcurrents.noaa.gov/harcon.html?unit=0&timezone=1&id=8651370&name=Duck&state=NC>. [Retrieved 16 October 2021].
- National Oceanic and Atmospheric Administration’s Climate Program Office (2020). U.S. Climate Resilience Toolkit: Storm Surge. <https://toolkit.climate.gov/topics/coastal/storm-surge>.
- National Weather Service (2018). Hurricane Irene August 26-27, 2011: Event Overview. <https://www.weather.gov/mhx/Aug272011EventReview>. [Retrieved 15 March 2018].
- Neuherz, R. A., Hoehler, D. C., Stuart, N. A., Lee, L., Keeter, K., Pelisier, J., Price, J., Vescio, M. D., Pietrafesa, L. J., and Janowitz, G. S. (1992). The use of hydrodynamic model for forecasting flooding around the North Carolina sounds. *13th Conference on Weather Analysis and Forecasts; American Meteorological Society Preprints*.
- North Carolina Department of Environmental Quality (2011). Fish Kill Historic Report. https://files.nc.gov/ncdeq/Water%20Quality/Environmental%20Sciences/FishKill/Event%20Maps/HistoricReport_2011.pdf. [Retrieved 18 October 2021].

- North Carolina Department of Environmental Quality (2021). Watershed Planning Documents. <https://deq.nc.gov/about/divisions/mitigation-services/dms-planning/watershed-planning-documents>. [Retrieved 31 October 2021].
- North Carolina Division of Marine Fisheries (2010). Eastern Oysters. <http://portal.ncdenr.org/web/mf/35eastern-oyster-ssr20110>. [Retrieved 19 October 2021].
- North Carolina Division of Marine Fisheries (2020). Chapter II: Commercial Fishery Statistics. <https://files.nc.gov/ncdeq/Marine-Fisheries/science---statistics/fisheries-statistics/big-book/Chapter-2-Commercial-Fishery-Statistics-with-Appendix.pdf>. [Retrieved 19 October 2021].
- Paerl, H., Crosswell, J., Dam, B. V., Hall, N., Rossignol, K., Osburn, C., Hounshell, A., Sloup, R., and Jr., L. H. (2018). Two decades of tropical cyclone impacts on North Carolina's estuarine carbon, nutrient and phytoplankton dynamics: implications for biogeochemical cycling and water quality in a stormier world. *Biogeochemistry*, 141:307–332.
- Peng, M., Xie, L., and Pietrafesa, L. J. (2004). A numerical study of storm surge and inundation in the Croatan-Albemarle-Pamlico Estuary System. *Estuarine, Coastal and Shelf Science*, 59:121–137.
- Pietrafesa, L. and Janowitz, G. (1991). The Albemarle-Pamlico Coupling Study. Technical report, Environmental Protection Agency.
- Pietrafesa, L., Janowitz, G., Chao, T., Weisberg, R., Askari, F., and Noble, E. (1986). The physical oceanography of Pamlico Sound. Technical Report UNC-WP-86-5, North Carolina Sea Grant.
- Pietrafesa, L. J., Xie, L., Morrison, J., Janowitz, G. S., Pelissier, J., Keeter, K., and Neuherz, R. A. (1997). Numerical modelling and computer visualization of the storm surge in and around the Croatan-Albemarle-Pamlico estuary system produced by Hurricane Emily of August 1993. *Mausam*, 48:567–578.
- Rayson, M. D., Gross, E. S., and Fringer, O. B. (2015). Modeling the tidal and sub-tidal hydrodynamics in a shallow, micro-tidal estuary. *Ocean Modelling*, 89:29–44.
- Renaissance Computing Institute (2016). <http://renci.org/>. [Retrieved 20 July 2016].
- Sebastian, A. G., Proft, J. M., Dietrich, J. C., Du, W., Bedient, P. B., and Dawson, C. N. (2014). Characterizing hurricane storm surge behavior in Galveston Bay using the SWAN+ADCIRC model. *Coastal Engineering*, 88:171–181.
- Sikiric, M. D., Janekovic, I., and Kuzmic, M. (2009). A new approach to bathymetry smoothing in sigma-coordinate ocean models. *Ocean Modelling*, 29(2):128–136.

- Szpilka, C., Dresback, K., Kolar, R., Feyen, J., and Wang, J. (2016). Improvements for the Western North Atlantic, Caribbean and Gulf of Mexico ADCIRC tidal database (EC2015). *Journal of Marine Science and Engineering*, 4:72.
- U.S. Geological Survey (2021). USGS Current Water Data for the Nation. <https://waterdata.usgs.gov/nwis/rt>. [Retrieved 31 October 2021].
- Westerink, J. J., Luettich Jr, R. A., Feyen, J. C., Atkinson, J. H., Dawson, C. N., Roberts, H. J., Powell, M. D., Dunion, J. P., Kubatko, E. J., and Pourtaheri, H. (2008). A Basin to Channel Scale Unstructured Grid Hurricane Storm Surge Model Applied to Southern Louisiana. *Monthly Weather Review*, 136:833–864.
- Williams, W., Beardsley, R., Irish, J., Smith, P., and Limeburner, R. (2001). Coupled economic-coastline modeling with suckers and free riders. *Deep-Sea Research Part II-Tropical Studies in Oceanography*, 48(1-3):179–197.
- Xie, L. and Pietrafesa, L. J. (1999). Systemwide modeling of wind and density driven circulation in Croatan-Albemarle-Pamlico estuary system. Part I: Model configuration and testing. *Journal of Coastal Research*, 18:1163–1177.
- Xie, X. and Li, M. (2018). Effects of wind straining on estuarine stratification: A combined observational and modeling study. *Journal of Geophysical Research-Oceans*, 123:2363–2380.
- Yin, K., Xu, S., Huang, W., and Xie, Y. (2017). Effects of sea level rise and typhoon intensity on storm surge and waves in Pearl River Estuary. *Ocean Engineering*, 136:80–93.

APPENDIX

APPENDIX

A

ADCIRC MODEL PARAMETERS

The Model Parameter and Periodic Boundary Condition File (fort.15) for the storm simulation.

```

Trimmed NC9 Mesh          ! 30 CHARACTER ALPHANUM RUN DESCRIPTION
Tidal Sequence Full Run  ! 20 CHARACTER ALPANAUMERIC RUN IDENTIFICATION
1 25.0 1 10 100.0       ! NFOVER NONFATA OVERRIDE,WARNING ELEV, FORT.69, KILL RUN
ELEV
0                        ! NABOUT - ABREVIATED OUTPUT
100                      ! NSCREEN - UNIT 6
567                      ! IHOT - HOT START
2                        ! ICS - COORDINATE SYSTEM
711112                  ! IM - MODEL TYPE  jgf20140502: corrected 111122
1                        ! NOLIBF - BOTTOM FRICTION TERM
2                        ! NOLIFA - FINITE AMPLITUDE TERM
1                        ! NOLICA - SPATIAL DERIVATIVE PORTION OF CONV. TERM
1                        ! NOLICAT - TIME DERIVATIVE PORTION OF CONVECTIVE TERM
3                        ! NWP jgf20140502:turned off wave refraction in swan
mannings_n_at_sea_floor
primitive_weighting_in_continuity_equation
surface_canopy_coefficient
1                        ! NCOR - VARIABLE CORIOLIS IN SPACE
1                        ! NTIP - TIDAL POTENTIAL
19                       ! NWS - WIND STRESS AND BAROMETRIC PRESSURE
1                        ! NRAMP - RAMP FUNCTION OPTION
9.81                    ! G - ACCELERATION DUE TO GRAVITY - DETERMINES UNITS
-3                      ! TAU0 - WEIGHTING FACTOR IN GWCE
0.5                    ! DT - TIME STEP (IN SECONDS) jgf20140502: 0.5s
0.0                    ! STATIM - STARTING TIME (IN DAYS)
0.0                    ! REFTIM - REFERENCE TIME (IN DAYS)
  2011 08 21 0000 1 0.9
23                      ! RNDAY - TOTAL LENGTH OF SIMULATION (IN DAYS)
6.0                    ! DRAMP - DURATION OF RAMP FUNCTION (IN DAYS)
0.0 1.0 0.0           ! TIME WEIGHTING FACTORS FOR THE GWCE EQUATION
0.1 0 0 .1           ! H0 - MINIMUM CUTOFF DEPTH
-79.0 35.0           ! SLAM0,SFEA0 - CENTER OF CPP DEGREES LONG/LAT
0.000 2. 10. 1.33333 ! FFACTOR - BOTTOM FRICTION COEFFICIENT
35.0                  ! ESL - LATERAL EDDY VISCOSITY COEFFICIENT
0.0                  ! CORI - CORIOLIS PARAMETER - IGNORED IF NCOR = 1
8                    ! NTIF
M2
  0.242334  1.405174E-004 0.693000 0.99887  36.88
S2
  0.112841  1.454426E-004 0.693000 1.00000  0.00
N2
  0.046398  1.378783E-004 0.693000 0.99887  331.65
K2
  0.030704  1.458408E-004 0.693000 1.02597  187.22
K1
  0.141565  7.292040E-005 0.736000 1.01855  183.72
O1
  0.100514  6.759704E-005 0.695000 1.02978  217.07
P1
  0.046843  7.252219E-005 0.706000 1.00000  167.53

```

Q1
 0.019256 6.495787E-005 0.695000 1.02978 151.84
 8 ! NBFR - TOTAL NUMBER OF FORCING FREQUENCIES ON OPEN
 BOUNDARIES
 M2
 1.405174E-004 0.99887 36.88
 S2
 1.454426E-004 1.00000 0.00
 N2
 1.378783E-004 0.99887 331.65
 K2
 1.458408E-004 1.02597 187.22
 K1
 7.292040E-005 1.01855 183.72
 O1
 6.759704E-005 1.02978 217.07
 P1
 7.252219E-005 1.00000 167.53
 Q1
 6.495787E-005 1.02978 151.84
 M2
 0.412918 354.052101
 0.412495 353.774359
 0.413119 353.760914
 0.413653 353.779417
 0.414470 353.794074
 0.415148 353.823253
 0.415994 353.875753
 0.416804 353.935866
 0.417714 354.004949
 0.418669 354.070645
 0.419655 354.141944
 0.420733 354.215672
 0.421812 354.289825
 0.422878 354.366128
 0.423955 354.442735
 0.424982 354.525743
 0.425940 354.612483
 0.426824 354.701045
 0.427589 354.788902
 0.428252 354.875090
 0.428754 354.964220
 0.429153 355.053350
 0.429303 355.134492
 0.428863 355.180713
 0.415872 350.205600
 0.416223 350.188685
 0.415981 350.235887
 0.415290 350.301375
 0.414202 350.381427

0.412839	350.479789
0.411134	350.592493
0.409142	350.712540
0.407072	350.835092
0.405045	350.954356
0.403176	351.065492
0.401517	351.167022
0.400195	351.252405
0.399212	351.319154
0.398518	351.373517
0.398141	351.409992
0.398080	351.423208
0.398279	351.419881
0.398690	351.401378
0.399324	351.365621
0.400234	351.307629
0.401770	351.274228
0.403458	351.293637
0.404249	351.419155
0.402015	351.720663

S2

0.071349	16.678074
0.071307	16.330281
0.071459	16.307920
0.071593	16.324391
0.071779	16.336620
0.071938	16.368947
0.072129	16.427898
0.072309	16.498623
0.072508	16.579277
0.072711	16.656820
0.072919	16.740442
0.073141	16.827961
0.073359	16.916198
0.073571	17.006723
0.073783	17.098818
0.073982	17.198147
0.074165	17.302305
0.074328	17.408548
0.074465	17.513539
0.074580	17.615650
0.074660	17.722326
0.074717	17.827939
0.074721	17.924688
0.074603	17.968805
0.070224	11.555048
0.070252	11.550683
0.070192	11.622856
0.070059	11.715396
0.069862	11.823055

0.069625	11.950080
0.069335	12.091450
0.069002	12.240028
0.068662	12.391969
0.068337	12.541490
0.068047	12.683274
0.067800	12.815377
0.067618	12.930400
0.067501	13.025331
0.067437	13.104939
0.067432	13.163607
0.067483	13.194229
0.067578	13.203981
0.067707	13.193880
0.067871	13.161572
0.068077	13.101375
0.068391	13.068965
0.068720	13.106719
0.068886	13.302951
0.068507	13.776511

N2

0.096457	335.097695
0.096367	334.741566
0.096506	334.727169
0.096628	334.745436
0.096811	334.763270
0.096961	334.793466
0.097146	334.850136
0.097323	334.913994
0.097519	334.988538
0.097728	335.060799
0.097942	335.139883
0.098177	335.222389
0.098413	335.306680
0.098646	335.393072
0.098881	335.479775
0.099104	335.572800
0.099311	335.670075
0.099501	335.767925
0.099666	335.863473
0.099807	335.956075
0.099912	336.051828
0.099994	336.145372
0.100020	336.228886
0.099914	336.271093
0.097429	331.302161
0.097480	331.283290
0.097398	331.315426
0.097220	331.362210
0.096957	331.421520

0.096637	331.496921
0.096243	331.584516
0.095789	331.678343
0.095318	331.775876
0.094858	331.872704
0.094433	331.964710
0.094055	332.050593
0.093752	332.124481
0.093524	332.183299
0.093361	332.231584
0.093269	332.265209
0.093247	332.278046
0.093283	332.276602
0.093367	332.261705
0.093500	332.231079
0.093694	332.179235
0.094025	332.153519
0.094387	332.181655
0.094548	332.314321
0.094059	332.641192

K2

0.020025	10.408693
0.020008	9.977233
0.020053	9.968171
0.020092	9.993664
0.020146	10.020046
0.020189	10.049928
0.020243	10.118861
0.020293	10.185809
0.020348	10.267784
0.020405	10.341636
0.020461	10.422323
0.020522	10.505363
0.020582	10.589852
0.020639	10.675123
0.020697	10.760138
0.020752	10.851632
0.020801	10.946791
0.020845	11.043611
0.020883	11.138926
0.020915	11.232435
0.020937	11.329487
0.020953	11.425897
0.020955	11.513225
0.020924	11.550954
0.019847	5.040049
0.019856	5.022366
0.019838	5.088664
0.019799	5.178392
0.019741	5.284170

0.019672	5.410509
0.019590	5.555370
0.019494	5.711116
0.019396	5.873086
0.019301	6.035881
0.019217	6.193622
0.019144	6.345764
0.019089	6.479502
0.019057	6.591675
0.019038	6.684300
0.019034	6.751835
0.019047	6.784483
0.019071	6.798401
0.019105	6.797633
0.019150	6.773862
0.019206	6.719183
0.019285	6.678135
0.019370	6.692321
0.019437	6.819375
0.019363	7.177178

K1

0.092879	176.234756
0.092874	176.037778
0.092827	176.098072
0.092796	176.119147
0.092748	176.184263
0.092716	176.188871
0.092687	176.216371
0.092656	176.209308
0.092629	176.209452
0.092603	176.196728
0.092582	176.187477
0.092557	176.173163
0.092538	176.159869
0.092521	176.146074
0.092508	176.128071
0.092496	176.108843
0.092487	176.088522
0.092475	176.064592
0.092465	176.039722
0.092463	176.015808
0.092461	175.985694
0.092463	175.959840
0.092464	175.930992
0.092494	175.903744
0.093243	178.009458
0.093295	178.063950
0.093285	178.136351
0.093271	178.189708
0.093255	178.225586

0.093235 178.249868
0.093216 178.262458
0.093199 178.262444
0.093181 178.251819
0.093161 178.229769
0.093140 178.197486
0.093114 178.154795
0.093086 178.106385
0.093050 178.052418
0.093011 177.995586
0.092965 177.940534
0.092925 177.888722
0.092891 177.838666
0.092864 177.789936
0.092854 177.745288
0.092869 177.699557
0.092917 177.677526
0.093009 177.691732
0.093357 177.892730
0.094249 178.124733

01

0.071007 181.144166
0.070953 180.900780
0.070754 181.188154
0.070558 181.291304
0.070279 181.540584
0.070055 181.573592
0.069872 181.696383
0.069678 181.700283
0.069501 181.726388
0.069305 181.717716
0.069103 181.701345
0.068912 181.670221
0.068710 181.628418
0.068505 181.571987
0.068330 181.491969
0.068159 181.397206
0.067989 181.294931
0.067822 181.162002
0.067663 181.016511
0.067523 180.861400
0.067388 180.645116
0.067270 180.460158
0.067135 180.265180
0.067133 180.020752
0.067871 186.986390
0.068049 186.914717
0.068323 186.922264
0.068587 186.920256
0.068831 186.924538

0.069052 186.933054
0.069255 186.934053
0.069444 186.916671
0.069606 186.884119
0.069735 186.830471
0.069830 186.759802
0.069878 186.677233
0.069886 186.600230
0.069851 186.537927
0.069794 186.500489
0.069736 186.496912
0.069708 186.515526
0.069711 186.551987
0.069749 186.600107
0.069835 186.655281
0.069969 186.713392
0.070190 186.826269
0.070583 187.098697
0.071803 187.803667
0.074816 188.019613

P1

0.029350 179.078595
0.029337 178.852183
0.029349 178.980205
0.029339 179.054693
0.029334 179.188172
0.029311 179.242048
0.029307 179.312299
0.029289 179.343457
0.029278 179.383995
0.029261 179.412969
0.029242 179.447452
0.029223 179.473145
0.029203 179.501231
0.029180 179.528403
0.029157 179.539227
0.029133 179.547861
0.029111 179.557139
0.029084 179.554447
0.029058 179.547181
0.029032 179.535755
0.028999 179.511210
0.028972 179.492392
0.028943 179.473195
0.028920 179.419925
0.029835 181.707650
0.029849 181.729722
0.029856 181.760565
0.029861 181.774727
0.029867 181.777616

0.029871 181.774165
0.029876 181.760357
0.029881 181.734422
0.029884 181.700467
0.029884 181.657505
0.029881 181.607722
0.029873 181.552677
0.029862 181.498384
0.029846 181.445663
0.029828 181.394733
0.029810 181.348129
0.029796 181.304257
0.029786 181.263169
0.029780 181.223886
0.029781 181.186181
0.029793 181.143408
0.029824 181.123963
0.029895 181.167940
0.030134 181.357935
0.030612 181.183791

Q1

0.013813 171.767646
0.013803 171.593041
0.013850 171.622219
0.013873 171.687752
0.013920 171.776522
0.013937 171.866085
0.013965 171.897357
0.013977 171.960055
0.013990 171.999273
0.013998 172.061487
0.014006 172.136135
0.014011 172.207142
0.014016 172.290779
0.014019 172.383598
0.014018 172.458006
0.014016 172.532713
0.014013 172.605300
0.014006 172.684083
0.013998 172.762225
0.013989 172.838779
0.013971 172.931508
0.013958 173.011460
0.013947 173.097332
0.013927 173.163060
0.014992 173.658618
0.014960 173.693369
0.014914 173.628131
0.014873 173.546584
0.014838 173.444487

```

0.014809 173.332985
0.014783 173.214024
0.014760 173.090338
0.014738 172.971651
0.014715 172.865759
0.014692 172.777859
0.014670 172.712400
0.014654 172.668110
0.014642 172.644376
0.014637 172.617793
0.014641 172.573769
0.014647 172.504336
0.014654 172.412193
0.014660 172.299091
0.014663 172.168673
0.014664 172.022762
0.014666 171.830631
0.014691 171.477379
0.014770 170.500353
0.014661 168.746907
110.0          ! ANGINN : INNER ANGLE THRESHOLD
0              ! NFFR
-5 0.0 30.0 3600 ! NOUTE,TOUTSE,TOUTFE,NSPOOLE:ELEV STATION OUTPUT INFO (UNIT
61)
10            ! TOTAL NUMBER OF ELEVATION RECORDING STATIONS
-75.519838 35.326875
-76.622778 35.537222
-75.704818 35.211632
-76.892778 35.813056
-75.700196 36.049921
-75.848740 36.370491
-75.987222 35.115278
-75.549722 35.796389
-77.061944 35.543333
-76.722778 35.915000
-5 0.0 30.0 3600 ! NOUTV,TOUTSV,TOUTFV,NSPOOLV :VEL STATION OUTPUT INFO (UNIT
62)
10            ! TOTAL NUMBER OF ELEVATION RECORDING STATIONS
-75.519838 35.326875
-76.622778 35.537222
-75.704818 35.211632
-76.892778 35.813056
-75.700196 36.049921
-75.848740 36.370491
-75.987222 35.115278
-75.549722 35.796389
-77.061944 35.543333
-76.722778 35.915000
0 0 0 0          ! MET
0

```

```

-5 0.0 30.0 1800          ! NOUTGE,TOUTSGE,TOUTFGE,NSPOOLGE : (UNIT 63)
-5 0.0 30.0 1800          ! NOUTGV,TOUTSGV,TOUTFGV,NSPOOLGV : (UNIT 64)
-5 0.0 30.0 1800          ! MET
0                          ! NHARF - NUMBER OF FREQUENCIES IN HARMONIC ANALYSIS
15.0 45.0 60 0.0         ! THAS, THAF, NHAINC,FMV
0 0 0 0                   ! NHASE,NHASV,NHAGE,NHAGV
5 172800                  ! NHSTAR,NHSINC
1 0 1.00E-07 25 0        ! ITITER,ISLDIA,CONVCR,ITMAX,ILUMP
4                          ! IDEN, 0=barotropic model run
2 0.005                   ! slip code and slip coefficient
0.01 0.01                 ! free surface and bottom roughnesses (const.
horiz)
0.5 0.5 0.5              ! time stepping coefficients (alpha 1,2,3)
1 11                       ! f.e. grid code, # nodes in f.e. grid
50 0.001 0.1             ! e.v. code, evmin, evcon coefficient
0.5 0.5                   ! THETA1, THETA2 included if IEVC = 50
0 0.0 5.0 3               ! DTS station output
0
-5 0.0 10.0 3600         ! velocity station output
10
-75.519838 35.326875
-76.622778 35.537222
-75.704818 35.211632
-76.892778 35.813056
-75.700196 36.049921
-75.848740 36.370491
-75.987222 35.115278
-75.549722 35.796389
-77.061944 35.543333
-76.722778 35.915000     ! coordinates of velocity station
0 0.0 5.0 3              ! turbulence station output
0                          ! coordinates of turbulence stations
-5 0.0 365 1800          ! DTS global output
-5 0.0 365 1800          ! velocity global output
0 0.0 23 3600            ! turbulence global output
4 0.0 0                   ! Boundary condition flags for elevation, temperature
RES_BC_FLAG, BCFLAG_LNM, BCFLAG_TEMP
3600 3600 3600           ! RBCTIMEINC
1209600 1209600 1209600 ! BCSTATIM
0.0                       ! sponge dist
2                          ! eq state
50.0 10.0                 ! NLSO, NVSD
50.0 10.0                 ! NLTD, NVTD
0.5                       ! APH4
NC STATE UNIVERSITY
Henry 2

```